METHODS FOR VOLTAGE MONITORING, ANALYSIS AND IMPROVEMENT IN ACTIVE DISTRIBUTION NETWORKS

Jingyuan Liu

A Dissertation Submitted to the Faculty of Graduate Studies in Partial Fulfillment of the Requirements for the Degree of Doctor of Philosophy

Graduate Program in Electrical Engineering and Computer Science
York University
Toronto, Ontario

April 2022

Abstract

Power Distribution Networks (DNs) deliver electricity from the transmission systems to the consumers. The proliferation of diverse load components and distributed generators in active DNs is drastically changing the power demand and supply patterns in the DN, which in turn has led to significant stress and uncertainty on the voltage profiles of the DNs. Nevertheless, the communication and computation capabilities of the modern DNs have enabled cyber-enabled power components such as DG (Distributed Generator) devices to make intelligent decisions through information exchanges [1]. As such, in this dissertation we leverage on this novel capability to present algorithms for voltage monitoring, analysis and improvement that allow the system operator to assess the voltage profile of the DN and to take preventative actions for enhancing voltage profiles and preventing undervoltage/overvoltage incidents. In the subsequent chapters, we present performance guarantees and simulation studies on the proposed algorithms, and compare the algorithms introduced in this dissertation with the state-of-the-art.

Table of Contents

Abstract ii

Table of Contents iii

List of Tables vi

List of Figures viii

List of Algorithms ix

List of Acronyms x

Nomenclature xii

1 Introduction 1

1.1 Overview of Smart Devices 3

1.2 Literature Survey 5

1.2.1 Grid Condition Monitoring 5

1.2.2 Probabilistic Load Flow 6

1.2.3 Topology Reconfiguration 8

1.3 Contributions of This Thesis 10

1.4 Thesis Outline 11

2 Background on Smart Distribution Networks 12

2.1 DN Settings and Assumptions 12

2.2 Notations 13
2.3 Models for DN Power Flow Relations 15
2.4 Modeling of Power Injection 22

3 Decentralized Grid Monitoring **23**
3.1 DN Settings and Problem Formulation 23
3.2 Design of the Monitoring Algorithm 25
3.3 Simulation Results 26
3.4 Chapter Summary 29

4 Data-Driven PLF for Voltage Analysis **30**
4.1 DN Settings and Problem Formulation 30
4.2 Brief Overview of GP Emulator 32
4.3 Proposed Kernel Design Methodology 36
4.4 Theoretical Performance Guarantees 38
4.5 Simulations on Practical Networks 42
4.6 Chapter Summary 51

5 Reconfiguration for Voltage Profile Improvement **52**
5.1 Problem Formulation 53
5.2 Decentralized DN Topology Reconfiguration 54
5.3 Theoretical Performance Guarantees 58
5.4 Simulation Results 59
5.5 Chapter Summary 63

6 Optimal Reconfiguration with Convex Relaxation **64**
6.1 Problem Formulation 65
6.2 Formulation of Reconfiguration Algorithm 67
6.3 Theoretical Performance Guarantees 74

6.4 Simulations on Practical DNs 82
6.5 Comparative Analysis 86
6.6 Chapter Summary 89

7 Conclusions and Future Work **90**
7.1 Dissertation Summary 90
7.2 Future Work 92

A Network Parameters for DNs **94**

Bibliography **111**

List of Tables

Page 11: Table 1.1: List of Publications.

Page 27: Table 3.1: Cluster ALE Loads in the 33-bus DN.

Page 34: Table 4.1: Examples of GP Emulator Kernels.

Page 45: Table 4.2:Impact of Initial Kernel Structure on Convergence Properties of Alg. 2.

Page 47: Table 4.3: R Values for the Proposed Method.

Page 50: Table 4.4: Comparison of KLD.

Page 51: Table 4.5: Comparison Between Simulation Time.

Page 86: Table 6.1: Comparison with Existing Work.

Page 95: Table A.1: Bus Parameters for the IEEE 33-Bus DN.

Page 96: Table A.2: Line Parameters for the IEEE 33-Bus DN.

Page 97: Table A.3: Bus Parameters for the IEEE 69-Bus DN.

Page 98: Table A.4: Line Parameters for the IEEE 69-Bus DN.

Page 99: Table A.5: Bus Parameters for the Brazilian 136-Bus DN (1).

Page 100: Table A.6: Bus Parameters for the Brazilian 136-Bus DN (2)..

Page 101: Table A.7: Line Parameters for the Brazilian 136-Bus DN (1).

Page 102: Table A.8: Line Parameters for the Brazilian 136-Bus DN (2).

Page 103: Table A.9: Bus Parameters for the IEEE 37-Bus DN.

Page 104: Table A.10: Line Parameters for the IEEE 37-Bus DN.

Page 104: Table A.11: Line Types for the IEEE 37-Bus DN.

Page 105: Table A.12: Bus Parameters for the IEEE 123-Bus DN (1).

Page 106: Table A.13: Bus Parameters for the IEEE 123-Bus DN (2).

Page 107: Table A.14: Bus Parameters for the IEEE 123-Bus DN (3).

Page 108: Table A.15: Line Parameters for the IEEE 123-Bus DN (1).

Page 109: Table A.16: Line Parameters for the IEEE 123-Bus DN (2).

Page 110: Table A.17: Line Types for the IEEE 123-Bus DN.

List of Figures

Page 2: Figure 1.1: Voltage Regulation Framework.

Page 3: Figure 1.2: Diagram of Contributions.

Page 14: Figure 2.1: Illustration of Notations in a Radial Network.

Page 24: Figure 3.1: Illustration of Clusters in a Radial Network.

Page 27: Figure 3.2: Simulations of Grid Condition Monitoring and ALE Integration.

Page 28: Figure 3.3: Illustration of Clusters in the 33-bus DN.

Page 46: Figure 4.1: Convergence Study for Alg. 2.

Page 48: Figure 4.2: Comparative Study for IEEE-33 DN.

Page 49: Figure 4.3: Comparison of Distributions for 123-87-B System.

Page 55: Figure 5.1: Illustration of the Three Cases.

Page 61: Figure 5.2: Simulations for the Switching Case.

Page 62: Figure 5.3: Simulations for the Branch Exchange Case.

Page 69: Figure 6.1: Illustration of Local and Perspective Variables.

Page 83: Figure 6.2: Topology of the 76-Bus DN.

Page 83: Figure 6.3: Impact of Initial Topology.

Page 85: Figure 6.4: Convergence Study for Alg. 4 under IT 01011.

Page 88: Figure 6.5: Comparative study with FNSGA.

List of Algorithms

Page 25: Alg. 1: Proposed Decentralized Monitoring Algorithm.

Page 38: Alg. 2: Proposed Kernel Design Algorithm.

Page 57: Alg. 3: Proposed Decentralized Topology Reconfiguration Algorithm.

Page 75: Alg. 4: Convex Reconfiguration for Voltage Improvement.

List of Acronyms

ALE Alternative Load Element

ADMM Alternating Direction Method of Multipliers

AMI Advanced Metering Infrastructure

CDM Constrained Direct Method

DN Distribution Network

DG Distributed Generator

DER Distributed Energy Resources

EV Electric Vehicle

FNSGA Fast Non-denominated Sorted Genetic Algorithm

GPU Graphical Processing Unit

GP Gaussian Process

GEN Generator

IEEE Institute of Electrical and Electronics Engineers

KLD Kullback-Leibler Divergence

LTP Load Tap Changers

LPF Linearized Power Flow

MCS Monte Carlo Simulation

MILP Mixed Integer Linear Programming

MISOCP Mixed Integer Second Order Cone Programming

MISDP Mixed Integer Semi-Definite Programming

MINLP Mixed Integer Non-Linear Programming

MLE Maximum Likelihood Estimation

NPF Nonlinear Power Flow

OSPF Open Shortest Path First

OS Order Set

PMU Phasor Measurement Unit

PLF Probabilistic Load Flow

PV PhotoVoltaics

QCP Quadratic Constrained Programming

QCQP Quadratic Constrained Quadratic Programming

RMSE Root Mean Square Error

SVC Static Var Compensators

SDP Semi-Definite Programming

SOCP Second Order Cone Programming

SCADA Supervisory Control And Data Acquisition

UDM Unconstrained Direct Method

Nomenclature

General Terms

$\mathcal{B}$	Set of buses
$\mathcal{E}$	Set of power lines
$\mathcal{P}$	Set of all potential parent sets
Ψ	Set of cycles
$\mathcal{R}$	Set of reconfigurable buses
$\mathcal{T}$	Topology of DN
$\mathcal{Z}$	Set of impedances along power lines

Bus Terms

$A_{r,m}$	Lowest common ancestor for $r, m \in \mathcal{B}$
$\mathcal{B}_r$	Bus set in the subtree rooted at $r \in \mathcal{B}$
C_r	Summation of loads for all buses in $\mathcal{B}_r$
f	Feeder bus
$\mathcal{K}_i$	Set of children for $i \in \mathcal{B}$
P_r, Q_r	Real and reactive loads at $r \in \mathcal{B}$
$\mathcal{P}_i$	Set of potential parents for $i \in \mathcal{R}$
$\overline{p}_r$, $\underline{p}_r$	Limits of real load at $r \in \mathcal{B}$
$\overline{q}_r$, $\underline{q}_r$	Limits of reactive load at $r \in \mathcal{B}$
Φ_r	Set of phases for $r \in \mathcal{B}$
S_r	Power injection/absorption at $r \in \mathcal{B}$
V_r	Voltage at $r \in \mathcal{B}$
V_r^{ϕ}	Voltage at $r \in \mathcal{B}$ at phase ϕ
$\hat{\mathcal{V}}_r$	Artificial voltage term, $\hat{\mathcal{V}}_r = V_r V_r^H$
$\overline{v}_r$, $\underline{v}_r$	Limits of voltage magnitude at $r \in \mathcal{B}$

Line Terms

$\mathcal{B}_{r,m}$	Set of terminal buses for $\mathcal{E}_{r,m}$
$\mathcal{E}_{r,m}$	Set of lines connecting $r, m \in \mathcal{B}$
$\mathcal{E}_f$	Set of fixed lines
$\mathcal{E}_s$	Set of switchable lines
I_{rl}	Current flow at line $(r, l) \in \mathcal{E}$

$\mathcal{I}_{rl}$	Artificial current term, $\mathcal{I}_{rl} = I_{rl} I_{rl}^H$	$\overline{S}_{rl}$	Upper limit of power flow at $(r, l) \in \mathcal{E}$
Φ_{rl}	Set of phases for line $(r, l) \in \mathcal{E}$	$\mathcal{S}_{rl}$	Artificial power term, $\mathcal{S}_{rl} = V_r^{\Phi_{rl}} I_{rl}^H$
S_{rl}	Power flow at line $(r, l) \in \mathcal{E}$	z_{rl}	Impedance at line $(r, l) \in \mathcal{E}$

Chapter 1

Introduction

The rapid proliferation of diverse Distributed Energy Resources (DERs) such as privately-owned photovoltaic generation systems can lead to significant uncertainty in the load/generation profile in the DN. According to the equations that govern the power flow in the DN (e.g. Kirchhoff's law), uncertainties in load/generation can lead to variations in DN bus voltages. As such, the highly varying voltage profile in active DNs caused by the integration of DERs poses pressing new challenges to the safe operation of the power networks [2]. Examples of these challenges include reverse power flow into the transmission system and increased power loss in the DNs. To address this issue, various proposals (e.g. [3, 4, 5, 6, 7, 8]) have formed a framework for voltage regulation based on the enhanced monitoring and actuation capabilities of cyber-enabled smart devices. This framework is formed by three components: DN monitoring, voltage analysis and voltage profile improvement. The relationship between these components and the DN is illustrated in Fig. 1.1.

The monitoring component inspects the voltage data gathered from smart devices such as micro-Phasor Measurement Units (PMUs) [3] and smart meters. Research areas associated with the monitoring component include 1) Measurement data integration, which studies efficient integration of measurement data gathered from heterogeneous data sources [6];2) Decentralized or distributed monitoring, which aims to increase the scalability and resiliency of monitoring architecture by removing the need for centralized decision makers [7]; 3) Measurement error correction,

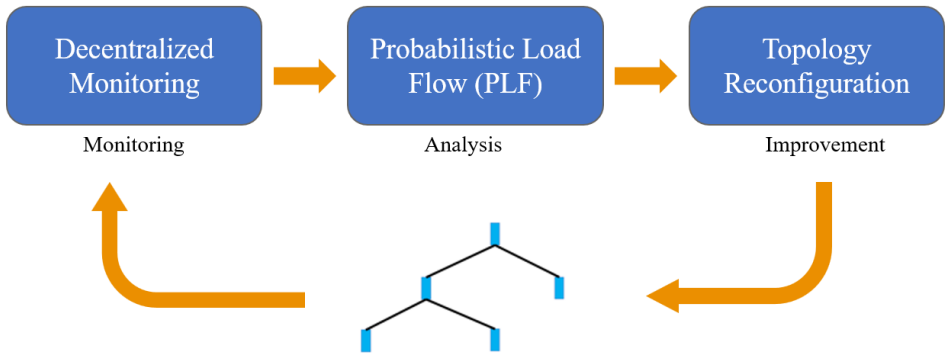

Figure 1.1: Voltage Regulation Framework.

which strives to mitigate the measurement errors incurred by various measurement devices such as smart meters and PMUs [8].

After the voltage data from various devices are gathered and inspected, the voltage analysis component studies the characteristics of voltage variables under diverse load/generation conditions in the DN. Some examples of proposals associated with the analysis component belong to the following categories: 1) Probabilistic Load Flow (PLF), which evaluates the characteristics of voltage variables under uncertainties in load and generation [9] and 2) Voltage estimation, which estimates DN voltage profiles from noisy and/or low quality measurement data [10].

When the characteristics of the voltage state variables have been analyzed, the improvement component coordinates smart actuators in the DN (e.g. automatic switches [11] and smart inverters [2]) to reduce the impact of adverse conditions and improve the voltage profile of the smart DNs. The hierarchical control architecture commonly employed in modern power systems [12] generally organizes voltage improvement techniques in a three-level structure. Improvement techniques belonging to the primary level are based on local measurements and keep the terminal voltages of the controllable resources (e.g. generators) around a set of set points. Improvement techniques belonging to the secondary level aim to maintain the stability of DN under different generation and loading situations and they operate through changing the set point values of controllable resources. Improvement techniques belonging to the tertiary level leverage forecast data to optimize the voltage profile of the DN. Research areas associated with the improvement component include

1) Topology reconfiguration, which recovers from DN outages caused by voltage collapse or improves the DN voltage profile by changing the underlying topology of the DN; 2) Reactive power control, which regulates bus voltages by controlling the injection of reactive power from smart actuators; and 3) Current flow control, which regulates bus voltages by controlling current injection from smart actuators.

Figure 1.2: Diagram of Contributions.

In this thesis, four main contributions to the voltage regulation framework are presented and these contributions are listed in Fig. 1.2. For the monitoring component, a decentralized grid condition monitoring algorithm based on consensus averaging is introduced. For the analysis component, a kernel design method for Gaussian Process (GP) based PLF calculation is proposed. For the improvement component, a decentralized DN topology reconfiguration algorithm based on game-theoretical constructs and a reconfiguration algorithm that finds the globally optimal DN topology through convex optimization constructs are presented.

1.1 Overview of Smart Devices

In this section, the capabilities of the cyber-enabled smart devices for voltage enhancement are reviewed. Then, a feasibility study on the methods introduced in this thesis is presented.

The smart devices can be generally divided into two categories: 1) Smart meters that are capable of data gathering and transmission, and 2) Smart actuators that mitigate voltage anomalies.

Currently, the data transmission capabilities of the smart meters are supported by both wireless and wired communication systems. In general, wireless systems such as WiMax, 3G, 4G and 5G are more scalable and less expensive than their wired counterparts (e.g. optical fiber and power line communication) [13, 14]. However, they are also more susceptible to interference and congestion [15]. While there are proposals for expanding the functionality of wireless systems by combining them with wired technologies [16], the disadvantages associated with wireless systems remain major issues of concern.

Due to the various limiting factors (i.e. topology, base voltage) present in the DNs, different types of smart actuators have been developed. These devices can be cataloged into two categories based on their method for voltage regulation. The first type of devices such as synchronous condensers and Static Var Compensators (SVCs) presented in reference [17] regulates voltage by injecting/absorbing reactive power. While these devices are ideal for higher voltage networks where the lines are mostly reactive, their effectiveness is reduced for lower voltage DNs with resistive lines. The second type of devices regulates voltage by controlling the current flow. As such, they are effective for both resistive and reactive DNs. Examples of devices in this category include smart inverters and Load Type Changers (LTPs). Smart inverters are capable of controlling both real and reactive power flow from power sources into the DN. However, the lack of regulation for private owned inverter-based DGs has also lead to operation challenges for power grids in Germany, Hawaii, and California [2]. As LTPs regulate voltage by adjusting transformer windings [17], their effectiveness for anomaly mitigation depends heavily on the location of the transformer relative to the anomalies. Moreover, switching operations conducted at the LTPs can lead to wear and tear over time and this also compromise the effectiveness of these devices [18].

In the current framework for information flow in the DN, data transmission to the central controller is often delegated to wireless technologies. Therefore, decentralized configuration for monitoring and improvement would further expand the functionality of wireless technologies by reducing congestion and dependencies on the central agent. While topology reconfiguration is mostly used for post-fault service restoration [11], its ability for voltage control through real power reg-

ulation has also attracted an increasing number of proposals. Cases where reconfiguration based voltage improvement can be particularly useful include mostly resistive DNs that satisfy the following conditions: 1) The utilities do not have control of the majority of the inverters, and 2) The standalone capacities of LTPs are insufficient.

1.2 Literature Survey

In this section, a detailed overview on the existing work in the areas of grid condition monitoring, probabilistic power flow and DN topology reconfiguration is provided.

1.2.1 Grid Condition Monitoring

Existing literature in the area of DN condition monitoring can be divided into two major categories. Works belonging to the first category treat cyber-enabled agents as independent nodes capable of reaching their own opinions on system states, and utilize data exchanges between agents to achieve consensus of opinions. Examples of proposals in this category include reference [19] where every bus in the DN calculates its own voltage sensitivity indices using information obtained from neighbouring buses, [20] where a distributed voltage monitoring technique based on synchrophasor measurements is introduced, reference [21] where decentralized voltage monitoring is performed via a distributed computing architecture and reference [22] where distributed control technique is employed for voltage monitoring. These proposals have shown that for specific applications such as DG dispatch and demand response, decomposition based approaches can be used to achieve consensus among agents. On the other hand, proposals belonging to the second category treat cyber-enabled agents as intermediaries that are only capable of gathering local information and passing it on to a central controller for information processing and decision making. Examples of proposals in this category include reference [23] where stochastic assessment of voltage indices is performed with integer optimization methods, reference [24] where matrix factorization is employed to analyze measurement data gathered from high renewable penetrated DNs, reference [25]

where analysis of bus voltages is performed via disagreement-based deep learning techniques, reference [26] which calculate the voltage indices from DN parameters, reference [27] where field tests of a decentralized DN monitoring technique are conducted in real world practical systems.

1.2.2 Probabilistic Load Flow

PLF is a technique for power flow evaluation that can be used to predict bus voltages under variable loading and generation conditions [9]. Proposals in PLF can be classified into four main categories depending on the theoretical constructs utilized to implement them.

Proposals belonging to the first category utilize Monte Carlo Simulation (MCS) based techniques to evaluate the statistical properties of power flow. The MCS technique utilizes repeated sampling to study the properties of power flow and the samples analyzed by the MCS can come from sensor measurements in practical DN systems or accurate models of power systems. Examples of MCS based PLF techniques include reference [28] where the data-centric technique of GP modelling is utilized to construct a surrogate model of the power system, reference [29] where the system model is obtained from deep learning, reference [30] where an efficient sampling technique based on Latin hypercube sampling is employed, reference [31] where an adaptive sampling method based on importance sampling and reinforcement learning is introduced, reference [32] where a DN modelling technique incorporating theoretical constructs from Bayesian networks is employed, reference [33] where the modelling technique of response surface is utilized to approximate the characteristics of power systems, reference [34] where an importance sampling technique based on the cross-entropy method is employed in conjunction with the MCS, reference [35] where a technique for accelerating deterministic power flow calculations via Graphical Processing Units (GPUs) is introduced, reference [36] which accelerates power flow calculations with parallel computation techniques based on OpenCL and reference [37] where a stochastic sampling method is deployed for generating of random samples. These proposals do not require any simplifying assumptions. However, these are associated with high computational overheads.

The second category is composed of PLF studies conducted via *analytical methods* that cal-

culate the stochastic properties of the DN from relaxed models of power flow relation and distributions of DN variables. Examples of PLF proposals in this category include reference [38] which employs probabilistic load integration techniques, reference [39] which approximates the power flow relation with the technique of multidimensional holomorphic embedding, reference [40] where the distribution of voltage variables are inferred with linearized power flow relations and mixed Gaussian load modeling, reference [41] where a distributed and privacy-preserving PLF technique based on Gaussian mixture modelling is proposed, reference [42] where a joint raw-moments based analytical method is employed and reference [43] which resolves the variable interdepencies in the power flow relation with affine arithmetic. These algorithms often use numerous mathematical approximations and assumptions about the electrical system (e.g. linear load flow relations, uncorrelated uncertainty sources) to allow for tractable computations, which can lead to mistakes in practical systems according to reference [44].

The third class uses *surrogate-based* techniques to build statistically similar analytical models for capturing PLF relations. Examples of proposals in this category include reference [45] where an analytical technique based on approximate Bayesian computations is employed, reference [46] which employs partial least square technique and polynomial chaos expansion, reference [47] where a fast method for calculating cumulants based on impulse-mixed probability density integration is proposed, reference [48] where a generalized polynomial chaos algorithm is utilized, reference [49] where a PLF method based on adaptive kernel density estimator is introduced, reference [50] where a decision tree based method is utilized to model the effect of fallout events on power flow properties and reference [51] where cumulant tensors of voltage variables are calculated with quadratic power flow models. Although these methods use fewer training data points, they also make simplifying assumptions about the system model and are dependent on in-built heuristics that require extensive parameter turning.

The final class of proposals are distinguished by the quantity of prior information about the DN (e.g. line impedance and DN topology) required for forming the PLF models. As such, references such as [29, 45, 52, 37] are classified as parameter-dependent since they incorporate extensive

knowledge of DN parameters in their construction of proposed algorithms. On the other hand, references such as [28, 50, 53] are classified as parameter-independent as they do not rely on internal information pertaining to the DN. Most parameter-independent proposals are however associated with various limitations caused by restrictions on training datasets and load types accommodated by the DN.

1.2.3 Topology Reconfiguration

DN topology reconfiguration problem is generally formulated as a NP-hard mixed integer combinatorial problem with non-linear and non-convex constraints [54]. Currently, work on DN reconfiguration can be divided into three main categories.

Works belonging to the first category guide the search process for the optimal DN configuration with a *meta-heuristic* technique that evolves a population of candidate solutions towards a better solution. Proposals in this category are generally not problem-specific. Meta-heuristic techniques employed in existing works include genetic algorithms [55, 56, 57] that evolve the candidate solutions with biologically inspired operators (e.g. crossover and mutation), particle swarm algorithms which guide the solution to the best known topology with regard to given criteria [58], harmonic search algorithms that iteratively replace the worst candidate [59], ant colony optimization algorithms that search for the best candidate through probabilistic analysis [60], memetic algorithms that use local search procedures to reduce the possibility of premature convergence [62], data-centric approaches which use deep learning techniques to reduce the number of candidate solutions [63, 64] and techniques that adopt Bayesian learning-based evolution algorithms [65]. As meta-heuristic techniques are capable of obtaining good solutions without making extensive assumptions about the underlying problem, they are often used to solve problems with highly nonconvex constraints. However, techniques of this kind often require significant amount of computation resources and are unable to provide performance guarantees on convergence speed or optimality.

The second class of existing literature utilizes *convex relaxations* methods to transform the

highly non-convex reconfiguration problem into problems that can be resolved with convex optimization techniques. Examples of proposals in this category include reference [66] where the current flow relation in the DN is linearized, reference [67] where the reconfiguration problem is first relaxed into a Mixed Integer Linear Programming (MILP) problem then resolved with a branch-and-cut algorithm, reference [54] where the reconfiguration problem is linearized into a Quadratic Constrained Programming (QCP) problem, references [54, 70] where the reconfiguration problem is solved as a Mixed Integer Second Order Cone Programming (MISOCP) problem, reference [71] where chordal relaxation techniques are employed to transform the reconfiguration problem into a Mixed Integer Semi-Definite Programming (MISDP) problem, reference [72] where a branch-and-bound algorithm is proposed to tackle the Quadratic Constrained Quadratic Programming (QCQP) reconfiguration problem, reference [73] where a conditionally exact relaxation technique is employed to resolve the reconfiguration problem, reference [74] where a relaxation technique based on Benders algorithm is utilized, reference [75] where a two-stage robust optimization model is introduced for the reconfiguration problems with uncertain loads, reference [76] where a MISOCP formulation of the DN reconfiguration problem is derived for the partial restoration scenario, reference [77] where an energy management scheme based on reconfiguration is performed on a linearized power flow model and reference [78] where a reconfiguration technique for reducing violations of voltage constraints is introduced. While convex relaxation based algorithms are capable of obtaining the globally optimal outcomes for relaxed problem formulations in a tractable manner, the relaxation process often leads to the exclusion of important physical attributes of the DN (e.g. ignoring reactive power and treating the DN as a single phase system).

Proposals belonging to the third category apply *graph-theoretic* methods for tractable computation. By offloading part of the computational and communication tasks to Energy Processing Units (EPUs) equipped agents in the DN that can act in parallel, graph theoretic algorithms solve the reconfiguration problem in a decentralized manner. Examples of algorithms in this category include branch exchange algorithm introduced in reference [4], hierarchical DN decomposition algorithm presented in reference [5], Open Shortest Path First (OSPF) algorithm proposed in ref-

erence [79], and best-first tree search algorithm introduced in reference [80]. However, methods belonging to this category often require highly granular parameter tuning specific to each system under consideration.

1.3 Contributions of This Thesis

Name of Publication	Conference/Journal	Acceptance Date
Distributed Assimilation of Grid Conditions and Load Integration via Social Learning [81]	IEEE *GlobalSIP* 2018	Aug. 2018
Decentralized Topology Reconfiguration in Multiphase Distribution Networks [83]	IEEE TSIPN	Feb. 2019
Adaptive Topology Reconfiguration in Smart Distribution Networks [84]	IEEE TSIPN	Oct. 2021
Kernel Structure Design for Data-Driven Probabilistic Load Flow Studies [82]	IEEE TSG	Mar. 2022

Table 1.1: List of Publications

Thus far, one conference paper and three journal articles based on this thesis's contribution in the area of voltage monitoring, analysis and improvement have been composed. These papers are presented in Table 1.1. The acronym IEEE stands for Institute of Electrical and Electronics Engineers. Compared to the monitoring state-of-the-art presented in Subsection 1.2.1, the work in [81] has made two major contributions: 1) It introduced a set of voltage monitoring metrics that can be updated in a decentralized manner through consensus averaging, and 2) It presented both theoretical and simulated studies on the convergence performance of the proposed metrics. Then, the work in [83] improves upon the existing works in 1.2.3 in the following aspects: 1) It introduced a reconfiguration algorithm that allows each smart agent in the DN to evaluate the global impact of its decisions with iterative information exchanges, and 2) It presented a game-theoretic formulation that leads to guarantees on algorithm convergence. Next, the work in [84] further improves upon [83] by presenting a reconfiguration algorithm based on convex relaxation techniques that guarantee convergence to global optimality. The published work in [82] then improves the state-of-the-art in PLF enumerated in Section 1.2.2 in the following two aspects: 1) It

presented a data-driven PLF method that can produce an accurate analysis of the distribution of voltage variables without prior knowledge of internal parameter of the DN (e.g. line admittances and DN topology), and 2) It introduced a game-theoretic technique for automatic model selection and parameter tuning for the proposed PLF method. All articles listed here have me as the first author and my advisor Dr. Srikantha as the corresponding author. The simulation results presented in this thesis are obtained from the MATPOWER simulation toolbox presented in reference [85] and the OpenDSS simulation toolbox introduced in reference [86].

1.4 Thesis Outline

The remainder of this thesis is organized as follows. In Chapter 2, the DN power flow models used in this thesis are introduced and their underlying assumptions are elaborated on. Chapters 3-6 provide a detailed overview of the grid condition monitoring, PLF and topology reconfiguration algorithms that constitute the main contributions of this thesis. In Chapter 7, the thesis is concluded by summarizing the contributions of my Ph.D. thesis and present possible directions for future work.

Chapter 2

Background on Smart Distribution Networks

To highlight the benefits of the proposed methods, this proposal focuses on cyber-enabled low-voltage active DNs with mostly resistive lines and uncertainties in its bus power injections. In this chapter, an overview of the system settings, assumptions, and notations for the DN studied is first presented. Next, the models for power flow relations in resistive multiphase DNs adopted by the various proposals is formulated. Then, a discussion on the methods used for modelling bus power injections in multiphase DNs is presented.

2.1 DN Settings and Assumptions

While DNs generally have meshed structures, they are commonly operated as radial networks where buses are connected by active lines (i.e. lines capable of sustaining current and power flows) [67]. In this proposal, the neighboring buses are defined as buses connected by a single active line. The assumptions listed below follow from the inherent properties of cyber-enabled low-voltage active DNs, the requirements for voltage regulation and the current state-of-the-art.

1. All buses in the DN possess the abilities to monitor local data, to communicate with neigh-

bors in the network, to perform basic computations, and to actuate local cyber-enabled components;

2. The acceptable range of voltage magnitudes for every non-feeder bus in the DN is assumed to be 1.0 ± 0.05 p.u;

3. Transient effects have no impact on system operations;

4. All loads in the DN are constant power loads;

5. The power injection/absorption at each bus is constant over five-second intervals;

6. Buses in the DN are capable of hosting distributed energy resources (e.g. generators, loads and storages).

Assumption 1 is supported by the current communication technologies and standards presented in reference [15]. Assumption 2 stems from the voltage constraints typically adopted by DN operators, which is more conservative than the actual tolerance margin prior to equipment failures in DNs (i.e. 1.0 ± 0.1 p.u.) [87]. The next assumption is supported by references such as [88, 89], which present recent advances that are capable of mitigating transient effects during normal operation of the DNs. Assumption 4 emphasizes the importance of voltage regulation by maximizing the negative incremental resistance phenomenon associated with constant-power loads [69]. Moreover, constant-power loads are becoming increasingly common in modern DNs as indicated by reference [69]. As long forecast horizons are typically associated with greater error margins [90], the shorter time interval indicated in Assumption 5 greatly reduces forecast errors. Finally, Assumption 6 is in line with the definitions of active DNs laid out in reference [91].

2.2 Notations

First, the DN notations and variables utilized in this proposal are introduced with a table of nomenclature presented at the beginning of this proposal. Then, these notations are illustrated in the

following radial network diagram. For the DN topology reconfiguration algorithms presented in this proposal, these notations refer to the current topology of the DN unless otherwise mentioned. Moreover, the labeling of iteration number is omitted to simplify notations unless otherwise specified.

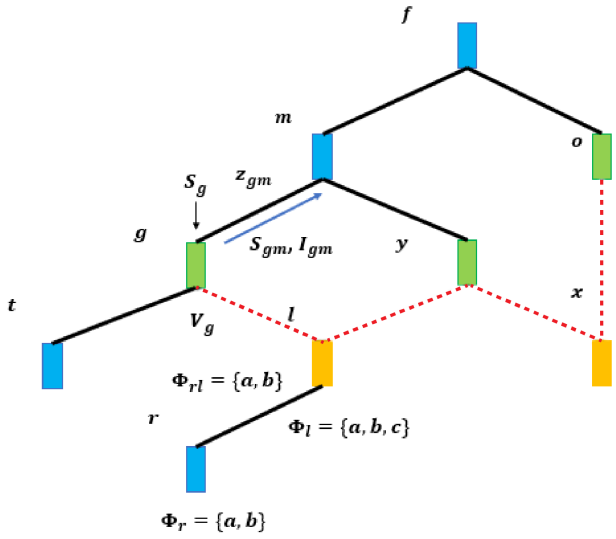

Figure 2.1: Illustration of Notations in a Radial Network.

The notations are illustrated in the radial DN presented in Fig. 2.1, where the feeder bus is denoted as f. While bus attributes S_r and V_r are illustrated for a single bus, these exist for all buses $b \in \mathcal{B}$. Similarly, line attributes z_{gm}, S_{gm} and I_{gm} apply to all lines $(g, m) \in \mathcal{E}$. To facilitate representation, the multiphase lines in the figure above are represented by single edges. For the topology presented in Fig. 2.1, the set of buses composing the subtree rooted at bus g is represented by $\mathcal{B}_g = \{g, t, l, r\}$. The sets of the potential parent buses and the child buses of g are denoted by $\mathcal{P}_g = \{m\}$ and $\mathcal{K}_g = \{t, l\}$ respectively. The set of lines (i.e. path) from bus r to bus g is $\mathcal{E}_{r,m} = \{(r, l), (l, g), (g, m)\}$, and the set of terminal buses for $\mathcal{E}_{r,m}$ is $\mathcal{B}_{r,m} = \{r, l, g, m\}$. Bus m is the lowest common ancestor $A_{r,x}$ for buses r and x. If $(r, l) \in \mathcal{E}$, then the relation between the related phase sets is $\Phi_r = \Phi_{rl} \subseteq \Phi_l$. The set of phases associated with bus r, bus l and line (r, l) are represented by $\Phi_r = \{a, b\}$, $\Phi_l = \{a, b, c\}$ and $\Phi_{rl} = \{a, b\}$, respectively. Moreover, superscripts are used to denote the projection of system states of the DN to specific phases in a set, where the projection of a state onto an undefined phase for the state is defined as 0. For example,

the projection of $V_r = \{V_r^a, V_r^b\}$ onto Φ_l is $V_r^{\Phi_l} = \{V_r^a, v_r^b, 0\}$ and the projection of V_l onto Φ_r is $V_l^{\Phi_r} = \{V_l^a, V_l^b, 0\}$. The fixed and switchable lines in Fig. 2.1 are illustrated by solid black lines and dotted red lines respectively. As such, the sets of fixed and switchable lines in this DN are $\mathcal{E}_f = \{(r,i),(t,g),(r,i),(g,m),(y,m),(m,f),(o,f)\}$ and $\mathcal{E}_s = \{(i,g),(i,y),(x,y),(x,o)\}$ respectively. The activated DN is composed of the switchable lines activated by the controller as well as the fixed lines. Moreover, the cycles in the DN topology is denoted by ϕ and Φ is the set containing all cycles in the DN. The only cycle in the DN in Fig. 2.1 is $\phi = \{(i,g),(g,m),(i,y),(y,m)\}$. To perform topology reconfiguration in the DN, the notion of *reconfigurable buses* is introduced where every reconfigurable bus is located at the downstream (i.e. farther away from the feeder bus) end of a switchable line. While non-reconfigurable buses can only have one potential parent, reconfigurable buses can have multiple potential parents. When a reconfigurable bus switch from one potential parent to another, the switchable line between it and the previous parent is deactivated. Moreover, the line between it and the next parent becomes activated. For the network presented in Fig. 2.1, the set of reconfigurable buses is $\mathcal{R} = \{l, x\}$. What is more, the sets of potential parents associated with these buses are $\mathcal{P}_l = \{g, y\}$ and $\mathcal{P}_x = \{y, o\}$, respectively. In Fig. 2.1, the reconfigurable buses and their parents are colored in yellow and green, respectively. When l switches from g to y, the line (l, g) is deactivated and the line (l, y) is activated.

2.3 Models for DN Power Flow Relations

In this section, the various models for representing power flow relations in a multiphase radial DN are introduced. The models presented here are based on different underlying assumptions on the DN. The first model presented is based on two assumptions: 1) The construction of the DN is nearly balanced; and 2) The power losses along power delivering lines have minor impact on bus voltages. The second model presented adopts the nearly balanced assumption and the assumption that the products of line powers from different phases are negligible. Moreover, the third model makes no assumption on the construction of the multiphase DN. While the first two models are

primarily used by proposals in DN optimization and control such as references [92, 93], the third model is commonly adopted by existing work on PLF such as references [94, 51].

The first model presented in this section calculates the power flow relations in a nearly balanced multiphase DN with minor line power losses. It is adopted by the proposal on voltage monitoring (i.e. reference [81]) and the proposal on topology reconfiguration based voltage improvement (i.e. reference [83]). For any line (r, l) on a multiphase DN, Ohm's law can be described as follows:

$$V_l^{\Phi_{rl}} = V_r - z_{rl} I_{rl} \tag{2.1}$$

By multiplying Eq. 2.1 with its own Hermitian transpose, the following voltage drop relation for multiphase DN is obtained:

$$\hat{\mathcal{V}}_l^{\Phi_{rl}} = \hat{\mathcal{V}}_r - (\mathcal{S}_{rl} z_{rl}{}^H + z_{rl} \mathcal{S}_{rl}^H) + z_{rl} \hat{\mathcal{I}}_{rl} z_{rl}{}^H \tag{2.2}$$

Furthermore, the power balance relations at bus r can be formulated using the aforementioned artificial variables defined for multiphase DNs:

$$\sum_{q:(q,r)\in\mathcal{E}} \mathcal{D}(\mathcal{S}_{qr} - z_{qr} \hat{\mathcal{I}}_{qr}) + S_r = \sum_{l:(r,l)\in\mathcal{E}} \mathcal{D}(\mathcal{S}_{rl})^{\Phi_r} \tag{2.3}$$

where $\mathcal{D}$ represents the diagonal elements of a matrix in vector form. To linearize the voltage drop and power balance relations, the assumption that the impact of line losses on the voltage profile of DN is negligible is made. While the resistive lines of low-voltage DNs are not lossless, reference [68] shows that the bus voltage deviation induced by power losses is within 0.0016 p.u. for various resistive DNs (i.e. IEEE-13 bus and IEEE-34 bus systems). As this deviation is minor in comparison to the aforementioned acceptable range of voltage magnitudes, this assumption is validated. The adoption of this assumption allows for the removal of power loss related terms $z_{rl} \hat{\mathcal{I}}_{rl} z_{rl}{}^H$ in Eq. 2.2 and $z_{qr} \hat{\mathcal{I}}$ in Eq. 2.3. Next, the assumption that bus voltages across the phases are *nearly* balanced for multiphase DNs is made, which implies the following relation introduced in reference [68] is satisfied for any $r \in \mathcal{B}$ where $\Phi_r = \{a, b, c\}$:

$$V_r^a \approx V_r^b e^{\mathbf{j}2\pi/3};\ V_r^b \approx V_r^c e^{\mathbf{j}2\pi/3};\ V_r^c \approx V_r^a e^{\mathbf{j}2\pi/3} \tag{2.4}$$

Comparing to *balanced* DN models where the phases are decoupled, this *nearly* balanced model approximates the coupling between phases in the following manner: If the terms α and υ are defined as $\alpha = e^{-\mathbf{j}2\pi/3}$ and $\upsilon = [1, \alpha, \alpha^2]^T$, then the power flow across $(r, l) \in \mathcal{E}$ can be represented by the following:

$$\mathcal{S}_{rl} = V_r^{\Phi_{rl}} I_{rl}^H \in range(\upsilon^{\Phi_{rl}}) \tag{2.5}$$

Suppose that Λ_{rl} is a vector whose elements represent the diagonal components of $\mathcal{S}_{rl}$. According to Eq. 2.5, the off-diagonal entries of $\mathcal{S}_{rl}$ can be approximated by Λ_{rl} as follows:

$$\mathcal{S}_{rl} = \gamma^{\Phi_{rl}} \text{Diag}(\Lambda_{rl}) \text{ where } \gamma = \begin{bmatrix} 1 & \alpha^2 & \alpha \\ \alpha & 1 & \alpha^2 \\ \alpha^2 & \alpha & 1 \end{bmatrix} \tag{2.6}$$

where the *Diag* operator creates a diagonal matrix whose diagonal elements are Λ_{rl}. The power flow relations model for multiphase DNs based on the aforementioned two assumptions was introduced in reference [68] as the Linearized Power Flow (LPF) model. The full formulation for the LPF model is presented as follows:

$$\sum_{m:(m,r)\in\mathcal{E}} \Lambda_{mr}^{\Phi_r} + S_r = \Lambda_{rl} \qquad r \in \mathcal{B}\backslash f \tag{2.7}$$

$$\mathcal{S}_{rl} = \gamma^{\Phi_{rl}}\text{Diag}(\Lambda_{rl}) = P_{rl} + \mathbf{j}Q_{rl} \qquad (r,l) \in \mathcal{E} \tag{2.8}$$

$$(P_{rl}^{\phi})^2 + (Q_{rl}^{\phi})^2 \leq \overline{S}_{rl}^2 \qquad \phi \in \Phi_{rl}, (r,l) \in \mathcal{E} \tag{2.9}$$

$$\hat{\mathcal{V}}_r - \hat{\mathcal{V}}_l^{\Phi_{rl}} = z_{rl}\mathcal{S}_{rl}^H + \mathcal{S}_{rl}z_{rl}{}^H \qquad (r,l) \in \mathcal{E} \tag{2.10}$$

$$S_r = P_r + \mathbf{j}Q_r \qquad r \in \mathcal{B} \tag{2.11}$$

$$\underline{p}_r \leq P_r^{\phi} \leq \overline{p}_r,\ \underline{q}_r \leq Q_r^{\phi} \leq \overline{q}_r \qquad \phi \in \Phi_r,\ r \in \mathcal{B} \tag{2.12}$$

$$\underline{v}_r \leq \hat{\mathcal{V}}_r^{\phi} \leq \overline{v}_r \qquad \phi \in \Phi_r, r \in \mathcal{B} \tag{2.13}$$

Eq. 2.7 and Eq. 2.8 maintain the power balance across the DN. Eq. 2.9 represents the apparent flow limit of each phase ϕ in Φ_{rl}, and Eq. 2.10 describes the relationship between voltage drop and power flow. The constraints on bus loads and voltage magnitudes for each phase are provided in Eq. 2.12 and 2.13, where the $\hat{\mathcal{V}}_r^{\phi}$ terms in Eq. 2.13 refers to the square of the voltage magnitude of bus r at phase ϕ (i.e. $\mathcal{D}(\hat{\mathcal{V}}_r)[\phi]$).

Through comprehensive accuracy analyses performed on practical resistive multiphase DNs with unbalanced loadings (e.g. IEEE 13-bus and IEEE-34 bus DNs), reference [68] demonstrated that the LPF model is capable of providing conservative estimations of the voltage values for the type of DNs this proposal focuses on. For example, the maximum difference between the actual bus voltage values for the test DNs and their LPF approximations is 0.0016 p.u., which is far smaller than the 0.05 p.u. voltage tolerance stated in Section 2.1. This conservative approximation for voltage values allows for the adoption of the LPF model as the basis for the proposals in references [81, 83].

The second model presented in this section is introduced by reference [95]. This model im-

proves upon the LPF model by accounting for the impact of line losses on the voltage profile of DN. Moreover, it considers the non-linear interdependencies between the voltage, current and power variables in the DN. It is adopted by the second proposal on topology reconfiguration based voltage improvement (i.e. reference [84]). In this thesis, this model is referred to as the Nonlinear Power Flow model (NPF). To derive the NPF model, it is first observed that the voltage change associated with each phase in any line in the DN can be obtained through grouping the terms in Eq. 2.2. For instance, the voltage drop relation for phase a in the three phase line $(r, l) \in \mathcal{E}$ can be described as follows:

$$V_r^a = V_l^a - z_{rl}^{aa}\frac{P_{rl}^a - \mathbf{j}Q_{rl}^a}{(V_l^a)^H} - z_{rl}^{ab}\frac{P_{rl}^b - \mathbf{j}Q_{rl}^b}{(V_l^b)^H} - z_{rl}^{ac}\frac{P_{rl}^c - \mathbf{j}Q_{rl}^c}{(V_l^c)^H} \tag{2.14}$$

where z_{rl}^{aa}, z_{rl}^{ab} and z_{rl}^{ac} are the first-row elements of the impedance matrix z_{rl} (i.e. $[1,0,0]z_{rl} = [z_{rl}^{aa}, z_{rl}^{ab}, z_{rl}^{ac}]$). Then, multiplying both sides of Eq. 2.14 with their respective conjugate counterparts leads to the following:

$$\begin{aligned}|V_r^a|^2 =& |V_l^a|^2 + |z_{rl}^{aa}|^2\frac{(P_{rl}^a)^2 + (Q_{rl}^a)^2}{|V_l^a|^2} + |z_{rl}^{ab}|^2\frac{(P_{rl}^b)^2 + (Q_{rl}^b)^2}{|V_l^b|^2} + |z_{rl}^{ac}|^2\frac{(P_{rl}^c)^2 + (Q_{rl}^c)^2}{|V_l^c|^2} + 2Re\Big(- (z_{rl}^{aa})^H(P_{rl}^a + \mathbf{j}Q_{rl}^a)\\ & - V_l^a(z_{rl}^{ab})^H\frac{P_{rl}^b + \mathbf{j}Q_{rl}^b}{V_l^b} - V_l^a(z_{rl}^{ac})^H\frac{P_{rl}^c + \mathbf{j}Q_{rl}^c}{V_l^c} + z_{rl}^{aa}(z_{rl}^{ab})^H\frac{(P_{rl}^a - \mathbf{j}Q_{rl}^a)(P_{rl}^b + \mathbf{j}Q_{rl}^b)}{(V_l^a)^H V_l^b})\\ & + z_{rl}^{aa}(z_{rl}^{ac})^H\frac{(P_{rl}^a - \mathbf{j}Q_{rl}^a)(P_{rl}^c + \mathbf{j}Q_{rl}^c)}{(V_l^a)^H V_l^c} + z_{rl}^{ab}(z_{rl}^{ac})^H\frac{(P_{rl}^b - \mathbf{j}Q_{rl}^b)(P_{rl}^c + \mathbf{j}Q_{rl}^c)}{(V_l^b)^H V_l^c}\Big)\end{aligned} \tag{2.15}$$

Next, the nearly balanced assumption stated in Eq. 2.4 is evoked to reduce couplings between different phases. Moreover, the product of line powers associated with different phases is assumed to be negligible. Based on these two assumptions, the voltage drop relation stated above can be transformed to the following system of equations:

$$l^a_{rl} = ((P^a_{rl})^2 + (Q^a_{rl})^2)/(\hat{\mathcal{V}}^a_l) \tag{2.16}$$

$$\begin{aligned}\hat{\mathcal{V}}^a_r =& \hat{\mathcal{V}}^a_l + |z^{aa}_{rl}|^2 l^a_{rl} + |z^{ab}_{rl}|^2 l^b_{rl} + |z^{ac}_{rl}|^2 l^c_{rl} - 2\big[r^{aa}_{rl} P^a_{rl} + x^{aa}_{rl} Q^{aa}_{rl} \\ &+ (-r^{ab}_{rl}/2 + \sqrt{3}x^{ab}_{rl})P^b_{rl} + (-\sqrt{3}r^{ab}_{rl}/2 + x^{ab}_{rl}/2)Q^b_{rl} \\ &+ (-r^{ac}_{rl}/2 + \sqrt{3}x^{ac}_{rl})P^c_{rl} + (\sqrt{3}r^{ac}_{rl}/2 + x^{ac}_{rl}/2)Q^c_{rl}\big]\end{aligned} \tag{2.17}$$

where $\hat{\mathcal{V}}^a_r$ is the aforementioned artificial voltage variable and the artificial current variable $l^a_{rl} = |I^a_{rl}|^2$ represents the squared current magnitude associated with phase a of the line (r, l). Moreover, r_{rl} and x_{rl} are the real and reactive components of the line impedance z_{rl} (i.e. $z_{rl} = r_{rl} + \mathbf{j}x_{rl}$). Repeating this procedure for the other phases leads to the following load flow relation in multiphase DNs:

$$\forall r \in \mathcal{B}:$$

$$\hat{\mathcal{V}}^{\Phi_{rl}}_l - \hat{\mathcal{V}}_r = 2(\bar{r}_{rl}P_{rl} + \bar{x}_{rl}Q_{rl}) + \bar{z}_{rl}l_{rl},\ \forall l \in \mathcal{P}_r \tag{2.18}$$

$$\hat{\mathcal{V}}_r \odot l_{rl} = (P_{rl})^{\odot 2} + (Q_{rl})^{\odot 2}, \forall l \in \mathcal{P}_r \tag{2.19}$$

$$P_r = \sum_{l \in \mathcal{P}_r}(P_{rl} - r_{rl}l_{rl}) - \sum_{m \in \mathcal{K}_r} P_{mr} \tag{2.20}$$

$$Q_r = \sum_{l \in \mathcal{P}_r}(Q_{rl} - x_{rl}l_{rl}) - \sum_{m \in \mathcal{K}_r} Q_{rl} \tag{2.21}$$

where:

$$\Gamma = \begin{bmatrix} 1 & e^{-j2\pi/3} & e^{j2\pi/3} \\ e^{j2\pi/3} & 1 & e^{-j2\pi/3} \\ e^{-j2\pi/3} & e^{j2\pi/3} & 1 \end{bmatrix}$$

$$\overline{r}_{rl} = Re\{\Gamma \odot r_{rl}\} - Im\{\Gamma x_{rl}\}$$

$$\overline{x}_{rl} = Re\{\Gamma \odot x_{rl}\} - Im\{\Gamma r_{rl}\}$$

$$\overline{z}_{rl} = |z_{rl}|^{\odot 2}$$

where $\odot$ denotes the element-wise product of two matrices and the superscript $\odot 2$ denotes the element wise square of a matrix. Moreover, $l_{rl} = [l^a_{rl}, l^b_{rl}, l^c_{rl}]^T$ is the vector of squared current magnitudes at the DL (r, l). Eq. 2.18 denotes the voltage change along the line (r, l). Then, the constraint Eq. 2.19 denotes the relation between the current, voltage and power magnitudes associated with the line (r, l). Next, Eqs. 2.20 and 2.21 are the real and reactive power balance relations across (r, l) respectively.

The third model presented in this section places no restriction on the characteristics of the DN and the power entities that connect to it. It is adopted by the proposal on voltage analysis with PLF (i.e. reference [82]). This model can be summarized with the following power balance equations:

$$S_r = P_r + \mathbf{j}Q_r = V_r \sum_{j=r}^{n} z^{-1}_{mr} V^H_m, \ \forall \ r \in \mathcal{B} \tag{2.22}$$

where n is the number of buses in the DN (i.e. $|\mathcal{B}| = n$). As can be observed from Eq. 2.22, this model describes the load flow relation in multiphase DN without making any assumption on the balance condition of the DNs or power losses along power-delivering lines.

2.4 Modeling of Power Injection

In this section, the models for the power injection at each bus are elaborated on. The bus injection considered in this proposal consists of three elements: 1) Non-EV consumer demand; 2) demand from EVs; and 3) Injection from Photovoltaics (PV) units.

For the works on voltage monitoring and improvement (i.e. references [81, 83, 84]), these three elements are modelled as deterministic injections into the bus loads. This is consistent with the approaches commonly undertaken by the state-of-the-art in monitoring and improvement (e.g. references [54, 70, 71]). In the work on voltage analysis (i.e. reference [82]), the load and generation profiles of these elements are modelled as probabilistic distributions. This is consistent with existing proposals on PLF such as references [28, 40, 53]. From references [96] and [97], the loads and generations associated with these power entities can be modelled via normal distributions. This approach is widely adopted by existing proposals such as references [98, 99, 100]. As these power injection elements are prevalent in densely populated urban/suburban residential areas, the decision to model their impact as normal distributions is supported by the Central Limit Theorem [101]. This approach is also adopted by this proposal and the specific parameters of the normal distributions utilized to model the various power uncertainties in the DN are presented in Chapter 4. For each phase of the buses under consideration, the mean values for the distribution is expressed as a percentage of the original demands.

Chapter 3

Decentralized Grid Monitoring

Existing literature in decentralized voltage monitoring and regulation such as reference [21] depend on purely local metrics such as battery capacity and state of charge to monitor the voltage profile of resistive DNs. In this section, a set of metrics introduced in reference [81] that allows each bus to measure the impact of their local voltage disturbances (e.g. those caused by Electric Vehicle (EV) charging) on the voltage profile of the DN is presented. Then, both theoretical and empirical studies on how these metrics can assist inverter regulation for maintaining the voltage profile are conducted. Some equations and figures presented in this section are included in the published work in reference [81]

3.1 DN Settings and Problem Formulation

To design the voltage evaluation metrics, the network model is first constructed by separating the buses $r \in \mathcal{B}$ of the DN into a set of clusters $\mathcal{U}$. Each cluster is rooted at a Generator (GEN)-bus with utility-regulated DG components, and the other buses in the cluster, termed Alternative Load Elements (ALE)-buses, have the ability to integrate ALE components such as EVs to their own loads. The ALE components are small scale load devices operated by the consumers and are not controlled by the utility. Whereas utility-regulated DG components serve to maintain the voltage profile of the DN, the ALE components introduce uncertainties to the power injection/absorption

at different buses which can cause fluctuations in DN voltages. Furthermore, the set of neighboring buses of r is denoted as $\mathcal{N}_r$, and the set of neighboring buses of r that resides in the same cluster as r as $\hat{\mathcal{N}}_r$. The ALE demand located on bus r is denoted as $\mathcal{A}^r$, and the aggregate demand of ALEs located in u is defined as $\mathcal{A}_u$. Moreover, the total ALE demand for the entire DN is defined as $\mathcal{A}$.

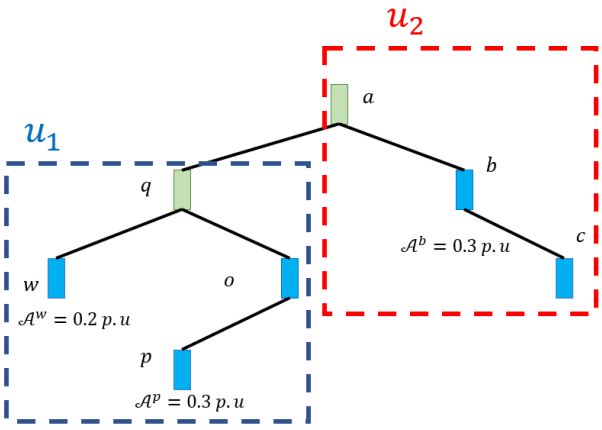

Figure 3.1: Illustration of Clusters in a Radial Network.

These notations are illustrated in Fig. 3.1. In this figure, the DN was partitioned into two clusters $u_1, u_2 \in \mathcal{U}$, where $u_1 = \{q, w, o, p\}$ and $u_2 = \{a, b, c\}$. The GEN-buses q and a are marked in green, and the ALE-buses are marked in blue. For bus q, $\mathcal{N}_q = \{a, w, o\}$, and $\hat{\mathcal{N}}_q = \{w, o\}$. The Aggregate demand of ALEs in u_1 is $\mathcal{A}_{u_1} = \mathcal{A}^w + \mathcal{A}^p = 0.5$ p.u, and the aggregate demand of the network is $\mathcal{A} = \mathcal{A}_{u_1} + \mathcal{A}_{u_2} = 0.8$ p.u. From these parameters, each bus agent r then computes the first metric for ALE impact measurement, which is termed the local opinion on ALE impact O_r. The formulation for this metric is $O_r = |u|\frac{\mathcal{A}}{\mathcal{A}_u}\Delta(\hat{V}_l - \hat{V}_r)$, where u is the host cluster of r and l is the parent of r. This metric serves to capture important information on the distribution of ALEs across the DN and their impact on the voltage profile of the DN. To measure the impact of ALE integration on the voltage profiles at cluster level, the opinion of cluster u on ALE impact O^u is defined as the average of the local opinions of all buses r residing in cluster u. Similarly, the global impact of ALE integration is measured by defining the global opinion O^g as the average opinion of all $r \in \mathcal{B}$.

3.2 Design of the Monitoring Algorithm

For decentralized computation of O^u and O^g, the following consensus averaging method based on the opinion propagation model introduced in reference [102] is proposed: Every $r \in \mathcal{B}$ first initializes its cluster perception variable O_r^u and global perception variable O_r^g with its opinion O_r. At each iteration t, every r exchanges its cluster perception variable with buses in $\hat{\mathcal{N}}_r$ and global perception variable with buses in $\mathcal{N}_r$. Then, r updates O_r^u with the average of the cluster perception variables of $m \in \hat{\mathcal{N}}_r$ and itself, and O_r^g with the average of the global perception variables of $l \in \mathcal{N}_r$ and itself. This process is repeated until O_r^u and O_r^g for all $r \in \mathcal{B}$ converge to O^u and O^g, respectively. This consensus averaging method is summarized in Alg. 1:

Alg. 1: Proposed Decentralized Monitoring Algorithm

Initialization:

- $O_r \rightarrow O_r^u, O_r \rightarrow O_r^g$ for every $r \in \mathcal{B}$.

Algorithm:

1. Every r broadcasts O_r^u to buses residing in $\hat{\mathcal{N}}_r$ and O_r^g to buses in $\mathcal{N}_r$.
2. Calculate $\hat{O}_r^u = (O_r^u + \sum_{m \in \hat{\mathcal{N}}_r} O_m^u)/(|\hat{\mathcal{N}}_r| + 1)$ and $\hat{O}_r^g = (O_r^g + \sum_{l \in \mathcal{N}_r} O_l^g)/(|\mathcal{N}_r| + 1)$.
3. If $\hat{O}_r^u = O_r^u$ and $\hat{O}_r^g = O_r^g$, terminate the iterative update process. Otherwise, let $\hat{O}_r^u \rightarrow O_r^u$ and $\hat{O}_r^g \rightarrow O_r^g$ then return to the first step.

The general form of opinion evolution for this iterative updating process can be represented by:

$$O(t) = TO(t-1) \tag{3.1}$$

where O is the vector of opinions of buses participating in the information exchange. Also, each component T_{rl} of the belief updating matrix T is defined as $T_{rl} = A_{rl}/(n_r + 1)$, where A is the adjacency matrix of the cluster or the DN and n_r is the number of buses in $\hat{\mathcal{N}}_r$ or $\mathcal{N}_r$ (depending on whether O^u or O^g is being computed).

From the convergence analysis performed in reference [102], the proposed consensus averaging

method is guaranteed to converge to a consensus. Moreover, the upper bound on the iteration number C for achieving consensus is represented by Eq. 3.2:

$$C \leq \left\lceil \frac{log(\frac{1}{\epsilon})}{log(\frac{1}{|\lambda_2(T)|})} \right\rceil \tag{3.2}$$

where ϵ is the residual and the second largest eigenvalue of T is denoted by $\lambda_2(T)$. This bound guarantees near real-time (i.e.$<$ 10 seconds) convergence behavior for O^u and O^g for a number of practical DNs. For example, the upper bound on the number of iterations necessary for O^g to converge for the IEEE 33-bus DN is 579 iterations when the residual is 10^{-5}. As the proposed monitoring algorithm is based on the assumption that each bus in the DN can only communicate with its neighbors in the network, wired communication technologies (e.g. power line communication) are adopted. From reference [103], the communication delay associated with each information exchange process for wired communication is within 5 milliseconds. Therefore, buses in the 33-bus DN can form a consensus on O^g within 3 seconds with the proposed consensus averaging method, and consensuses on each O^u can be formed in even less time.

3.3 Simulation Results

Based on the aforementioned impact assessment metrics, the following algorithm for reducing the impact of ALE integration on the voltage profile of the DN is proposed: Before an ALE-bus r integrates an ALE component, it first requests the GEN-bus g_u at the root of its host cluster u to supplement the power requested by the ALE. If g_u approves of the request, then the new ALE will only affect the voltage values of buses within the subtree $\mathcal{B}_u$ and the opinions of other buses within the cluster u. Next, buses in the cluster u form the post ALE integration opinion consensus $O^{u'}$ through iterative information exchange using the aforementioned consensus averaging method and the power flow model introduced in Section 2.3. As individual ALE loads tend to be much smaller than typical bus loads, the assumption that the inclusion of individual ALE has a negligible impact on the global opinion consensus O^g is made. Hence, if $O^{u'}$ is much higher than O^g, then

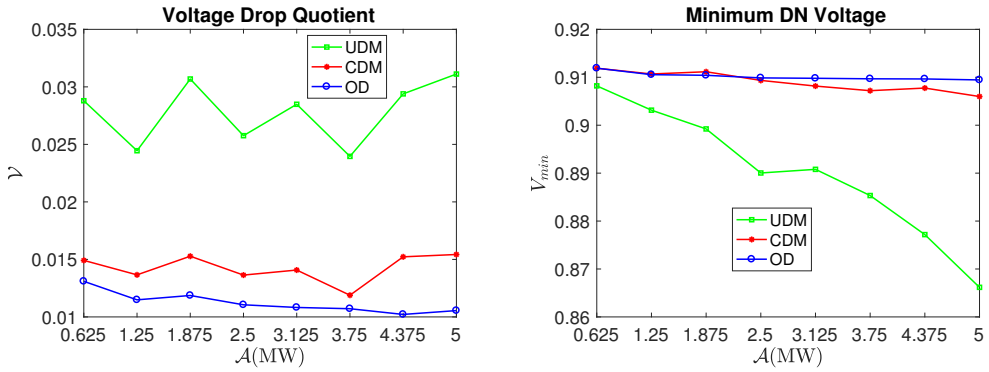

(a) Reduction quotient ©2018 IEEE. (b) $|V_{min}|$ ©2018 IEEE

Figure 3.2: Simulations for Grid Condition Monitoring and ALE Integration

the integration of the new ALE would disproportionately impact the voltage values of buses within u. Therefore, the algorithm instructs r to reject the ALE if $O^{u'} - O^{g}$ is higher than a threshold τ obtained through simulation results.

The performance of the proposed grid condition monitoring metric and its application on ALE integration is evaluated on the 12.66kV IEEE 33-bus DN, for which parameters were detailed in reference [4]. The test DN is partitioned into four clusters where each cluster hosts a randomly selected percentage of ALE loads as indicated in Table. 3.1.

Cluster Name	**ALE Percentage**
Cluster 1	10%
Cluster 2	22%
Cluster 3	50%
Cluster 4	18%

Table 3.1: Cluster ALE Loads in the 33-bus DN ©2018 IEEE.

The clusters and the GEN-buses are illustrated in Fig. 3.3 where different clusters are indicated by dashed lines of different colours and GEN-buses are illustrated in orange. The numbers in Fig. 3.3 denote the buses in the DN. The proposed method, which was termed Opinion Dynamics (OD), was compared with the Unconstrained Direct Method (UDM) where ALE integration requests are never turned down, and the Constrained Direct Method (CDM), where ALE integration requests are only turned down when it would lead to bus voltage constraint violations. Furthermore, the

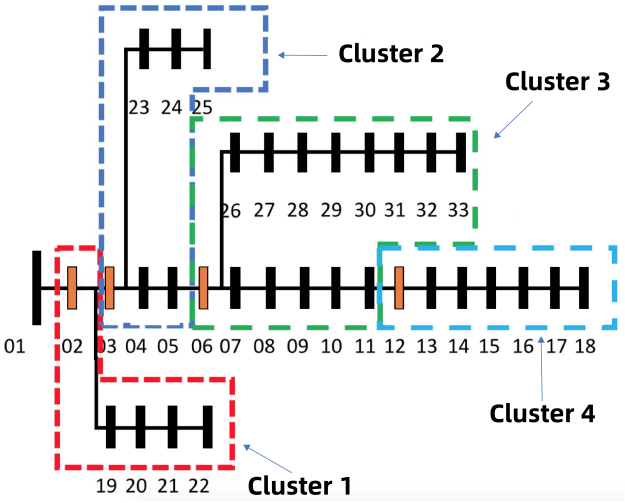

Figure 3.3: Illustration of Clusters in the 33-bus DN.

voltage reduction quotient $\mathcal{V}$ is introduced to represent the impact of ALE integration on the voltage profile. The formulation for $\mathcal{V}$ is expressed as follows:

$$\mathcal{V} = \frac{1}{\mathcal{A}} \sum_{b \in \mathcal{B}} \Delta(|V_b|^2) \tag{3.3}$$

where $\Delta(|V_b|^2)$ represents the change in bus voltage magnitude due to ALE integration. Moreover, the value of τ for this simulation is selected as $2 * 10^{-4}$. In Fig. 3.2a, the proposed monitoring and integration technique can successfully mitigate the voltage reduction effects caused by unregulated integration of ALEs. Also, the proposed method consistently leads to smaller voltage reduction across the network than the CDM. Moreover, Fig. 3.2b shows that the proposed method is more effective at safeguarding the minimum bus voltage of the DN than CDM in scenarios with high ALE penetration. As such, Figs 3.2a and 3.2b demonstrate the detrimental effects of unregulated ALE integration on the voltage profile of the DN and illustrate the effectiveness of the proposed algorithm in mitigating these effects.

3.4 Chapter Summary

This chapter presents a decentralized algorithm for grid condition monitoring. Next, it proves through theoretical constructs associated with social learning that the monitoring algorithm allows for near real-time monitoring of grid conditions for practical DNs. Then, it introduces a technique that allows cyber-enabled smart buses to collaboratively reduce the impact of ALE penetration on the DN based on the monitoring algorithm. Impact of the integration method on the DN voltage profile at various rates of ALE penetration have been demonstrated with simulations conducted on the practical IEEE 33-bus DN.

Chapter 4

Data-Driven PLF for Voltage Analysis

From the literature review conducted in Chapter 1.2.2, current proposals in data-driven PLF such as reference [29] generally require both arduous tuning process for their machine learning models and extensive knowledge pertaining to the internal parameters of the DN (e.g. line impedances and DN topology). Moreover, no existing proposal in data-driven PLF offers guarantees on the performance of their machine learning algorithms. In this section, the assumptions as well as the network and load models adopted by this work are first detailed. Then, a brief summary for the machine learning techniques utilized in this work is presented. Next, a GP emulator-based data-driven method for PLF is proposed. This PLF method automates the model selection and parameter tuning processes and requires no internal parameter of the DN. Then, the theoretical performance guarantees for the proposed method are introduced. Both the proposed method and the guarantees on its performance are first established in reference [82]. The equations, tables and figures presented in this section are included in the published work in reference [82]

4.1 DN Settings and Problem Formulation

In this proposal, no simplifying assumptions regarding the physical attributes of the DN (e.g. number of phases and availability of line parameters) is made. As such, this proposal provides an accurate analysis of the bus voltage behaviours associated with practical multiphase DNs. The only

assumptions made in this work are pertaining to the availability of the training/testing datasets and the settings for the GP emulator. Owing to the extensive application of Advanced Metering Infrastructure (AMI) and Supervisory Control And Data Acquisition (SCADA) technologies in modern smart DNs [104], this proposal adopts the assumption that the datasets of net power injections, bus voltage magnitudes and voltage phase angles at each bus in the DN are readily available. Next, the input feature vector for the GP emulator is set to be a composite vector that includes the net power injections associated with every bus in the DN. The net power injection at a bus is defined as the overall power generation from distributed sources (e.g. rooftop PV panels) residing at that bus subtracted by the overall demand at that bus. Then, the output from the GP emulator is set to be a single DN state entity for simplifying the notations adopted in this work. The extension of the output of GP emulator to multiple state entities can be easily done without loss of generality as demonstrated in reference [82].

The datasets utilized by the proposed PLF technique can come from either data repositories maintained by utility companies or from DN simulation toolboxes such as MATPOWER and OpenDSS. In this proposal, the latter method is adopted to generate the training and testing datasets from the IEEE 33-bus, 37-bus and 123-bus DNs. Specifically, the datasets associated with the balanced DNs (i.e. the IEEE 33-bus DN) are generated from MATPOWER and the datasets associated with the unbalanced DNs (i.e. the IEEE 37-bus and 123-bus DNs) are generated from OpenDSS. These two simulation toolboxes generate the DN datasets from the following power balance relations:

$$S_r = V_r \sum_{j=r}^{n} z_{mr}^{-1} V_m^H, \ \forall \ r \in \mathcal{B} \tag{4.1}$$

The system parameters used for generating the datasets (e.g. impedance matrices) are obtained from reference [131] for all DNs studied. Next, the load and generation models that govern the net power injection at each bus are detailed. As mentioned in Section 2.4, the bus injection considered in this proposal is the summary of three components: non-EV consumer demands, demand from EVs and injection from photovoltaic DGs. Here, the cumulative consumer loads are modelled

as a normal distribution whose means and standard deviations are selected to be 125% and 5% of the original loads respectively. These values aim to capture the diversity in power demands. Moreover, the chosen variance values are also used by the state-of-the-art in PLF methods such as reference [28]. Next, the net injection from the EVs is modelled as a normal distribution whose means and standard deviations are set to be 75% and 5% of the original loads respectively. The penetration rate of EVs considered in this proposal is significantly higher than those considered by the existing literature (e.g. the penetration rates adopted in references [105] and [106] are 10% and 20% respectively). This allows for the consideration of greater variability in power demands. Furthermore, existing proposals studying the impact of EVs in DNs such as reference [98] have also selected the standard deviation to 5%. Then, the power injection from PVs is modelled as a normal distribution whose means and standard deviations are set as 100% and 20% of the original demands respectively. The means selected allow the power generated by the PVs to supply all of the original demands in the DN on average. The standard deviations selected for the PV generation have also been adopted in reference [100].

4.2 Brief Overview of GP Emulator

The machine learning technique of GP emulator is adopted in this work to construct surrogate models of practical DNs. Here, the input feature vector x into the GP emulator is an stochastic vector that includes the real and reactive net bus power injections associated with all phases in the DN. As such, the realization of x at any instance i is denoted by x^i and the dimension of this realization is denoted by d_i (i.e. $x^i \in \mathcal{R}^{d_i}$). As the set of phases for bus $r \in \mathcal{B}$ is denoted by Φ_r and x accounts for both real and reactive power injections, $d_i = \sum_{r=1}^{|\mathcal{B}|} 2|\Phi_r|$. The training dataset for the emulator is denoted by the matrix X and each row of X is a realization of the emulator input x that contains a snapshot of the DN net bus power injections at a specific time instance. The size of this training set is denoted by n_X (i.e. $X \in \mathcal{R}^{n_X \times d_i}$). Next, the system output corresponding to the input realization x^i is denoted by $f(x^i)$ and the collection of system outputs corresponding to

X is represented as $f(X) = [f(x^1), ..., f(x^{n_X})]$. As the technique of GP emulator is adopted by this proposal, the predictive distribution of input x is a GP whose realization is denoted by $g(x)$. The predictive posterior distribution $p(g(x)|f(X), X, \mu(.), k(., .))$ is then defined as the following:

$$
\begin{aligned}
&p(g(x)|f(X), X, \mu(.), k(., .)) = \mathcal{N}(m(x), \Sigma(x)) \\
&m(x) = \mu(x) + k(x, X)k(X, X)^{-1}(f(X) - \mu(X)) \\
&\Sigma(x) = k(x, x) - k(x, X)k(X, X)^{-1}k(X, x)
\end{aligned}
\tag{4.2}
$$

where

$$
\mu(X) = \begin{bmatrix} \mu(x^1) \\ \vdots \\ \mu(x^{n_X}) \end{bmatrix}, \quad k(X, X) = \begin{bmatrix} k(x^1, x^1) & \dots & k(x^1, x^{n_X}) \\ \vdots & \ddots & \vdots \\ k(x^{n_X}, x^1) & \dots & k(x^{n_X}, x^{n_X}) \end{bmatrix}
$$

$$
k(x, X) = [k(x, x^1), ..., k(x, x^{n_X})], \quad k(X, x) = \begin{bmatrix} k(x^1, x) \\ \vdots \\ k(x^{n_X}, x) \end{bmatrix}
$$

In Eq. 4.2, μ and k denote the prior mean and covariance functions for the GP respectively. The μ and k functions represent the prior knowledge of DN power flow relations available to the data engineer. Next, the predictive posterior distribution $p(g(x)|f(X), X, \mu(.), k(., .))$ is the distribution of $g(x)$ for a GP emulator trained on $(X, f(X))$ that has prior mean and covariance functions μ and k. Moreover, The predictive posterior mean $m(x)$ serves as an approximation for $f(.)$ and the predictive posterior covariance $\Sigma(x)$ represents the precision of such an approximation. Since no prior information of the DN is assumed to be available to the data engineer, this work sets the GP prior mean function μ to 0 for all DNs studied. From reference [107], GP emulators with zero prior mean are capable of accurate prediction of physical system behaviours after the training process. Moreover, the accuracy of predictions for zero mean GP emulators are highly

reliant on the engineer's selection of prior covariance functions. The prior covariance k is typically represented by a kernel function whose associated set of hyper-parameters θ are inferred during the training process. An example of the kernel function is the Squared-Exponential (SE) kernel defined as $k(x, x') = \sigma_f^2 exp(-\frac{\|x-x'\|^2}{2l^2})$ where $\|.\|$ denotes the L_2 norm. The set of hyper-parameters associated with this kernel is $\theta = \{\sigma_f, l\}$ where σ_f and l represent the signal variance and length-scale for the kernel respectively. The SE kernel is adopted by the state-of-the-art in GP emulator based PLF in reference [28]. Other examples of kernel functions for GP emulators are included in Table 4.1:

Kernel Name	**Kernel Function Formulation**
Rational Quadratic	$\sigma^2 \left(1 + \frac{\|x-x'\|^2}{2\alpha\ell^2}\right)^{-\alpha}$
Periodic	$\sigma^2 \exp\left(-\frac{2\sin^2(\pi\|x-x'\|/p)}{\ell^2}\right)$
Linear	$\sigma_b^2 + \sigma_v^2(x-c)(x'-c)$

Table 4.1: Examples of GP Emulator Kernels ©2022 IEEE

The hyper-parameters for GP kernels are typically trained with the Maximum Likelihood Estimation (MLE) method [28]. The MLE aims to maximize the marginal likelihood function over the training dataset through the optimization of hyper-parameters. The expression for the marginal likelihood function associated with a zero-mean GP emulator $\mathcal{GP}(0, k(.,.))$ trained on the dataset $(X, f(X))$ can be expressed as the following equation:

$$\begin{aligned} L(k(.,.)|X, f(X)) &= p(f(X)|X, k(.,.)) \\ &= \mathcal{N}(f(X)|0, k(X,X)) \\ &= (2\pi)^{-\frac{n_X}{2}} \times [det(k(X,X))]^{-\frac{1}{2}} \\ &exp\{-\frac{1}{2} f(X)^T k(X,X)^{-1} f(X)\} \end{aligned} \tag{4.3}$$

where the determinant of a matrix is denoted by $det(.)$. According to Eq. 4.3, the marginal likeli-

hood L for an GP emulator with input matrix X and kernel $k(.,.)$ is the conditional probability for the emulator output to be equal to the system output $f(X)$. As such, higher L values corresponds to higher accuracy for the prediction by the GP emulator. From reference [108], the likelihood L is a balanced metric that is widely adopted for the computation of kernel hyper-parameters. Moreover, L is associated with an intuitive interpretation where the component $[det(k(X,X))]^{-\frac{1}{2}}$ of L controls the representative capacity of the emulator and the component $exp\{-\frac{1}{2}f(X)^T k(X,X)^{-1} f(X)\}$ evaluates the emulator's fit with data. As such, MLE based training of kernel hyper-parameters leads to balanced kernels capable of representing complicated relations such as those existing in PLF studies.

To capture the complex relations between the various elements of the input feature vector and the system output, simple kernels such as those presented in Table 4.1 are combined in order to construct *additive kernels* via summations and products. The simple kernels used for constructing the additive kernels are referred to as base kernels. In the studies conducted in this work, SE kernels with one dimensional inputs are adopted as the base kernels. While the base kernels can capture the relationship between individual elements of the input vector, they have difficulty extrapolating to the entire input space as only local interactions are accounted for. As such, the m^{th} order additive kernel $k_{add_m}(x, x')$ is defined as follows:

$$k_{add_m}(x, x') = \sigma_m^2 \sum_{\mathscr{C} \in \mathscr{C}_{d_i}^m} [\Pi_{r \in \mathscr{C}} k_r(x_r, x'_r)] \tag{4.4}$$

where x and x' are the two inputs of k_{add_m} and both of them are vectors with dimension d_i. Moreover, $\mathscr{C}_{d_i}^m$ is the set for all possible m digit combinations of integers in the range of 1 to d_i and $k_r(x_r, x'_r)$ is the base kernel. As such, k_{add_m} is the summary of all combinations of m^{th} order products from the base kernels. When $m = 0$, the kernel k_{add_0} is set to be an SE kernel. Additive kernels of different orders are then combined together to form the final kernel k:

$$k(x, x') = \sum_{s_m \in S} s_m k_{add_m}(x, x') \tag{4.5}$$

where $s_m \in \{0, 1\}$ and the additive kernel k_{add_m} is included in the final kernel if and only if $s_m = 1$. If $s_m = 1$ for every $1 \leq m \leq d_i$, the resulting final kernel will be an intricate entity that is capable of modelling the highly complex interdependences in the training dataset. However, this kernel is also prone to over-fitting and does not generalize well to new datasets. On the other hand, setting $s_m = 0$ for every m will result in the standard SE kernel that does not extrapolate well. As such, the values selected for s_m decide the structure of the final kernel and plays a critical role in determining the performance of the GP emulator.

4.3 Proposed Kernel Design Methodology

To decide the optimal values of s_m and the hyper-parameters associated with the final kernel, the kernel design problem is formulated and this problem is a bi-level optimization problem. The Order Set (OS) S is first defined as the collection of s_m for every $1 \leq m \leq d_i$. The input dimension d_i is generally a large number and this is especially true for large scale DNs. As such, a limit o is placed on the order number m to limit the complexity of kernel and curb overfitting. Hence, every order set S now contains o elements (i.e. $S = \{s_1, ..., s_o\}$). As S is composed of information on which additive kernel is incorporated in the final kernel k, it represents the structure of k.The final kernel whose structure is represented by the OS S is denoted by $k_{AK_S}(., .|S, \theta_S)$. The kernel design problem is then formulated as the composition of two subproblems: 1) The upper level subproblem $\mathcal{P}_{k_u}$ which calculates the optimal OS S using the dataset $(X_u, f(X_u))$; and 2) The lower level subproblem $\mathcal{P}_{K_l}$ which trains the hyper-parameters associated with the specific OS S over the dataset $(X_l, f(X_l))$. This formulation adheres to the structure of bi-level optimization problems laid out in reference [109]. The upper level problem $\mathcal{P}_{k_u}$ searches for the optimal OS S whose elements are binary numbers (i.e. $C1$) on the dataset $(X_u, f(X_u))$ using the set of optimal hyper-parameters obtained in $\Theta(S)$ (i.e. $C2$). Then, the lower level problem $\mathcal{P}_l$ computes the hyper-parameters for a specific OS S over the data set $(X_l, f(X_l))$. As there exists no overlapping elements between $(X_u, f(X_u))$ and $(X_l, f(X_l))$, the issue of over-fitting can be avoided. Since the objective

is to maximize the likelihood of observing the outputs $f(X_u)$ given the input X_u, the OS S and the set of hyper-parameters θ_S associated with S, the objective functions for both subproblems are selected to be the negative marginal log likelihood function.

$$\mathcal{P}_{K_u} : \min_{S,\theta_S} F(S,\theta_S) = -L(k_{AK_S}(.,.|S,\theta_S)|X_u, f(X_u))$$

$$s.t.\ \ s_m \in \{0,1\}\ \forall\ 1 \le m \le o,\ S = \{s_1,\ldots,s_o\} \qquad [C1]$$

$$\theta_S \in \Theta(S) \qquad [C2]$$

$$\mathcal{P}_{K_l} : \min_{\theta_S} G(S,\theta_S) = -L(k_{AK}(.,.|S,\theta_S)|X_l, f(X_l))$$

The kernel design problem is a NP-hard bi-level problem that is difficult to solve directly. As such, an iterative algorithm for overcoming these obstacles is introduced. To construct the framework for the proposed iterative algorithm, the hyper-parameters computed in $\mathcal{P}_{K_l}$ is substituted by the equivalent mapping $\theta_S = v(S, X_l, f(X_l))$. This allows for the reformulation of the bi-level kernel design problem as the optimization problem $\mathcal{P}_K$:

$$\mathcal{P}_K : \min_{S} F(S) = -L(k_{AK_S}(.,.|S, v(S,X_l,f(X_l)))|X_u, f(X_u))$$

$$s.t.\ \ s_m \in \{0,1\}\ \forall\ 1 \le m \le o,\ S = \{s_1,\ldots,s_o\} \qquad (4.6)$$

To iteratively solve the reformulated problem $\mathcal{P}_K$, the current OS examined S^c is first initialized with a random set of binary numbers. Next, the local neighbourhood of S^c is defined as the set that contains all OSs that differ from S^c by an element and denote it by $\hat{\mathcal{S}}_o^c$. Then, at every iteration an OS in $\hat{\mathcal{S}}_o^c$ is randomly examined and S^c is replaced with the OS examined if it is associated with a lower cost (i.e. F) than S^c. This iterative examination and replacement procedure is continued until no OSs in $\hat{\mathcal{S}}_o^c$ is associated with a lower cost than S^c. The proposed algorithm for kernel

design is summarized in Alg. 2:

Alg. 2: Proposed Kernel Design Algorithm

Initialization:

- Initialize S^c with an OS whose elements are randomly selected from $\{0, 1\}$.
- Denote the set of OS examined by V_c and initialize it with the empty set $\emptyset$.

Algorithm:

1. Randomly select S from $\hat{\mathcal{S}}_o^c \setminus V_c$ for evaluation.
2. If $F(S) >= F(S^c)$, replace V_c with $V_c \cup S$. Otherwise, replace S^c with S and set V_c as $\emptyset$.
3. If $V_c = \hat{\mathcal{S}}_o^c$, then terminate the iterative update process. Otherwise, return to the first step.

4.4 Theoretical Performance Guarantees

Next, a two-fold study of the theoretical performance of the proposed PLF method is conducted. First, the performance guarantees for the kernel design algorithm presented in Alg. 2 are established. Then, a study on the approximation capabilities for the GP emulator utilized in the proposed PLF method is presented. To establish the performance guarantees for Alg. 2, a game-theoretic formulation $\mathcal{G}_K(\mathcal{P}, \mathcal{L}, C)$ of this algorithm is presented. Here, $\mathcal{P}$ is the set of players participating in the game. The sets of strategies available to the players are included in $\mathcal{L}$. Moreover, the cost functions for these strategies are included in C. In the formulation for $\mathcal{G}_K$, every element of S^c is represented by a player in $\mathcal{P}$ and the strategies available to each player is $\{0, 1\}$. Furthermore, the cost functions for all players as well as the global cost function for $\mathcal{G}_K$ are set to be the cost function F of $\mathcal{P}_K$. In this setup, at every iteration a player $m \in \mathcal{P}$ in $\mathcal{G}_K$ is randomly selected. This player then makes the decision regarding whether to change its current strategy according to the

cost function laid out in C. This iterative revision process is terminated when no player in $\mathcal{G}_K$ is capable of making further changes. Next, the set of strategies for any player $m \in \mathcal{P}$ and the set of strategies adopted by other players are denoted by $L_m \in \mathcal{L}$ and L_{-m} respectively. For the player m contemplating a switch from strategy $a \in L_m$ to strategy $b \in L_m$, the change in its local cost $C_m \in C$ incurred by this switch is identical to the change in global cost C due to this switch:

$$C_m(a, L_{-m}) - C_m(b, L_{-m}) = C(a, L_{-m}) - C(b, L_{-m}),\ m \in \mathcal{P} \tag{4.7}$$

As such, $\mathcal{G}_K$ is an exact potential game according to reference [119]. From the properties of exact potential game, any stationary point of $\mathcal{G}_K$ is a Nash Equilibrium and its corresponding solution in Alg. 2 is a local optimum for $\mathcal{P}_K$. Since strategy changes in $\mathcal{G}_K$ only happens when it results in the reduction of the global cost C, the global cost C decreases at every iteration. What is more, the number of strategies available to each player in $\mathcal{G}_K$ is finite. Therefore, according to the definition of exact potential games presented in reference [119] $\mathcal{G}_K$ will always converge to a stationary point in finite time. Thus, Alg. 2 will always converge to a local optimum of $\mathcal{P}_K$. The convergence result produced by Alg. 2 is denoted by S^* and the kernel associated with this result by $k_{AK_{S^*}}$. Hence, the zero-mean GP utilized by the proposed PLF method and its predictive mean are $\mathcal{GP}(0, k_{AK_{S^*}}(.,.))$ and $m_{AK_{S^*}}(.)$ respectively. The supremum norm defined on the set of real numbers $\mathbb{R}$ is then denoted by $\|.\|_\infty$. From reference [110], the posterior mean $m_{AK_{S^*}}(.)$ is an arbitrary close approximation of the system output $f(.)$ if the supremum norm of their differences (i.e. $\|m_{AK_{S^*}}(.) - f(.)\|_\infty$) tends to 0 as the number of samples in the training set $(X, f(X))$ goes to infinity. Leveraging theoretical constructs associated with the Representer Theorem detailed in reference [111], it can be established that the posterior mean $m_{AK_{S^*}}(.)$ can be an arbitrarily close approximation of $f(.)$ if the kernel $k_{AK_{S^*}}$ can be expressed as a function the squared difference between its two inputs.

To prove the emulator posterior mean $m_{AK_{S^*}}(.)$ can approximate the system output $f(.)$ arbitrarily closely under practical conditions, functions obtained by substituting any $x \in \mathbb{R}^{d_i}$ into the second input of the kernel function $k_{AK_{S^*}}(.,.)$ are first designated as $k_{AK_{S^*}}(.,.)$ partially evaluated

at x and denoted as $k_{AK_{S^*}}(.,x)$. As the kernel function $k_{AK_{S^*}}(.,.)$ maps $\mathbb{R}^{d_i} \times \mathbb{R}^{d_i}$ to $\mathbb{R}$, the partially evaluated function $k_{AK_{S^*}}(.,x)$ maps $\mathbb{R}^{d_i}$ to $\mathbb{R}$. Next, the set of all functions that can be represented as a weighted sum of $k_{AK_{S^*}}(.,x)$ where $x \in X$ are designated as $\mathcal{K}^X$. Similarly, the set containing all functions that can be written as a weighted sum of infinitely many additive kernels where each additive kernel $k_{AK_{S^*}}(.,.)$ is partially evaluated at a different input obtained from sampling $\mathbb{R}^{d_i}$ is denoted by $\lim_{n_X \to \infty} \mathcal{K}^X$. That is:

$$\mathcal{K}^X = \sum_{i}^{n_X} \alpha_i k_{AK_{S^*}}(.,x^i), x^i \in X, \alpha_i \in \mathbb{R}\}$$

$$\lim_{n_X \to \infty} \mathcal{K}^X = \lim_{n_X \to \infty} \sum_{i}^{n_X} \alpha_i k_{AK_{S^*}}(.,x^i), x^i \in X, \alpha_i \in \mathbb{R}\}$$

The non-negative and the positive real number sets are denoted as $\mathbb{R}_{\geq 0}$ and $\mathbb{R}_{>0}$ respectively. Next, the mathematical concepts and terms (e.g. Borel measure) utilized in this proof are elaborated on. According to reference [112], the sigma-algebra $\mathcal{A}$ defined for the set X is a family of subsets of X such that the unions, the intersections and the complements of elements of $\mathcal{A}$ are in $\mathcal{A}$. Moreover, X itself is also included in $\mathcal{A}$. That is:

- If $M \in \mathcal{A}$, then $X \setminus M \in \mathcal{A}$.
- If $M, N \in \mathcal{A}$, then $M \cup N \in \mathcal{A}$.
- If $M, N \in \mathcal{A}$, then $M \cap N \in \mathcal{A}$.
- $X \in \mathcal{A}$.

Next, a Borel measure $\hat{\mu}$ defined on the set X is a function mapping the Borel sigma-algebra of X to $\mathcal{R}_{\geq 0}$, whereas the Borel sigma-algebra for X is defined as the intersection of all sigma-algebras containing the open subsets of X. Furthermore, a subset U of the n-dimensional real space $\mathcal{R}^n$ is an open set if for every point x in U there exists a real value $\epsilon \in \mathcal{R}_{>0}$ such that any $y \in \mathcal{R}^n$ is in U if and only if $||x - y|| < \epsilon$. Moreover, a closed set is a the set whose complements is an open set.

What is more, an open neighborhood O_x associated with a point x in X is an open subset of X such that there exist $V \in X$ satisfying $V \in O_x, x \in V$. Finally, the support of a measure $\hat{\mu}$ defined on the set X is defined as the largest closed subset of X where the measure for every open neighborhood at every point in the subset is positive.

Thus, if the additive kernel $k_{AK_{S^*}}(.,.)$ can be rewritten as an equivalent function $h_{AK_{S^*}}(t)$ where $t = \|x - x'\|^2$, then according to reference [110] there exists a Borel measure $\hat{\mu}_{AK_{S^*}}(\sigma)$ defined on $\mathbb{R}_{\geq 0}$ (i.e. $\sigma \in \mathbb{R}_{\geq 0}$) such that for all $t \in \mathbb{R}_{\geq 0}$, $h_{AK_{S^*}}(t)$ can be reformulated into the following Lebesgue integral:

$$h_{AK_{S^*}}(t) = \int_{\mathbb{R}_{\geq 0}} e^{-t\sigma} d\hat{\mu}_{AK_{S^*}}(\sigma)$$

From reference [110], for every non-constant function $h_{AK_{S^*}}(t)$ the support of the sigma-algebra $\hat{\mu}_{AK_{S^*}}(\sigma)$ shall be contained in $\mathbb{R}_{>0}$. According to Theorem 17 presented in the same reference, if the support of $\hat{\mu}_{AK_{S^*}}(\sigma)$ is a subset of $\mathbb{R}_{>0}$ and $d_o = 1$ then there must be a $q^* \in \lim_{n_X \to \infty}$ that approximates $f(.)$ arbitrarily closely. As such, there must exist such $q^*(.)$ providing $k_{AK_{S^*}}(.,.)$ is not constant. For the dataset $(X, f(X))$, the statement that $\|f(x^i) - q^*(x^i)\|^2 \leq \frac{\epsilon}{2^i}$ for every $\epsilon \in \mathbb{R}_{>0}$ without loss of generality is valid as $q^*(.)$ approximates $f(.)$ arbitrarily closely. Therefore, the summation of all $\|f(x^i) - q^*(x^i)\|^2$ when $n_X \to \infty$ is upper bounded by every $\epsilon \in \mathbb{R}_{>0}$:

$$\lim_{n_X \to \infty} \sum_{i=1}^{n_X} \|f(x^i) - q^*(x^i)\|^2 \leq \lim_{n_X \to \infty} \sum_{i=1}^{n_X} \frac{\epsilon}{2^i} = \epsilon$$

According to the Representer Theorem detailed in reference [111], the predictive posterior mean $m_{AK_{S^*}}(.)$ associated with the zero-mean GP $\mathcal{GP}(0, k_{AK_{S^*}}(.,.))$ trained on $(X, f(X))$ satisfies $m_{AK_{S^*}}(.) \in \mathcal{K}^X$ and is the only solution to the following problem:

$$\min_{q \in \mathcal{K}^X} \sum_{i=1}^{n_X} \|f(x^i) - q(x^i)\|^2$$

From the previous derivations, there exists $q^*(.) \in \lim_{n_X \to \infty}$ such that $\sum_{i=1}^{n_X} \|f(x^i) - q^*(x^i)\|^2$ is finite.

Thus, as $n_X \to \infty$ the posterior mean $m_{AK_{S^*}}(.)$ trained on $(X, f(X))$ satisfies $m_{AK_{S^*}}(.) \in \underset{n_X \to \infty}{lim}$ and is the unique solution to the problem:

$$\underset{q \in \lim\limits_{n_X \to \infty} \mathcal{K}^X}{min} \lim_{n_X \to \infty} \sum_{i=1}^{n_X} \|f(x^i) - q(x^i)\|^2$$

Since $m_{AK_{S^*}}(.)$ is the sole solution to the above problem, the following can be derived:

$$\lim_{n_X \to \infty} \sum_{i=1}^{n_X} \|f(x^i) - m_{AK_{S^*}}(x^i)\|^2 \leq \lim_{n_X \to \infty} \sum_{i=1}^{n_X} \|f(x^i) - q^*(x^i)\|^2 \leq \epsilon$$

For every $\epsilon \in \mathbb{R}_{>0}$. From the above relation, it can be concluded that every $x \in \mathbb{R}^{d_i}, \epsilon \in \mathbb{R}_{>0}$ satisfies $\|f(x) - m_{AK_{S^*}}(x)\|^2 \leq \epsilon$. As such, the posterior mean $m_{AK_{S^*}}(.)$ produced by Alg. 2 is capable of approximating $f(.)$ arbitrarily closely.

4.5 Simulations on Practical Networks

To assess the performance of the proposal on PLF, simulation studies conducted on three test systems based on practical IEEE benchmark DNs have been conducted. These test systems are: 1) Bus 15 for the Balanced 12.66 kV IEEE 33-bus DN; 2) Bus 21, Phase C for the Unbalanced 4.8 kV IEEE 37-bus DN; and 3) Bus 87, Phase B for the Unbalanced 4.16 kV IEEE 123-bus DN. These test systems are denoted as 33-15, 37-21-C and 123-87-B respectively. The specifications of these benchmark DNs can be found in reference [131]. In the simulations presented here, the kernels are designed to emulate the voltage magnitude of a bus at a phase. Moreover, the bus-phase combinations for each test system are selected at random. Comparative analysis with the state-of-the-art in data-driven PLF methods introduced in reference [28] is also included. To generate the datasets utilized for training and validating the proposed PLF method, the emulator input x is set to contain the net power injections at each phase of every bus in the DN under consideration. As the net injections are stochastic in nature, the input features X in the dataset are generated through sampling the bus net power injections detailed in Section 2.4. The outputs in the dataset

which are bus voltage magnitudes are then generated through power system simulation toolboxes MATPOWER and OpenDSS [85, 86]. The total number of datapoints for the training dataset $(X, f(X))$ and the testing dataset $(X_t, f(X_t))$ are set to be 400 and 100 respectively. These sizes are comparable to those adopted by the state-of-the-art in PLF such as reference [113] and the 80/20 split of training/testing datasets adheres to the dataset partitioning principles proposed by [114]. For the proposed method, the training dataset is first equally partitioned into $(X_l, f(X_l))$ and $(X_u, f(X_u))$. Then, the kernel with structure obtained from Alg. 2 is trained on the training dataset $(X, f(X))$. The hyper-parameters of GP kernels are trained with the GPflow library [115]. Next, the maximum kernel order o is set to 8. As such, the number of unique kernel structures available is 2^8. This choice of maximum order serves to limit overfitting with commonly associated with overly complex models [114]. Furthermore, the iteration number of the proposed design method is defined as the number of times a kernel is evaluated.

For evaluating the performance of the proposed method, three different metric is then introduced. The first metric is the likelihood difference factor D which measures the difference between the likelihood values of kernels obtained from the training set and the optimal kernel for the testing set. The second metric is the Root Mean Squared Error (RMSE) R which evaluates the emulator output's fit with data. The third metric is the Kullback-Leibler Divergence (KLD) D_{KL} which provides a quantitative evaluation of the difference between two random variables. The formulation for the difference factor D is presented as follows:

$$D = \frac{log(L(k(.,.)|X_E, f(X_E))) - log(L(k_\omega(.,.)|X_E, f(X_E)))}{log(L(k_\alpha(.,.)|X_E, f(X_E))) - log(L(k_\omega(.,.)|X_E, f(X_E)))} \tag{4.8}$$

where k is the kernel evaluated by this metric and $(X_E, f(X_E))$ is the dataset this metric is evaluated on. The first term $log(L(k(.,.)|X_E, f(X_E)))$ in the numerator of this metric is the log likelihood value for the kernel k. Moreover, the second terms in both the numerator and the denominator are identical to each other and both of them are $log(L(k_\omega(.,.)|X_E, f(X_E)))$. This term is the log likelihood

value for the GP kernel k_ω whose structure results in the worst performance (i.e. least likelihood value) for $(X_E, f(X_E))$. Furthermore, the first term $log(L(k_\alpha(.,.)|X_E, f(X_E)))$ in the denominator of D is the log likelihood value for the GP kernel k_α whose structure results in the best performance (i.e. highest likelihood value) for $(X_E, f(X_E))$. The kernel structures for k_ω and k_α are obtained from iterative examination of the performance associated with all possible kernel structures. As such, the metric D provides normalized insights into the performance of k with respect to the kernels associated with the best and worst structures. From the formulation provided in Eq. 4.8, the values for D ranges from 0 to 1. If the performance of k evaluated on $(X_E, f(X_E))$ is close to that associated with the optimal kernel, then the value of D is close to 1. On the other hand, if the performance of k is close to the worst kernel then D will be close to 0. Next, the formulation for the metric R is presented as follows:

$$R = \sqrt{\frac{(||m(X_E) - f(X_E)||)^2}{n_E^X}} \tag{4.9}$$

where $m(.)$ is the predictive mean whose expression is detailed in Eq. 4.2, $(X_E, f(X_E))$ denotes the dataset this metric is evaluated on, and n_E^X denotes the size (i.e. the number of samples) of $(X_E, f(X_E))$. The numerator term $||m(X_E) - f(X_E)||)^2$ then measures the distance between $m(.)$ and the system output $f(.)$ the emulator is designed to emulate. Next, the expression for D_{KL} is presented as follows:

$$D_{KL}(\pi_1||\pi_2) = \int_{-\infty}^{\infty} \pi_1(r) log(\frac{\pi_1(r)}{\pi_2(r)}) dr \tag{4.10}$$

where the distributions of the two random variables to be evaluated are denoted by π_1 and π_2 respectively. According to reference [116], $D_{KL}(\pi_1||\pi_2)$ can also be interpreted as a measure of the information loss when π_1 is approximated by π_2.

To study the convergence characteristics of Alg. 2, the impact of the initial kernel structure on

DN System	$\mu(I_t)$	$\sigma(I_t)$	**Dataset**	$\mu(D_0)$	$\mu(D_{I_t})$
33-15	21.6	9.89	$(X_l, f(X_l))$	0.823	0.908
			$(X_u, f(X_u))$	0.864	0.932
			$(X_t, f(X_t))$	0.843	0.900
37-21-C	16.6	4.765	$(X_l, f(X_l))$	0.384	0.493
			$(X_u, f(X_u))$	0.352	0.500
			$(X_t, f(X_t))$	0.371	0.503
123-87-B	13.3	2.5407	$(X_l, f(X_l))$	0.685	0.977
			$(X_u, f(X_u))$	0.683	0.975
			$(X_t, f(X_t))$	0.656	0.934

Table 4.2: Impact of Initial Kernel Structure on Convergence Properties of Alg. 2 ©2022 IEEE.

convergence is first evaluated. The evolution characteristics of D for the three DNs at every iteration are then studied. In Table 4.2, the effect of different initial kernel structures on the convergence characteristics of Alg. 2 is presented. For each of the three test systems examined, 10 different initial kernel structures whose maximum kernel order $o = 8$ are randomly generated. Then, Alg. 2 is carried out for each initial structure generated. The number of iterations required for Alg. 2 to achieve convergence is denoted by I_t. In Table 4.2, the average and the standard deviation values of the iteration numbers for the 10 runs associated with every test system are denoted by $\mu(I_t)$ and $\sigma(I_t)$ respectively. Moreover, the average values of D for the initial kernel structures and the kernel structures produced by Alg. 2 are denoted by $\mu(D_0)$ and $\mu(D_{I_t})$ respectively. From Table. 4.2, the average iteration number required for convergence (i.e. $\mu(I_t)$) varies for different test systems. Nevertheless, all $\mu(I_t)$ values presented are much smaller than the number of kernel structures that need to be examined for computing the optimal kernel structure via the brute force approach. Moreover, for all systems studied the standard deviations for convergence iterations are smaller than half of the averages for convergence iterations. As such, the convergence of Alg. 2 is consistently fast for all test systems and the convergence iterations for different starting kernel configurations do not depart considerably from the average convergence iteration. Furthermore,

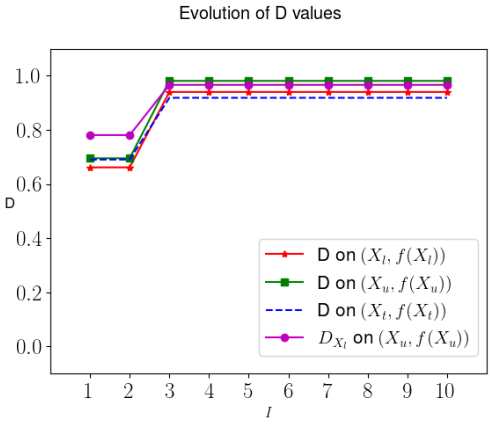

(a) System 33-15 ©2022 IEEE.

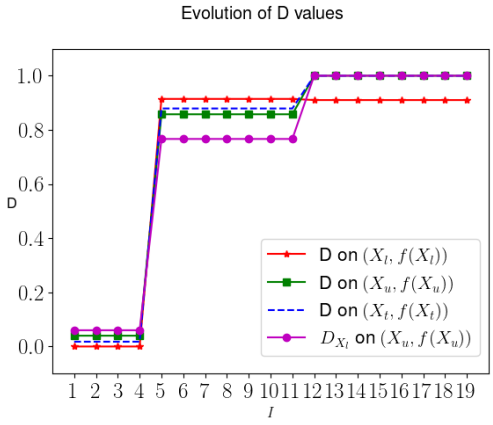

(b) System 37-21-C ©2022 IEEE.

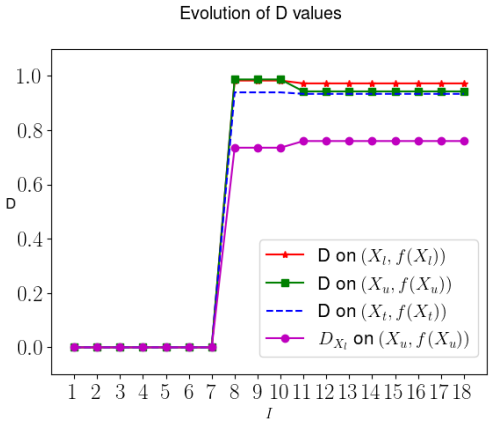

(c) System 123-87-B ©2022 IEEE.

Figure 4.1: Convergence Study for Alg. 2.

for all test systems examined the $\mu(D_0)$ values associated with different datasets are similar and the $\mu(D_{I_t})$ values for different datasets are also close to each other. What is more, for all test systems and datasets examined $\mu(D_{I_t})$ are notably higher than $\mu(D_0)$. Thus, the proposed kernel design algorithm in Alg. 2 generally results in notable improvements in kernel performance regardless of the initial structure selected. As the performance of Alg. 2 does not degrade for systems with high dimensional input vectors, the proposed design algorithm can be easily scaled to large scale systems.

Next, Figs 4.1a-4.1c charts the evolution of the D values at every iteration of Alg. 2 for all test systems. Here, the D values associated with the kernels trained on $(X, f(X))$ and $(X_l, f(X_l))$ are represented by D and D_{X_l} respectively. For the simulations presented in these figures, the

initial kernel structures used by Alg. 2 are represented by zero vector OS. In these figures, it can be observed that the D_{X_l} values evaluated on $(X_u, f(X_u))$ monotonously increase for all test systems. Moreover, the D values associated with the same test system stay the same at specific iterations while changing in other iterations. This behaviour is expected as Alg. 2 only allows change in kernel structure when the change leads to smaller cost for $\mathcal{P}_K$. Since there exists no significant divergence among the evolution trends of the D values calculated on different datasets, the improvements in kernel performances enabled by Alg. 2 generalize well to different datasets belonging to the same test system.

To assess the performance of the proposed method on the training dataset $(X, f(X))$ and testing dataset $(X_t, f(X_t))$, the R values for the three test cases considered is evaluated. These values are recorded in Table 4.3. As shown by these results, the R values associated with the training and testing datasets are close to each other for all the test systems considered. As such, the kernels produced by the proposed method generalize well to out-of-sample datapoints. What is more, the R values associated with all test cases are in the order of 10^{-3} p.u. Therefore, the predictive means produced by the emulator are close to their respective system outputs.

DN System	**Dataset**	R (p.u)
33-15	$(X, f(X))$	0.00212
	$(X_t, f(X_t))$	0.00322
37-21-C	$(X, f(X))$	0.00089
	$(X_t, f(X_t))$	0.00071
123-87-B	$(X, f(X))$	0.00031
	$(X_t, f(X_t))$	0.00049

Table 4.3: R Values for the Proposed Method ©2022 IEEE.

Next, the performance of the proposed method is compared against those of the state-of-the-art in data-driven PLF introduced in reference [28] and the traditional MCS based PLF method commonly adopted as a benchmark in proposals such as reference [50]. First, the D values associated with the proposed PLF method and the method introduced in reference [28] are compared

against those associated with the optimal solution for $\mathcal{P}_K$ for the testing datasets associated with all buses in the IEEE 33-bus DN. Then, the distributions of the output random variables obtained from the proposed method and the SE based state-of-the-art are evaluated against those obtained from the benchmark MCS based method for PLF. Finally, a comparison between the computational performance of the proposed PLF method and that of the MCS method is presented.

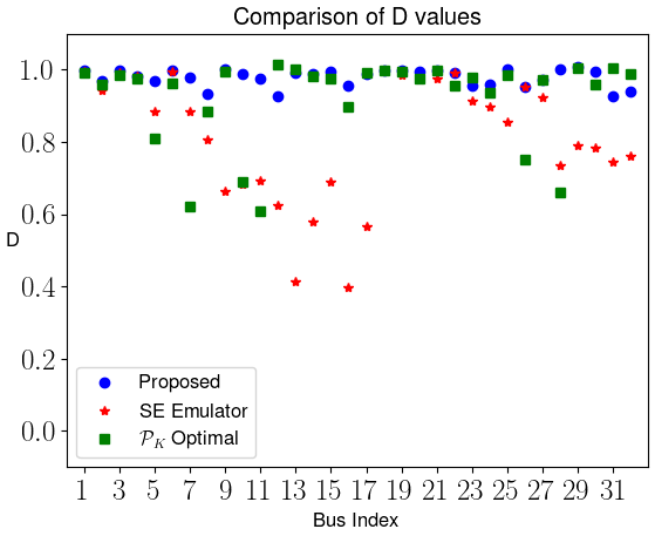

Figure 4.2: Comparative Study for IEEE-33 DN ©2022 IEEE.

The D values for the testing datasets associated with all buses in the IEEE-33 DN are plotted in Fig. 4.2 for the three PLF methods considered. This figure refers to the proposed method, the method introduced in reference [28] and the method associated with the optimal kernel for $\mathcal{P}_K$ as Proposed, SE Emulator and $\mathcal{P}_K$ Optimal respectively. As can be observed from Fig. 4.2, the PLF method associated with the optimal solution for $\mathcal{P}_K$ leads to D values that are notably lower than 1 for multiple buses in the DN. This phenomenon can be attributed to the overfitting of the optimal kernel on the dataset $(X_u, f(X_u))$. What is more, the PLF method presented in reference [28] also leads to D values that are significant lower than 1 for multiple buses and this can be attributed to the inability of the SE kernel to extrapolate well [108]. On the other hand, the proposed PLF method leads to D values that are close to 1 for all buses in the DN. As such, it can be observed from Fig. 4.2 that the proposed algorithm results in near optimal performance for the testing dataset and this

is a notable improvement over the state-of-the-art.

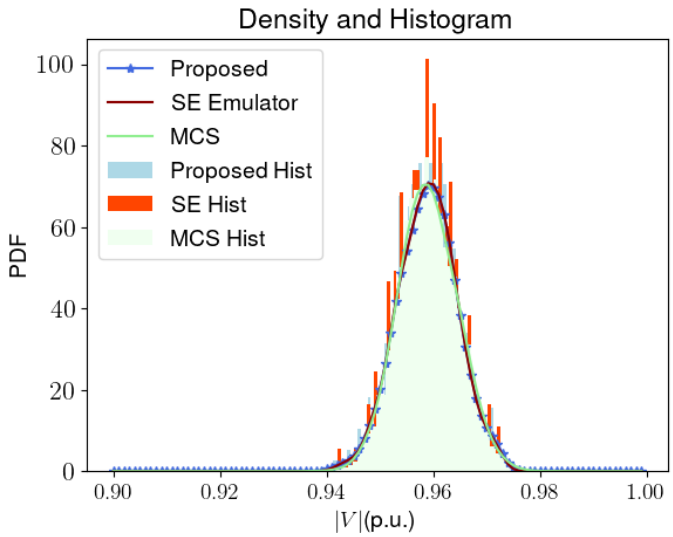

Figure 4.3: Comparison of Distributions for 123-87-B System ©2022 IEEE.

In Fig. 4.3, the histograms and Probability Distribution Functions (PDFs) associated with the output variables obtained from the proposed PLF method are plotted against those obtained from the SE Emulator based proposal and the benchmark MCS method for the 123-87-B test system. The distributions presented in this figure are plotted over voltage magnitudes ranging from 0.85 p.u to 1 p.u to facilitate presentation. Moreover, a sample size of 10000 is adopted by all proposals for generating the distributions presented. From Fig. 4.3, it can be observed that the distributions generated by the proposed technique result in a closer approximation of the benchmark results than the SE Emulator based method. To provide a quantitative assessment of the proposed method's ability for approximating benchmark results, the KLDs for the distribution obtained from the proposed method and the SE Emulator based technique are then listed in Table 4.4. These KLD values are evaluated against the benchmark distributions. From Table 4.4, it can be observed that the distributions obtained from the proposed method are associated with lower KLD values (i.e. better approximations) than the SE based method for all test cases examined. As such, it can be concluded the proposed method results in better approximations of the benchmark distribution than the SE based method.

DN System	**PLF Methods**	D_{KL}
33-15	Proposed	0.00863
	SE Emulator	0.1037
37-21-C	Proposed	0.00596
	SE Emulator	0.00629
123-87-B	Proposed	0.0083
	SE Emulator	0.00981

Table 4.4: Comparison of KLD ©2022 IEEE.

In Table 4.5, the average time required for simulating over 600 inputs for both the proposed PLF method and the benchmark MCS method are presented for all three test systems examined. From these results, it can be observed that this proposal requires lesser time for each simulation than the benchmark MCS method. This is expected as the computational complexities of the proposed method and the MCS method are $O(n)$ and $O(n^2)$ respectively. From Eq. 4.3, the computational complexity of the proposed PLF method is determined by the complexities of the kernel produced by Alg. 2 and the inferencing process of the GP emulator. As can be observed from Eqs. 4.4 and 4.5, the kernel utilized by the proposed method is calculated from all base kernels. Moreover, the number of base kernels is the same as the number of features. As the number of features is linear in terms of the number of buses in the system, the computational complexity of the kernel adopted by the proposed PLF method can be expressed as $O(n)$ where n is the number of buses in the system. Then, according to reference [117], the complexity of each simulation with a GP emulator is linear with regard to the size of the training dataset. As the size of the training dataset is a constant, the complexity of the proposed PLF method is also $O(n)$. Furthermore, the computational complexity of the MCS method for each simulation is the complexity for evaluating the load flow relations which is $O(n^2)$ according to reference [118].

DN System	PLF Methods	Simulation Time (s)
33-15	Proposed	0.0007
	MCS	0.0029
37-21-C	Proposed	0.0007
	MCS	0.0025
123-87-B	Proposed	0.0021
	MCS	0.0060

Table 4.5: Comparison Between Simulation Time ©2022 IEEE.

4.6 Chapter Summary

This chapter presents a kernel design algorithm for efficient approximation of underlying DN power flow relations captured by the training datasets. In this chapter, it is demonstrated via both theoretical and practical studies that the proposed design algorithm converges to the local optimum of the kernel design problem. Moreover, the kernel resulting from the design algorithm is shown to efficiently approximate the underlying distributions of voltage random variables. Comparative studies that demonstrates the advantage of the proposed algorithm over the state-of-the-art are also included.

Chapter 5

Reconfiguration for Voltage Profile Improvement

Current work in decentralized topology reconfiguration for resistive DNs such as reference [5] generally employ hierarchical structures that require extensive and system-specific tuning process. Moreover, no existing work in decentralized reconfiguration offers guarantees on algorithm performance or convergence. In this section, a decentralized DN reconfiguration method for voltage improvement that does not depend on highly granular tuning processes is first presented. Then, the general guarantees on the performance of the proposed method is introduced. Next, sufficient conditions for the optimal convergence of the proposed method are presented. Both the proposed method and the study on its convergence are first established in reference [83]. The equations, tables and figures presented in this section are included in the published work in reference [83].

Two different scenarios for topology reconfiguration are considered by this work. These two scenarios are designated as the *switching* and the *branch exchange* scenarios respectively. Both scenarios require the topology of the activated DN to maintain the radial structure (i.e. connected and acyclic). Under the switching scenario, only the power lines connecting reconfigurable buses and their potential parents are equipped with switches. Under the branch exchange scenario, all power lines in the DN are equipped with switches. As such, the branch exchange scenario can be

regarded as a special case of switching scenario where all buses in the DN are reconfigurable buses. Thus, this work first develops the reconfiguration algorithm for the switching case then simulate it on both switching and branch exchange cases.

5.1 Problem Formulation

To develop a topology reconfiguration technique for voltage profile improvement under the switching scenario, the following formulation for the reconfiguration problem was considered:

$$\mathcal{P}_{TR-rec}:$$

$$\min_{\mathcal{T}(\mathcal{R},\mathcal{P})} F(\mathcal{T}) := \sum_{r\in\mathcal{B}}\sum_{\phi\in\Phi_r}(\hat{\mathcal{V}}_f^{\phi} - \hat{\mathcal{V}}_r^{\phi})\ s.t.$$

$$\sum_{m:(m,r)\in\mathcal{E}} \Lambda_{mr}^{\Phi_r} + S_r = \Lambda_{rl} \qquad r\in\mathcal{B}\backslash f \tag{5.1}$$

$$\mathcal{S}_{rl} = \gamma^{\Phi_{rl}}\mathrm{Diag}(\Lambda_{rl}) = p_{rl} + \mathbf{j}q_{rl} \qquad (r,l)\in\mathcal{E} \tag{5.2}$$

$$(p_{rl}^{\phi})^2 + (q_{rl}^{\phi})^2 \le \overline{s}_{rl}^2 \qquad \phi\in\Phi_{rl}, (r,l)\in\mathcal{E} \tag{5.3}$$

$$\hat{\mathcal{V}}_r - \hat{\mathcal{V}}_l^{\Phi_{rl}} = z_{rl}\mathcal{S}_{rl}^H + \mathcal{S}_{rl}z_{rl}^H \qquad (r,l)\in\mathcal{E} \tag{5.4}$$

$$S_r = p_r + \mathbf{j}q_r \qquad r\in\mathcal{B} \tag{5.5}$$

$$\underline{p}_r \le p_r^{\phi} \le \overline{p}_r,\ \underline{q}_r \le q_r^{\phi} \le \overline{q}_r \qquad \phi\in\Phi_r,\ r\in\mathcal{B} \tag{5.6}$$

$$\underline{v}_r \le \hat{V}_r^{\phi} \le \overline{v}_r \qquad \phi\in\Phi_r, r\in\mathcal{B} \tag{5.7}$$

The objective function $F(\mathcal{T})$ of $\mathcal{P}_{TR-rec}$ represents the sum of voltage square magnitude drop of every phase in all buses in DN with respect to the feeder bus f. This formulation is inspired by the voltage profile optimization and voltage regulation criterion in existing works such as [5] and [55]. Furthermore, the problem was defined on the aforementioned LPF model. The LPF model is adopted here as it linearized the reconfiguration problem and allows for decentralized DN optimization on nearly balanced multiphase DNs. The challenges associated with resolving

$\mathcal{P}_{TR-rec}$ are two-fold. First, the reconfiguration problem is highly nonlinear as the topology variable $\mathcal{T}$ is discrete. Second, the highly coupled nature of the power and voltage constraints in Eqs. 5.2, 5.3 and 5.4 hampers the implementation of decentralized optimization techniques.

5.2 Decentralized DN Topology Reconfiguration

To formulate a decentralized reconfiguration strategy for the $\mathcal{P}_{TR-rec}$ problem, it is first inferred from Eqs. 5.2 and 5.4 that the voltage magnitude drop from the feeder bus f to any of its descendent h can be expressed as:

$$\hat{\mathcal{V}}_f - \hat{\mathcal{V}}_h = -\sum_{(m,r)\in\mathcal{E}_{h,f}} 2Re(z_{mr}^H C_m) \tag{5.8}$$

where $Re(.)$ denotes the real component and $C_m = \sum_{p\in\mathcal{B}_m} S_p$. From Eq. 5.8, it can be observed that the change in voltage drop from f to h caused by reconfiguration action at bus i only depends on the cumulative load C_i and the impedances associated with the power delivering lines shared by $\mathcal{E}_{h,f}$ and $\mathcal{E}_{i,f}$. From these observations, it can be concluded that the reconfiguration decision by $i \in \mathcal{R}$ only affects the voltage magnitudes of buses in $\mathcal{B}_{A_{j_i,k_i}}$. Moreover, all $h \in \mathcal{B}_{A_{j_i,k_i}}$ whose voltages are affected by reconfiguration can be separated into three cases based on impact of reconfiguration on their voltage profiles: Case 1 encompasses all $h \in \mathcal{B}_i$; Case 2 includes all $h \notin \mathcal{B}_i$ located in the subtree rooted at the immediate descendant of A_{j_i,k_i} that also belongs to the set $\mathcal{B}_{j_i,A_{j_i,k_i}}$; and Case 3 includes all $h \notin \mathcal{B}_i$ located in the subtree rooted at the immediate descendant of A_{j_i,k_i} that also belongs to the set $\mathcal{B}_{k_i,A_{j_i,k_i}}$. The three cases are illustrated in Fig. 5.1.

For any h in Case 1, its voltage drop change $\sum_{\phi\in\Phi_h} \Delta(\hat{\mathcal{V}}_f^\phi - \hat{\mathcal{V}}_h^\phi)$ caused by the reconfiguration action can be decomposed into three components: 1) Difference between the original voltage terms of the old parent j_i and new parent k_i of bus i before the switching action (i.e. $\sum_{\phi\in\Phi_h}(\hat{\mathcal{V}}'^\phi_{j_i} - \hat{\mathcal{V}}'^\phi_{k_i})$). 2) Voltage change due to the difference in impedance between line (i, k_i) and line (i, j_i) (i.e. $-\sum_{\phi\in\Phi_h}[({z_{ik_i}}^H - {z_{ij_i}}^H)C_i + C_i^H(z_{ik_i} - z_{ij_i})]^\phi$), and 3) Voltage change due to the addition of C_i to the power flow of lines in $\mathcal{E}_{k_i,A_{j_i,k_i}}$ (i.e. $-\sum_{(r,l)\in\mathcal{E}_{k_i,A_{j_i,k_i}}} \sum_{\phi\in\Phi_h}({z_{rl}}^H C_i + C_i^H z_{rl})^\phi$). Combining these

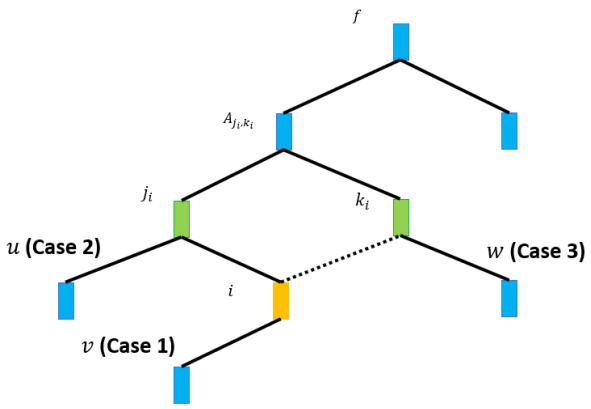

Figure 5.1: Illustration of the Three Cases.

components together leads to the following expression for voltage drop change for every $r \in \mathcal{B}_i$:

$$\sum_{\phi\in\Phi_h} \Delta(\hat{\mathcal{V}}_f^{\phi} - \hat{\mathcal{V}}_h^{\phi}) = \sum_{\phi\in\Phi_h} \left\{(\hat{\mathcal{V}}'^{\phi}_{j_i} - \hat{\mathcal{V}}'^{\phi}_{k_i}) - [({z_{ik_i}}^H - {z_{ij_i}}^H)C_i + C_i^H(z_{ik_i} - z_{ij_i})]^{\phi} - \sum_{(r,l)\in\mathcal{E}_{k_i A_{j_i k_i}}} ({z_{rl}}^H C_i + C_i^H z_{rl})^{\phi}\right\} \tag{5.9}$$

where $\hat{\mathcal{V}}'_{j_i}$ and $\hat{\mathcal{V}}'_{k_i}$ refer to the voltage terms at j_i and k_i before the switching action, respectively. For voltage change of buses in Cases 2 and 3, it is noted that the reconfiguration action decreases the power flow in lines belonging to $\mathcal{E}_{A_{j_i,h},A_{j_i,k_i}}$ by C_i and increases the power flow in lines belonging to $\mathcal{E}_{A_{k_i,h},A_{j_i,k_i}}$ by the same amount. Therefore, the voltage change $\sum_{\phi\in\Phi_h} \Delta(\hat{\mathcal{V}}_f^{\phi} - \hat{\mathcal{V}}_h^{\phi})$ for h in Case 2 can be expressed by $\sum_{(r,l)\in\mathcal{E}_{A_{j_i h A_{j_i k_i}}}} \sum_{\phi\in\Phi_h} ({z_{rl}}^H C_i + C_i^H z_{rl})^{\phi}$, and the voltage change for h in Case 3 is $-\sum_{(r,l)\in\mathcal{E}_{A_{k_i h A_{j_i k_i}}}} \sum_{\phi\in\Phi_h} ({z_{rl}}^H C_i + C_i^H z_{rl})^{\phi}$.

From the above relations, the effect of the switching operation on the voltage magnitude drop for every $h \in \mathcal{B}_{A_{j_i,k_i}}$ can be derived. This allows for the presentation of the following formulation for the cost change f_{j_i,k_i} incurred by the switching action at $i \in \mathcal{R}$:

$$f_{j_i k_i} = F(\mathcal{T}^{j_i}) - F(\mathcal{T}^{k_i}) = \sum_{\phi \in \Phi_f} \Big\{ (\hat{\mathcal{V}}'_{k_i} - \hat{\mathcal{V}}'_{j_i} + ((z_{ik_i}{}^H - z_{ij_i}{}^H)C_i + C_i^H(z_{ik_i} - z_{ij_i})))^{\phi} |\mathcal{B}_i^{\phi}| \tag{5.10}$$

$$+ \sum_{(r,l) \in \mathcal{E}_{j_i A_{j_i k_i}}} ((z_{rl}{}^H C_i + C_i^H z_{rl})^{\phi} (|\mathcal{B}_r'^{\phi}| - |\mathcal{B}_i^{\phi}|)) - \sum_{(r,l) \in \mathcal{E}_{k_i A_{j_i k_i}}} ((z_{rl}{}^H C_i + C_i^H z_{rl})^{\phi} (|\mathcal{B}_r'^{\phi}| + |\mathcal{B}_i^{\phi}|)) \Big\}$$

where $|\mathcal{B}_r'^{\phi}|$ is the number of buses in subtree $\mathcal{B}_r$ that have phase ϕ prior to the switch, and $|\mathcal{B}_i^{\phi}|$ is the number of buses with phase ϕ in $\mathcal{B}_r$ post switching. For the formulation of the decentralized algorithm, every bus r in the DN is allowed to monitor the cardinality of its own subtree $\mathcal{B}_r$, the minimal bus voltage $\hat{V}_{r_{min}}$ of buses in $\mathcal{B}_r$ and the impedances of the lines directly connected to it. Additionally, every $i \in \mathcal{R}$ is allowed to monitor the voltage values of its current and potential parents and the power flow in its directly connected lines. From Eq. 5.10, this arrangement allows every $i \in \mathcal{R}$ to calculate the global cost change $f_{j_i k_i}$ through iteratively accessing the local data of buses in $\mathcal{B}_{j_i, A_{j_i k_i}}$ and $\mathcal{B}_{k_i, A_{j_i k_i}}$.

For maintaining the topology constraint associated with the reconfiguration problem, the notion of *fundamental cycles* is introduced for every reconfigurable bus $i \in \mathcal{R}$. The fundamental cycle O_{i,j_i,k_i} associated with the switching action from $j_i \in \mathcal{P}_i$ to $k_i \in \mathcal{P}_i$ is defined as the cycle formed by the lines connecting i to j_i and k_i as well as the lines in $\mathcal{E}_{j_i, A_{j_i k_i}}$ and $\mathcal{E}_{k_i, A_{j_i k_i}}$ (i.e. $O_{i,j_i,k_i} = \{\mathcal{E}_{j_i, A_{j_i k_i}} \cup \mathcal{E}_{k_i, A_{j_i k_i}} \cup (i, j_i) \cup (i, k_i)\}$). To maintain the radial topology of the activated DN, the activated DN must be connected. Moreover, either (i, j_i) or (i, k_i) must be deactivated. Since the initial topology for the activated DN are radial and switching action does not change the number of lines in the activated DN, the activated DN is connected for the switching scenario so long as $(i, j_i) \notin \mathcal{E}_{k_i, A_{j_i k_i}}$ and $(i, k_i) \notin \mathcal{E}_{j_i, A_{j_i k_i}}$.

In reference [83], a reconfiguration algorithm is introduced that allows every $i \in \mathcal{R}$ to switch from j_i to k_i when the two following conditions are satisfied: 1) The switching leads to a reduction in global cost. (i.e. $f_{j_i k_i} > 0$); And 2) The switching action does not incur any constraint violations. The costs are calculated using data gathered by buses residing in $\mathcal{B}_{j_i, A_{j_i k_i}}$ and $\mathcal{B}_{k_i, A_{j_i k_i}}$. Furthermore, the voltage and topology constraints are maintained through calculating the changes to the minimal

bus voltages and monitoring the statuses of fundamental cycles respectively. These switching decisions are made at random exponentially distributed time intervals determined by the parameter λ, which prevents two buses from switching at the same time. The algorithm is terminated when no more switching can take place. The proposed reconfiguration algorithm is presented in Alg. 3.

Alg. 3: Proposed Decentralized Topology Reconfiguration Algorithm

Initialization:

- Every reconfigurable bus $i \in \mathcal{R}$ randomly selects a strategy revision time t_i based on the exponential distribution defined by the parameter λ.

Algorithm:

1. Each bus $b \in \mathcal{B}$ monitors $|\hat{V}_{b_{min}}|$ and $|B_b^{\phi}|$ $\forall$ $\phi \in \Phi_f$ with iterative information propagation from leaf to root.
2. At time t_i, the reconfigurable bus i randomly selects a switching strategy k_i from $\mathcal{P}_i$.
3. Bus i transmits signal containing C_i, $|B_i|$ and initial cost $f_{j_i k_i} = 0$ along $\mathcal{E}_{j_i A_{j_i k_i}}$ and $\mathcal{E}_{k_i A_{j_i k_i}}$. This signal also checks the fundamental cycle O_{i,j_i,k_i} for violations of radial constraints.
4. When signal arrives at bus r residing in the paths $\mathcal{E}_{j_i A_{j_i k_i}}$ or $\mathcal{E}_{k_i A_{j_i k_i}}$, this bus computes the change of cost from strategy k_i and adds it to $f_{j_i k_i}$. Change in power flow in lines in $\mathcal{E}_{j_i A_{j_i k_i}}$ and $\mathcal{E}_{k_i A_{j_i k_i}}$ is also computed to check for power flow constraint violations.
5. When the cost signals converge at bus $A_{j_i k_i}$, the bus combines these to compute the cost $f_{j_i k_i}$ and sends this to node i. This bus also check for voltage constraint violations for buses in Cases 1-3 with $\hat{V}_{r_{min}}$.
6. If any constraint is violated or $f_{j_i k_i} \leq 0$, then i aborts the switch. Otherwise the switching operation is carried out.
7. After the decision, bus i updates t_i by randomly selecting another time interval.
8. If the termination condition is met (i.e. $f_{j_i k_i} \leq 0$ $\forall$ $k_i \in \mathcal{P}_i$), then bus i terminates the strategy revision process. Otherwise, return to the first step.

5.3 Theoretical Performance Guarantees

To analyze the convergence characteristics of Alg. 3, a game-theoretic formulation $\mathcal{G}(\mathcal{N}, \mathcal{S}, \mathcal{V})$ of the algorithm is first introduced. This formulation starts by defining the potential of this game $\mathcal{F}$ as the objective function F of the reconfiguration problem. Then, the set of rational players $\mathcal{N}$ is defined as the set of buses capable of performing reconfiguration (i.e. $\mathcal{N} = \mathcal{R}$). The set of strategies $S_i \in \mathcal{S}$ available to the player $i \in \mathcal{N}$ is defined as the set of parents $\mathcal{P}_i$ for reconfigurable bus i. The cost function $V_i \in \mathcal{V}$ for player $i \in \mathcal{N}$ is defined as the change in F induced by the reconfiguration at bus i. Furthermore, the strategy currently selected by player i is denoted as $s_i \in S_i$ and the collection of strategies selected by all players other than i is denoted as $s_{-i} \in S_{-i}$. From the decision-making process presented in Alg. 3, the following relation between player cost V_i and the potential $\mathcal{F}$ is satisfied for all $i \in \mathcal{N}$, any two $x, y \in S_i$ and any $s_{-i} \in S_{-i}$:

$$V_i(x, s_{-i}) - V_i(y, s_{-i}) = \mathcal{F}(x, s_{-i}) - \mathcal{F}(y, s_{-i}) \tag{5.11}$$

Since the proposed game $\mathcal{G}(\mathcal{N}, \mathcal{S}, \mathcal{V})$ satisfies Eq. 5.11 and has a finite set of players $\mathcal{N}$, it is classified as an exact potential game according to reference [119]. Next, a study on the trajectory of the game potential F due to the iterative switching process detailed in Alg. 3 is presented. In the proposed algorithm, each $i \in \mathcal{R}$ only switches from j_i to k_i when the switching action reduces the objective function (i.e. $f_{j_i k_i} = F(\mathcal{T}^{j_i}) - F(\mathcal{T}^{k_i}) > 0$). Therefore, every strategy revision performed by each player $i \in \mathcal{R}$ reduces the potential $\mathcal{F}$ of the proposed game. If the sequence of strategy revisions that results in the reduction of the system potential is defined as the *improvement path*, then from reference [119] every improvement path ζ for the exact potential game $\mathcal{G}$ is finite as both $\mathcal{N}$ and $\mathcal{S}$ are discrete and finite. Furthermore, by the end of all improvement paths no player i will be able to reduce V_i further by switching. As the pure-strategy Nash Equilibrium condition is defined as the state where no further improvement to the cost can be attained by any player, every ζ converges to a pure strategy Nash Equilibrium in finite time. Hence, Alg. 3 always converges to a local optimum of the reconfiguration problem $\mathcal{P}_{TR-rec}$ in finite time.

Furthermore, in this proposal the condition of *discrete concavity* presented in reference [120] is utilized to derive conditions in the DN that guarantee optimality for the proposed algorithm. First, the statuses for all reconfigurable buses $i \in \mathcal{R}$ are represented by the *status vectors* $x \in \mathbb{R}^{|\mathcal{R}|}$. If bus $i \in \mathcal{R}$ is connected to its original parent, then its corresponding element x_i in the status set x is 1, otherwise x_i is 0. Hence, each status vector corresponds to an unique DN topology configuration. The set of status vectors is denoted as $\mathcal{X}$. If the first norm is denoted as $\|.\|$, then for any $x, y \in \mathcal{X}$, $\|x - y\| = 1$ if the topologies represented by x and y differ by the status of a single reconfigurable bus. Next, the utility value corresponding to any status vector $x \in \mathcal{X}$ is defined as $U(x) = -F(\mathcal{T})$, where $\mathcal{T}$ is the DN topology corresponding to x. Based on these definitions, the definition of the discrete concavity condition for the reconfiguration problem can be expressed as the following:

$$\max_{x,y,z \in X: \|x-z\| = \|y-z\| = 1} U(z) = \begin{cases} > \min(U(x), U(y)), \text{ if } U(x) \neq U(y) \\ \geq U(x) = U(y), \text{otherwise} \end{cases} \tag{5.12}$$

From this expression, it can be concluded that the reconfiguration problem is discretely concave if for any $x, y, z \in \mathcal{X}$ that satisfy $\|x - y\| = 2$, $\|x - z\| = 1$ and $\|y - z\| = 1$, the smaller value between $U(x)$ and $U(y)$ is lower than the highest $U(z)$. Since local optima for discretely concave problems are globally optimal according to reference [120], the proposed algorithm always lead to globally optimum solutions for DN reconfiguration problems that satisfy the discrete concavity condition.

5.4 Simulation Results

To evaluate the performance of the proposed algorithm, comparative analyses between it and the FNSGA introduced in [55] are made for both the switching and the branch exchange scenarios. For the switching scenario, both reconfiguration algorithms are tested on the following five radial DNs: 1) The 12.66kV IEEE 33-bus radial DN introduced in reference [4], which has five remote controlled switches and is denoted by the name 33-5; 2) The 12.66kV IEEE 69-bus radial DN introduced in reference [121], which has five remote controlled switches and is denoted by the name

69-5; 3) A modified 69-bus DN created by randomly adding two remotely controllable switches to the 69-5. This new DN is denoted by the name 69-7; 4) Another modified 69-bus DN created by randomly adding three remotely controllable switches to 69-7. This new DN is denoted by the name 69-10; 5) A 13.8kV DN with 136 buses and 21 remotely controllable switches that is based in Brazil [122], which is denoted by the name 136-21. Among these five test DNs, the 33-5, 69-5 and 69-7 test DNs are discretely concave for the switching scenario, whereas the 69-10 and 136-21 test DNs are not. For the branch exchange scenario, both algorithms are simulated on the 33-5 and 69-5 test DNs as well as two test DNs created by modifying 33-5. These two test DNs are designed as 33-3 and 33-7 and they are created by randomly removing and adding two tie switches to the 33-5 test DN respectively. To measure the convergence rate of both algorithms, the iteration number I_t is defined as the number of times the state of DN is evaluated before convergence is achieved. Furthermore, both algorithms are simulated over 200 randomly generated initial DN topology configurations to reduce the impact of initial topology configuration on the quality of the solution. For evaluating the effectiveness of both algorithms, the term of *improvement factor* $\mathcal{I}$ is introduced. This term is defined as follows:

$$\mathcal{I}_k = \frac{F(\mathcal{T}) - F(\mathcal{T}_k)}{F(\mathcal{T}) - F(\mathcal{T}_{opt})} \tag{5.13}$$

where $\mathcal{T}$ refers to the initial DN topology, $\mathcal{T}_k$ refers to the DN topology at iteration k resulting from the algorithm under evaluation, and $\mathcal{T}_{opt}$ refers to the topology corresponding to the optimal outcome for $\mathcal{P}_{TR-rec}$. The figures displayed in this chapter adopt the confidence interval of 95%.

The performances for both the proposed reconfiguration algorithm and the Fast Non-denominated Sorted Genetic Algorithm (FNSGA) under the switching scenario are presented in Fig. 5.2. The FNSGA introduced in reference [55] is a genetic algorithm that solves the reconfiguration problem by calculating the load flow values for a limited number of candidate topologies. From reference [55], the FNSGA can solve non-linear optimization problems in short computation time. In Fig. 5.2a, the proposed algorithm can be observed to consistently obtain the globally optimal configuration for the discretely concave 33-5, 69-5 and 69-7 test DNs, and nearly optimal configuration

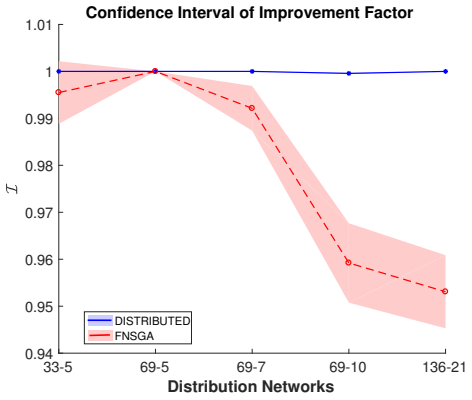

(a) Confidence interval for $\mathcal{I}$.

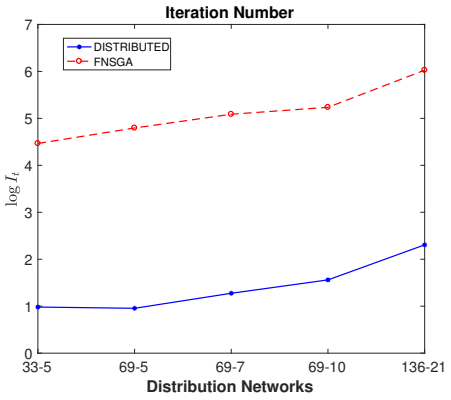

(b) Average I_t.

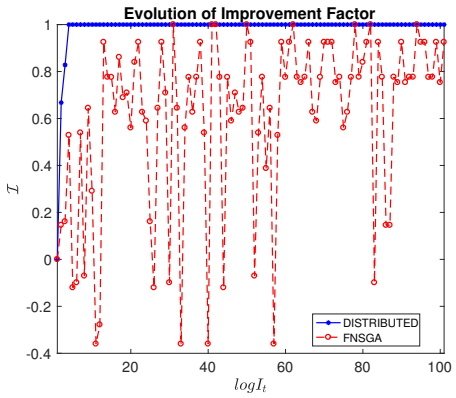

(c) Evolution of $\mathcal{I}$ for 33-5 DN.

Figure 5.2: Simulations for the Switching Case.

for the 69-10 and 136-21 test DNs. This demonstrates the improvement of the proposed algorithm over FNSGA, which performance is heavily affected by the initial network configuration for all test cases other than the 69-5 test DN. The average iteration number I_t for both the proposed algorithm and the FNSGA algorithm are presented in Fig. 5.2b, which showcases the rapid convergence property for the proposed algorithm. Finally, the improvement factor evolution for both the proposed algorithm and FNSGA for the 33-5 test DN is shown in Fig. 5.2c. Unlike FNSGA, the proposed algorithm is capable of rapidly converging to the optimal solution without any oscillatory behavior as indicated by this figure.

Next, the performance for the proposed algorithm and FNSGA under the branch exchange scenario is displayed in Fig. 5.3. As all buses in the DN have the ability to perform switching actions under the branch exchange scenario, the condition of discrete concavity is less likely to

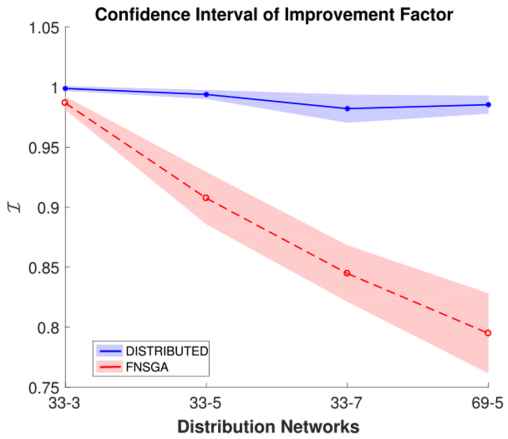

(a) Confidence interval for $\mathcal{I}$.

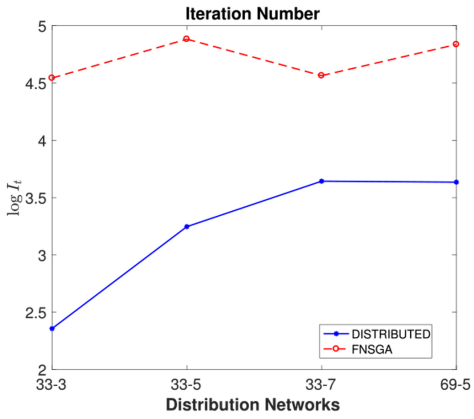

(b) Average I_t.

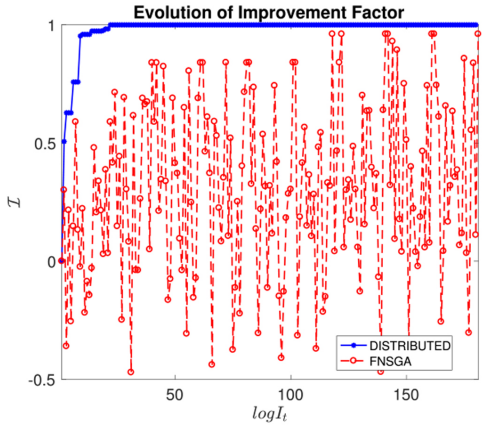

(c) Evolution of $\mathcal{I}$ for 33-5 DN.

Figure 5.3: Simulations for the Branch Exchange Case.

hold for this particular scenario. As evidenced from Fig. 5.3a, the solutions obtained from the proposed algorithm deviates slightly from the optimal solution for all test DNs studied while the solutions obtained from FNSGA diverge significantly from the optimal solution. Moreover, the performances for both the proposed algorithm and FNSGA deteriorates as the size of the DN and the number of switchable lines in the DN increase. In Fig. 5.3b, it can be further observed that the proposed algorithm is associated with a lower I_t than the FNSGA for all test DNs examined and this result is similar to the switching scenario results displayed in Fig. 5.2b. As illustrated in Fig. 5.3c, the proposed algorithm exhibits swift convergence to near-optimal solution while FNSGA is associated with heavy oscillatory behaviour.

5.5 Chapter Summary

This chapter introduces a decentralized algorithm that allows intelligent buses in the DN to improve the DN voltage profile through the reconfiguration of topologies. As the proposed algorithm is both decentralized and converges in real time, it can significantly improves the DN's resilience against voltage fluctuations. The algorithm is based on a iterative information exchange process that allows for effective coordination between cyber-enabled smart buses in the DN. This exchange process is designed by leveraging theoretical constructs associated with potential games as well as discrete concavity along with the attributes of DN topologies. The performance of the proposed reconfiguration algorithm is demonstrated via simulations conducted on the practical IEEE 33-bus, 69-bus and the Brazilian 136-bus DNs.

Chapter 6

Optimal Reconfiguration with Convex Relaxation

While the reconfiguration method introduced in the previous section can lead to locally optimal results and even global optimality under certain practical conditions, it does not account for the complex non-linear interdependencies inherent in the power flow relation and provides no guarantees of global optimality. In this chapter, a formulation of the reconfiguration problem based on the NPF model elaborated in Chapter 2 is first presented. Then, a decentralized reconfiguration method for voltage improvement is proposed that resolves the electrical interdependencies with a convex relaxation technique based on ADMM. Next, the theoretical foundations for the proposed method are introduced and proof for the globally optimal convergence of the proposed method is presented. The performance guarantees for the proposed method is first established in reference [84]. Also, the reconfiguration algorithm presented in this section is developed for the switching scenario. The equations, tables and figures presented in this section are included in the published work in reference [84]

6.1 Problem Formulation

To account for the electrical interdependencies in the DN, the reconfiguration problem $\mathcal{P}_{TR-rec}$ presented in the previous section is first formulated using the NPF model detailed in Section 2.3. The objective function F of the reformulated problem $\mathcal{P}_{TR-ref}$ serves to improve the voltage profile of the DN. Then, Eqs. 6.1-6.7 of the reformulated problem represent the multiphase NPF model introduced in Sec. 2.3 and maintain the electrical attributes as well as safe operating margins of the DN. Next, Eqs.6.8-6.14 address the impact of topology reconfiguration on the attributes of the DN. The reformulated reconfiguration problem $\mathcal{P}_{TR-ref}$ is presented as follows:

$$\mathcal{P}_{TR-ref} : \min_{\hat{\mathcal{V}},\beta,l,P,Q} F(\hat{\mathcal{V}},\beta,l,P,Q)$$

$$s.t.\ \forall i \in \mathcal{B} :$$

$$\underline{v}_i \leq \hat{V}_i^{\phi} \leq \overline{v}_i \qquad \phi \in \Phi_i \tag{6.1}$$

$$0 \leq l_{ij}^{\phi} \leq \bar{l}^2 \qquad \forall j \in \mathcal{P}_i, \forall \phi \in \Phi_{ij} \tag{6.2}$$

$$\hat{\mathcal{V}}_j^{\Phi_{ij}} - \hat{\mathcal{V}}_{ij} = 2(\overline{r}_{ij}P_{ij} + \overline{x}_{ij}Q_{ij}) + \overline{z}_{ij}l_{ij} \qquad \forall j \in \mathcal{P}_i \tag{6.3}$$

$$\hat{\mathcal{V}}_{ij} \odot l_{ij} = (P_{ij})^{\odot 2} + (Q_{ij})^{\odot 2} \qquad \forall j \in \mathcal{P}_i \tag{6.4}$$

$$\hat{\mathcal{V}}_i = \hat{\mathcal{V}}_{ip} \qquad \forall (i,p) \in \mathcal{E}_f \tag{6.5}$$

$$P_i = \sum_{j \in \mathcal{P}_i}(P_{ij} - r_{ij}l_{ij}) - \sum_{m \in \mathcal{K}_i} P_{mi} \tag{6.6}$$

$$Q_i = \sum_{j \in \mathcal{P}_i}(Q_{ij} - x_{ij}l_{ij}) - \sum_{m \in \mathcal{K}_i} Q_{ij} \tag{6.7}$$

$$\forall r \in \mathcal{R} :$$

$$0 \leq \beta_{rg} \leq 1 \qquad \forall (r,g) \in \mathcal{E}_s^r \tag{6.8}$$

$$\beta_{rg}(\beta_{rg} - 1) \geq 0 \qquad \forall (r,g) \in \mathcal{E}_s^r \tag{6.9}$$

$$\sum_{(u,v)\in\psi} \beta_{uv} \leq |\psi| - 1 \qquad \forall \psi \in \Psi \tag{6.10}$$

$$\sum_{(u,v)\in\mathcal{E}_s} \beta_{uv} = |\mathcal{B}| - 1 - |\mathcal{E}_f| \tag{6.11}$$

$$(\beta_{rg} - 1)\overline{v}_r^2 \leq \hat{\mathcal{V}}_{rg}^{\phi} - \hat{\mathcal{V}}_{r}^{\phi} \leq (1 - \beta_{rg})\overline{v}_r^2 \qquad \forall (r,g) \in \mathcal{E}_s^r, \forall \phi \in \Phi_{rg} \tag{6.12}$$

$$-\beta_{rg}\overline{v}_g^2 \leq \hat{\mathcal{V}}_{g}^{\phi} - \hat{\mathcal{V}}_{rg}^{\phi} \leq \beta_{rg}\overline{v}_g^2 \qquad \forall (r,g) \in \mathcal{E}_s^r, \forall \phi \in \Phi_{rg} \tag{6.13}$$

$$0 \leq l_{rg}^{\phi} \leq \beta_{rg}\overline{l}^2 \qquad \forall (r,g) \in \mathcal{E}_s^r \forall \phi \in \Phi_{rg} \tag{6.14}$$

Eq. 6.1 serves to maintain the voltage magnitude constraint at every bus in the DN. Moreover, Eq. 6.2 maintains the line current constraints at every line in the DN. As such, Eqs. 6.1 and 6.2 serve to maintain the electrical integrity of the DN. The linear constraint in Eq. 6.3 denotes the voltage drop along every $(i, j) \in \mathcal{E}$. The non-linear and non-convex interdependencies between the current, voltage and power pertaining to every line in the DN is represented by Eq. 6.4. The equality constraint in Eq. 6.5 enforces the consistency of bus voltage magnitudes associated with fixed lines. Eqs. 6.6 and 6.7 are the real and reactive power balance relations at every bus i. The continuous constraints in Eqs. 6.8 and 6.9 force the switching variable $\beta_{r,g}$ associated with every switchable line $(r, g) \in \mathcal{E}_s^r$ to take values in the intersection between the intervals $[0, 1]$ and $(-\infty, 0] \cup [0, \infty)$. As such, the value of every β is restricted to be either 0 or 1. Since Eq. 6.8 is a linear constraint, it is convex in terms of $\beta_{r,g}$. However, the quadratic constraint 6.9 is non-convex in terms of $\beta_{r,g}$. Eq. 6.10 prevents activated lines from forming cycles by forcing at least one switchable line in every cycle ψ in the DN to be deactivated. Eq. 6.11 constraints the number of activated lines in the DN to $|\mathcal{B}| - 1$. As such, Eqs. 6.10 and 6.11 maintain the radial structure of the activated DN. To provide an illustrative example of how the radial topology is maintained by these two constraints, the DN presented in Fig. 5.1 is considered. In this example, the total number of buses $|\mathcal{B}| = 9$, the number of switchable line $|\mathcal{E}_s| = 2$ and the number of fixed line $|\mathcal{E}_f| = 7$. From Eq. 6.11, the maximum number of active switchable line in this DN is

$|\mathcal{B}| - |\mathcal{E}_f| - 1 = 1$. When Eq. 6.11 is violated during the operation of the DN, either both switchable lines are active (which violates the acyclic condition) or both switchable lines are inactive (which violates the connected condition). From Eq. 6.10, the number of active lines residing in the only cycle $\psi = \{(i, j_i), (i, k_i), (j_i, A_{j_i,k_i}), (k_i, A_{j_i,k_i})\}$ in the DN shall be no greater than $|\psi| - 1 = 3$. Since at least one switchable line in every cycle must be deactivated, this constraint serves to enforce the acyclic condition. Eqs. 6.12 and 6.13 then connect the line status variable βrg associated with every switchable line $(r, g) \in \mathcal{E}_s$ to the line voltage magnitude variable $\hat{\mathcal{V}}_{rg}$ by setting $\hat{\mathcal{V}}_{rg}$ to $\hat{\mathcal{V}}_r$ in case $\beta_{rg} = 1$ and to $\hat{\mathcal{V}}_g$ in case $\beta_{rg} = 0$. Next, Eq. 6.14 sets the current across all deactivated switchable lines in the DN to 0. From the formulation of $\mathcal{P}_{TR-ref}$, the reformulated reconfiguration problem is a QCQP Problem that is associated with two sources of non-convexities: 1) The constraint in Eq. 6.4 which is related to voltage, current and power magnitudes; and 2) The constraint in Eq. 6.9 which is related to the status variables of switchable lines.

6.2 Formulation of Reconfiguration Algorithm

To resolve the non-convexities present in the reformulated reconfiguration problem, a strategic decomposition technique is first applied. This technique serves to decompose $\mathcal{P}_{TR-ref}$ into a set of QCQP sub-problems where each sub-problem only contains variables associated with a specific bus. Then, every non-convex sub-problem is further decomposed into QCQP-1 problems (i.e. QCQP problems where each problem only has a single non-convex quadratic constraint) using the principle of *additive separability*. Next, the exact convex relaxations for these non-convex QCQP-1 problems are derived using a convex relaxation technique based on Schur's complement and S-procedure. These sub-problems are then solved to obtain the solution to $\mathcal{P}_{TR-ref}$ using theoretical constructs from the Alternating Direction Method of Multipliers (ADMM). While references [123] and [124] have applied the ADMM decomposition technique on DN optimization problems, this proposal differs from them in two major aspects: 1) This proposal is the first work to apply ADMM decomposition techniques to the mixed-integer topology reconfiguration problems; and 2) This

proposal introduced a novel technique for exact convex relaxation of QCQP problems with multiple non-convex constraints (QCQP-n).

To decompose $\mathcal{P}_{TR-ref}$ for each bus $i \in \mathcal{B}$ in the DN, couplings amongst state variables associated with different buses need to be removed. An example of the couplings can be found in Eqs. 6.3 and 6.6 where the line current variable l_{ij} is used in computations for both $\hat{\mathcal{V}}_j$ and P_i. Therefore, l_{ij} must be present in the computations at both i and j. To eliminate the couplings, the set of state variables associated with every bus is first expanded through the inclusion of *perspective variables*. With this expansion, the set of state variables maintained by every $i \in \mathcal{B}$ can be divided into two subsets: 1) The set of native variables x_i which contains all state variables at i itself and those at the lines connecting i to its parent buses in $\mathcal{P}_i$; and 2) The set of perspective variables y_i which includes local estimations of the non-local native variables in the constraints bus i is subjected to. The accuracy of such estimation is represented by the consensus residual, which is defined as the 2-norm of the differences between the native and perspective variables (i.e. $r = ||x - y||$) . The variable sets x_i and y_i associated with every $i \in \mathcal{B}$ are included in Eqs. 6.15 and 6.16 respectively:

$$x_i = \{\hat{V}_i^x, \hat{V}_{ij}^x, \beta_{ig}^x,\ l_{ij}^x,\ P_{ij}^x,\ Q_{ij}^x,\ \mid j \in \mathcal{P}_i, (i,g) \in \mathcal{E}_s^i\ \} \tag{6.15}$$

$$\begin{aligned} y_i = \{&\hat{V}_{i,i}^y, \hat{V}_{j,i}^y,\ \hat{V}_{ij,i}^y, \beta_{ig,i}^y, l_{ij,i}^y, P_{ij,i}^y, Q_{ij,i}^y, P_{mi,i}^y, Q_{mi,i}^y \\ &\mid j \in \mathcal{P}_i, m \in \mathcal{D}_i, (i,g) \in \mathcal{E}_s\} \end{aligned} \tag{6.16}$$

The variables in x_i and y_i have the superscripts x and y respectively. Moreover, the subscript for every variable in y_i is formed by two components where the first component represents the bus or line whose variable is being estimated and the second component denotes the bus performing the estimation. For instance, the perspective variable $\hat{\mathcal{V}}_{j,i}^y$ is the estimation of the voltage variable at the bus j by the bus i. The sets of local and perspective variables for the reconfigurable bus $i \in \mathcal{R}$ are illustrated in Fig. 6.1 for the DN topology presented in Fig. 5.1.

For every $i \in \mathcal{B}$, all sets of local variables satisfying the non-convex constraints in $\mathcal{P}_{TR-ref}$

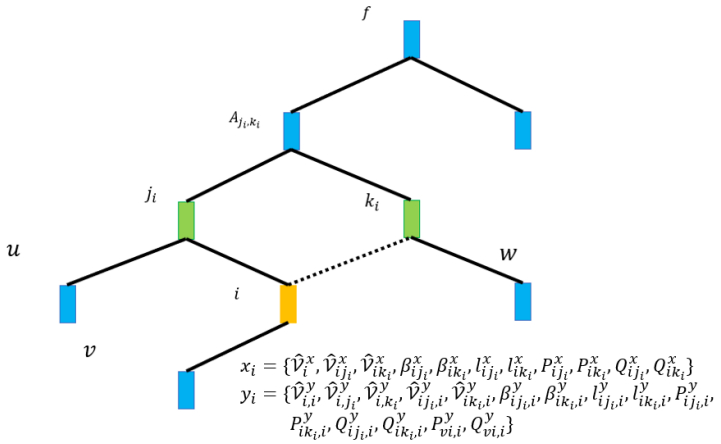

Figure 6.1: Illustration of Local and Perspective Variables ©2021 IEEE.

that is associated with i are first denoted as $\mathcal{X}_i$ where x_i take values from $\mathcal{X}_i$ (i.e. $x_i \in \mathcal{X}_i$). Then, all sets of perspective variables satisfying all convex constraints associated with i are denoted as $\mathcal{Y}_i$, where y_i take values from $\mathcal{Y}_i$ (i.e. $y_i \in \mathcal{Y}_i$). Next, $\mathcal{P}_{TR-ref}$ is reformulated into an equivalent optimization problem $\mathcal{P}_{TR-ref-e}$ defined on all $\mathcal{X}_i$ and $\mathcal{Y}_i$ through the establishment of consensus constraints between local variables and their corresponding estimations in perspective variables:

$$\mathcal{P}_{TR-ref-e}: \min_{x_i \in \mathcal{X}_i, y_i \in \mathcal{Y}_i \forall i \in \mathcal{B}} \sum_{i \in \mathcal{B}} F_i(x_i)$$

$$s.t.\ \hat{V}_{i,i}^y = \hat{V}_i^x,\ \hat{V}_{j,i}^y = \hat{V}_j^x,\ \hat{V}_{ij,i}^y = \hat{V}_{ij}^x,\ P_{ij,i}^y = P_{ij}^x,\ Q_{ij,i}^y = Q_{ij}^x,$$

$$P_{ij,j}^y = P_{ij}^x,\ Q_{ij,j}^y = Q_{ij}^x,\ l_{ij,i}^y = l_{ij}^x,\ \forall\ i \in \mathcal{B},\ \forall\ j \in \mathcal{P}_i$$

$$\beta_{rg,r}^y = \beta_{rg}^x,\ \forall\ (r,g) \in \mathcal{E}_s$$

The technique of ADMM is then utilized to decompose the topological reconfiguration problem $\mathcal{P}_{TR-ref-e}$ into sub-problems solvable by each bus. With the ADMM technique, every bus i in the DN solves its associated sub-problem in a iterative manner with information gathered from a limited number of buses in the DN and these buses are designated as the peer buses of i. First, the augmented Lagrangian $\mathcal{L}_\rho^{TR-ref-e}(x, y, v)$ for $\mathcal{P}_{TR-ref-e}$ is constructed as follows:

$$\mathcal{L}_{\rho}^{TR-ref-e}(x, y, v) = \sum_{i \in \mathcal{B}} F_i(x_i) + v_i^T(Ax - By) + \frac{\rho}{2}||Ax - By||_2^2 \tag{6.17}$$

where the consensus constraints in $\mathcal{P}_{TR-ref-e}$ are represented by the notion of $Ax - By = 0$. Moreover, $\rho > 0$ is a parameter used for penalizing consensus constraint violations and v is a vector formed by the dual variables associated with the consensus constraints. The ADMM-based iterative update process of the variables in $\mathcal{P}_{TR-ref-e}$ can then be expressed as:

$$x^{k+1} = \underset{x \in \mathcal{X}}{\operatorname{argmin}}\ \mathcal{L}_{\rho}^{TR-ref-e}(x, y^k, v^k) \tag{6.18}$$

$$y^{k+1} = \underset{y \in \mathcal{Y}}{\operatorname{argmin}}\ \mathcal{L}_{\rho}^{TR-ref-e}(x^{k+1}, y, v^k) \tag{6.19}$$

$$v^{k+1} = v^k + \rho(Ax^{k+1} - By^{k+1}) \tag{6.20}$$

where variables with the superscripts k and $k + 1$ on the right side of Eqs. 6.18-6.20 represent constants computed in the previous iteration and the current iteration respectively. The problems in 6.18-6.20 are solved in a iterative manner until the residual of consensus (i.e. $||Ax - By||_2^2$) falls below a pre-determined threshold value $\epsilon \approx 0$. As such, $Ax - By$ reduces to 0 and $\mathcal{L}_{\rho}^{TR-ref-e}(x, y, v)$ reduces to $\mathcal{P}_{TR-ref-e}$ when the iterative update process is concluded. To enable distributed computation of the reconfiguration problem, the problems in Eqs. 6.18-6.20 are then decomposed into sub-problems solvable by each bus $i \in \mathcal{B}$ through the reformulation of augmented Lagrangians. Terms in $\mathcal{L}_{\rho}^{TR-ref-e}(x, y^k, v^k)$ with variables included in x_i are grouped together to form the x-layer update problem for bus i. Similarly, terms in $\mathcal{L}_{\rho}^{TR-ref-e}(x^{k+1}, y, v^k)$ with variables included in y_i are grouped together to form the y-layer update problem for bus i. Moreover, the dual variables v_i associated with bus i are updated via a gradient update technique. The three update layers associated with bus i are presented in the following:

$$x_i^{k+1} = \underset{x_i \in \mathcal{X}_i}{\operatorname{argmin}} \mathcal{L}_\rho^{TR-ref-e}(x, y^k, v^k) \tag{6.21}$$

$$y_i^{k+1} = \underset{y_i \in \mathcal{Y}_i}{\operatorname{argmin}} \mathcal{L}_\rho^{TR-ref-e}(x^{k+1}, y, v^k) \tag{6.22}$$

$$v_i^{k+1} = v_i^k + \rho(Ax^{k+1} - By^{k+1}) \tag{6.23}$$

For the iterative update process associated with the distributed problems presented in Eqs. 6.21-6.23, at every iteration $k \geq 1$ each bus i first exchanges its associated dual variables v_i^k computed in the previous iteration (i.e. $k-1$) with its peer buses in the DN. This procedure is then repeated for x_i after the x-layer update process in Eq. 6.21 and y_i after the y-layer update process in Eq. 6.22. The update process continues until the consensus residual $\|Ax - By\|_2^2$ drops below the pre-determined threshold ϵ. The y-layer update is convex since the convex augmented Lagrangian $\mathcal{L}_\rho^{TR-ref-e}(x, y^k, v^k)$ is minimized over the convex set of $\mathcal{Y}_i$. However, the x-layer update is non-convex as $\mathcal{X}_i$ is a non-convex set.

To resolve the non-convexities present in the x-layer update process, a convex relaxation technique for the non-convex QCQP-n problem $\mathcal{P}_x^i$ associated with every $i \in \mathcal{B}$ is derived where $n > 1$ represents the number of non-convex constraints. The variables in x_i are further partitioned into the local voltage variable $\hat{\mathcal{V}}_i^x$, the switching variable at neighbouring switchable lines β_{ig}^x and the variables associated with neighbouring lines $x_{ij} = \{\hat{\mathcal{V}}_{ij}^x, l_{ij}^x, P_{ij}^x, Q_{ij}^x\}$. Applying this to $\mathcal{P}_x^i$ leads to:

$$\mathcal{P}_x^i : \min_{x_i}[\hat{V}_i^{x\mathbf{T}}(Q_{vi})\hat{V}_i^x + u_{vi}^{\mathbf{T}}\hat{V}_i^x] + \sum_{(i,g)\in\mathcal{E}_s^i}[\beta_{ig}^x(Q_{ig})\beta_{ig}^x + u_{ig}\beta_{ig}^x] + \sum_{j\in\mathcal{P}_i}[x_{ij}^{\mathbf{T}}(Q_{ij})x_{ij} + u_{ij}^{\mathbf{T}}x_{ij}]$$

$$s.t.\ \ (\beta_{ig}^x)^2 - \beta_{ig}^x \geq 0 \qquad \forall (i,g) \in \mathcal{E}_s^i$$

$$x_{ij}^{\mathbf{T}}G_{ij}x_{ij} + w_{ij}^{\mathbf{T}}x_{ij} \geq 0 \qquad \forall\, j \in \mathcal{P}_i$$

where

$$Q_{vi} = \frac{\rho I_{|\Phi_i|}}{2}(|\mathcal{D}_i| + 1) \qquad u_{vi} = v^V_{i,i} - \rho V^y_{i,i} + \sum_{m \in \mathcal{D}_i} (v^V_{i,m} - \rho V^y_{i,m})$$

$$Q_{ig} = \frac{\rho |\mathcal{R}|}{2} \qquad u_{ig} = v^\beta_{ig,i} - \rho \beta^y_{ig,i} + \sum_{u \in (\mathcal{R} \setminus i)} (v^\beta_{ig,u} - \rho \beta^y_{ig,u})$$

$$Q_{ij} = \frac{1}{2}\begin{bmatrix} \rho \mathbf{I}_{|\Phi_{ij}|} & 0 & 0 & 0 \\ 0 & \rho \mathbf{I}_{|\Phi_{ij}|} & 0 & 0 \\ 0 & 0 & 2\rho \mathbf{I}_{|\Phi_{ij}|} & 0 \\ 0 & 0 & 0 & 2\rho \mathbf{I}_{|\Phi_{ij}|} \end{bmatrix} \qquad u_{ij} = \begin{bmatrix} v^V_{ij,i} - \rho \hat{V}^y_{ij,i} \\ (\mathbf{I}_{1,|\Phi_{ij}|} R_{ij})^T + v^l_{ij,i} - \rho l^y_{ij,i} \\ (v^P_{ij,j} + v^P_{ij,i}) - \rho (P^y_{ij,j} + P^y_{ij,i}) \\ (v^Q_{ij,j} + v^Q_{ij,i}) - \rho (Q^y_{ij,j} + Q^y_{ij,i}) \end{bmatrix}$$

$v^V_{i,i}$ and $v^V_{i,m}$ denote the dual variables associated with the voltage consensus constraints. Moreover, $\mathbf{I}_{|\Phi|}$ is the $|\Phi|$ by $|\Phi|$ dimension identity matrix. Leveraging the relations established in Eqs. 6.5, 6.12 and 6.13, the quadratic constraints associated with different lines (i.e. Eq. 6.4) are decoupled in this formulation of $\mathcal{P}^i_x$. As such, the QCQP-n $\mathcal{P}^i_x$ is an *additively separable* problem since it can be decomposed into the following sub-problems with no shared variables or constraints [125]:

$$\mathcal{P}^{vi}_x : \min_{V^x_i} \quad \hat{V}^{x\mathbf{T}}_i (Q_{vi}) \hat{V}^x_i + u^{\mathbf{T}}_{vi} \hat{V}^x_i$$

$$\mathcal{P}^{ig}_x : \min_{\beta^x_{ig}} \quad \beta^x_{ig} (Q_{ig}) \beta^x_{ig} + u_{ig} \beta^x_{ig}$$

$$s.t. \; -(\beta^x_{ig})^2 + \beta^x_{ig} \leq 0$$

$$\mathcal{P}^{ij}_x : \min_{x_{ij}} \quad x^{\mathbf{T}}_{ij} (Q_{ij}) x_{ij} + u^{\mathbf{T}}_{ij} x_{ij}$$

$$s.t. \; -x^{\mathbf{T}}_{ij} G_{ij} x_{ij} - w^{\mathbf{T}}_{ij} x_{ij} \leq 0$$

As the sub-problems $\mathcal{P}^{vi}_x$, $\mathcal{P}^{ig}_x$ and $\mathcal{P}^{ij}_x$ have no shared variables, the optimal solution for $\mathcal{P}^i_x$ can be expressed as the combination of the optimal solutions of the sub-problems. While $\mathcal{P}^{vi}_x$ is a convex problem whose optimal solution can be readily obtained with any convex solver, both $\mathcal{P}^{ig}_x$

and $\mathcal{P}_x^{ij}$ are non-convex QCQP-1 problems. Next, the exact convex relaxations are presented for these non-convex sub-problems. The expressions for the respective optimal solutions β_{ig}^{x*} and x_{ij}^* for these two QCQP-1 problems are first derived. These solutions are obtained in terms of their respective optimized Lagrangian multipliers λ_{ig}^* and λ_{ij}^* by setting the gradients of their associated Lagrangians to 0 (i.e. the first-order optimality condition):

$$\beta_{ig}{}^{x*} = -\frac{1}{2}(Q_{ig} - \lambda_{ig}^*)^{-1}(u_{ig} + \lambda_{ig}^*) \tag{6.24}$$

$$x_{ij}^* = -\frac{1}{2}(Q_{ij} - \lambda_{ij}^* G_{ij})^{-1}(u_{ij} - \lambda_{ij}^* w_{ij}) \tag{6.25}$$

Then, the concave dual problem $\mathcal{D}_x^{ig}$ of $\mathcal{P}_x^{ig}$ and the dual problem $\mathcal{D}_x^{ij}$ of $\mathcal{P}_x^{ij}$ are converted into their respective equivalent Semi-Definite Programming (SDP) problems $\mathcal{S}_x^{ig}$ and $\mathcal{S}_x^{ij}$ with the Shur's complement method presented in reference [126].

$$\begin{aligned}
\mathcal{S}_x^{ig} : & \max_{\lambda_{ig},\gamma_{ig}} \gamma_{ig} \\
& s.t. \lambda_{ig} \geq 0 \\
& \begin{bmatrix} Q_{ig} - \lambda_{ig} & \frac{1}{2}(u_{ig} + \lambda_{ig}) \\ \frac{1}{2}(u_{ig} + \lambda_{ig}) & -\gamma_{ig} \end{bmatrix} \geq 0 \\
\mathcal{S}_x^{ij} : & \max_{\lambda_{ij},\gamma_{ij}} \gamma_{ij} \\
& s.t. \lambda_{ij} \geq 0 \\
& \begin{bmatrix} Q_{ij} - \lambda_{ij} G_{ij} & \frac{1}{2}(u_{ij} - \lambda_{ij} w_{ij}) \\ \frac{1}{2}(u_{ij} - \lambda_{ij} w_{ij}) & -\gamma_{ij} \end{bmatrix} \geq 0
\end{aligned}$$

As both $\mathcal{S}_x^{ig}$ and $\mathcal{S}_x^{ij}$ are concave problems, their respective optimal solutions λ_{ig}^* and λ_{ij}^* can be readily obtained. Next, these solutions are substituted into Eqs. 6.24 and 6.25 to compute $\beta_{ig}{}^{x*}$ and x_{ij}^*. To establish the optimality of these values, the theoretical constructs of S-procedure

established in reference [127] are leveraged. For the strictly feasible QCQP-1 problem $\mathcal{P}$ defined as follows,

$$\mathcal{P}: \min_{x} \quad x^T A_0 x + b_0^T x + c_0$$
$$s.t. \quad x^T A_1 x + b_1^T x + c_1 <= 0$$

if there exists a $\lambda \geq 0$ and a lower bound γ for the cost function such that the parameters of $\mathcal{P}$ satisfy the following:

$$\begin{bmatrix} A_0 & \frac{1}{2}b_0 \\ \frac{1}{2}b_0^T & c_0 - \gamma \end{bmatrix} + \lambda \begin{bmatrix} A_1 & \frac{1}{2}b_1 \\ \frac{1}{2}b_1^T & c_1 \end{bmatrix} \geq 0$$

then the optimal values associated with $\mathcal{P}$ and its dual problem are identical (i.e. zero duality gap) regardless of the convexity of the constraint or the cost function of $\mathcal{P}$. Since both x-layer and y-layer updates can now be computed with convex optimization methods, the proposed reconfiguration method can be expressed as a iterative refinement process which is presented in Alg. 4.

6.3 Theoretical Performance Guarantees

To derive the convergence guarantees of Alg. 4, it is first noted that distributed ADMM based iterative optimization process always converges to the globally optimal solution when the sub-problems are all convex [128]. In Alg. 4, the formulation of the non-convex problem $\mathcal{P}_{TR-ref}$ is decomposed into QCQP sub-problems where every sub-problem is either convex or contains a single non-convex constraint. As such, to prove the convergence and optimality of Alg. 4 the following two conditions must be established: 1) Any QCQP-1 problem with a single non-convex constraint has zero duality gap and therefore can be resolved exactly with convex relaxation method based on Schur's complement; and 2) The convex relaxation technique adopted for solving non-convex

Alg. 4: Convex Reconfiguration for Voltage Improvement

Initialization:

- For every $i \in \mathcal{B}$, set $x_i \leftarrow x_i^0$, $y_i \leftarrow y_i^0$, $v_i \leftarrow 0$ and the residual $\epsilon_i^{k+1} \leftarrow \infty$. $\mathcal{G}_i$ is the set of all neighbours of i.

Algorithm:

1. At iteration k, every $i \in \mathcal{B}$ first performs its x update:

   For $i \in \mathcal{B}$, $x_i^{k+1} \leftarrow \{\hat{V}_i^{x,k+1}, \beta_{ig}^{k+1}, x_{ij}^{k+1}, \}$ where:

   $\hat{V}_i^{k+1}$: Solved from $\mathcal{P}_x^{vi}$ directly.

   $x_{ij}^{x,k+1}$: Solved from substituting λ_{ij} in Eq. 6.24, where λ_{ij} is obtained by solving $\mathcal{S}_x^{ij}$;

   β_{ig}^{k+1}: Solved from substituting λ_{ig} in Eq. 6.25, where λ_{ig} is obtained by solving $\mathcal{S}_x^{ig}$;

2. Every $i \in \mathcal{B}$ exchanges its updated x variables with $j \in \mathcal{G}_i$.

3. Every $i \in \mathcal{B}$ performs its y update based on Eq. 6.22.

4. Every $i \in \mathcal{B}$ exchanges its updated y variables with $j \in \mathcal{G}_i$.

5. Consensus dual variable v is updated for $i \in \mathcal{B}$ using Eq. 6.23.

6. These are broadcast to $j \in \mathcal{G}_i$ and the residual for iteration k is updated: $\epsilon_i^{k+1} \leftarrow \|Ax_i^{k+1} - By_i^{k+1}\|$

7. If $\epsilon_i^{k+1} \leq \epsilon$, then the iterative update process is terminated. Otherwise, $k \leftarrow k + 1$ and return to the first step.

QCQP-1 problems preserves the convergence properties of the standard iterative computations entailed in ADMM. In this section, the specific conditions under which the convergence and the optimality guarantees hold true are established.

To prove the duality gap of any strictly feasible non-convex QCQP-1 problem $\mathcal{P}$ is zero, it is first noted that the concave dual problem of $\mathcal{P}$ can be transformed into an equivalent SDP problem $\mathcal{S}$ by leveraging a technique based on Schur's complement. According to the technique presented in reference [129], the general formulation for the SDP equivalent $\mathcal{S}$ of the concave dual of the QCQP-1 problem $\mathcal{P}$ can be expressed as:

$$
\begin{aligned}
&\mathcal{S}: \max_{\lambda,\gamma} \gamma \\
&\quad s.t.\ \ \lambda \geq 0 \\
&\quad \begin{bmatrix} A_0 & \frac{1}{2}b_0 \\ \frac{1}{2}b_0^T & c_0 - \gamma \end{bmatrix} + \lambda \begin{bmatrix} A_1 & \frac{1}{2}b_1 \\ \frac{1}{2}b_1^T & c_1 \end{bmatrix} \geq 0
\end{aligned}
$$

If the maximum objective function γ^* of the SDP problem $\mathcal{S}$ is a lower bound for the cost function $x^T A_0 x + b_0^T x + c_0$ of the non-convex problem $\mathcal{P}$ and there exists a x^* in the feasibility region of $\mathcal{P}$ such that $x^{*T} A_0 x^* + b_0^T x^* + c_0 = \gamma^*$, then the optimal cost for $\mathcal{P}$ can be obtained by solving $\mathcal{S}$. Next, it is noted from theoretical constructs pertaining to the S-procedure presented in reference [127] that one and only one of the following statements can be true:

1. $\exists \lambda \geq 0, \begin{bmatrix} A_0 & \frac{1}{2}b_0 \\ \frac{1}{2}b_0^T & c_0 - \gamma \end{bmatrix} + \lambda \begin{bmatrix} A_1 & \frac{1}{2}b_1 \\ \frac{1}{2}b_1^T & c_1 \end{bmatrix} \geq 0.$

2. $\exists x,\ x^T A_1 x + b_1^T x + c_1 \leq 0,\ x^T A_0 x + b_0^T x + c_0 - \gamma < 0.$

Since the feasibility sets of $\mathcal{S}$ and $\mathcal{P}$ are defined by statement 1 and $x^T A_1 x + b_1^T x + c_1 \leq 0$ respectively, it can be concluded that all γ residing in the feasibility set of $\mathcal{S}$ can serve as lower bound to the cost function of $\mathcal{P}$. Then, the existence of x^* is proved through contradiction. Assume

there exists no such x^* satisfying $x^{*T}A_0x^* + b_0^Tx^* + c_0 = \gamma^*$. Leveraging equivalence relations presented in reference [127], $\mathcal{S}$ can be rewritten as the quadratic problem $\mathcal{S}_1$:

$$\begin{aligned}\mathcal{S}_1 : \max_{\lambda,\gamma}\ & \gamma \\ & \exists\ \lambda \geq 0 \\ & x^TA_0x + b_0^Tx + c_0 + \lambda(x^TA_1x + b_1^Tx + c_1) \geq \gamma,\ \forall x\end{aligned}$$

From the formulations of $\mathcal{S}$ and $\mathcal{P}$, $\lambda \geq 0$ and $x^TA_1x + b_1^Tx + c_1 \leq 0$ is valid for all x. As such, the optimal γ^* for $\mathcal{S}$ and $\mathcal{S}_1$ can be obtained from $\gamma^* = \min_x x^TA_0x + b_0^Tx + c_0$ and this proves the existence of x^*. Therefore, the optimal solution of $\mathcal{P}$ can be obtained by solving $\mathcal{S}$.

To derive the convergence characteristics of Alg. 4, the notations are simplified by overloading the variables and terms in the DN. For every vector m, the expression $m \geq 0$ represents that every element of m is a non-negative real number and $m < 0$ if every element in m is a negative real number. In Alg. 4, the primal variable x for the x-layer update process is obtained from the corresponding dual variable λ (i.e. (6.24) and (6.25)) and denote the transformation process from the dual to the primal variable is denoted as $x = z(\lambda)$. Next, the values of the objective function at iteration k (i.e. $F(f(\lambda^k))$) and the optimal value of the objective function (i.e. $inf\{F(f(\lambda))|Af(\lambda) - By = 0\}$) are denoted by p^k and p^* respectively. The consensus residual at iteration k is represented by r^k (i.e. $r^k = Af(\lambda^k) - By^k$). Hence, the reconfiguration problem $\mathcal{P}_{TR-ref-e}$ is reformulated as the following:

$$\begin{aligned}\mathcal{P}_{RS} :\ & \min_{\lambda \geq \mathbf{0}, y \in \mathcal{Y}} F(z(\lambda)) \\ & s.t.\ Az(\lambda) - By = 0\end{aligned}$$

The augmented Lagrangian $\mathcal{L}_\rho^{RS}(z(\lambda), y, v)$ associated with $\mathcal{P}_{RS}$ and the ADMM-based iterative

update process for solving $\mathcal{P}_{RS}$ can be expressed as:

$$\mathcal{L}_{\rho}^{RS}(z(\lambda), y, v) = F(z(\lambda)) + v^T(Az(\lambda) - By) + \frac{\rho}{2}||Az(\lambda) - By||_2^2$$

and

$$\begin{aligned}
\lambda^{k+1} &= \underset{\lambda \geq \mathbf{0}}{\operatorname{argmin}}\ \mathcal{L}_{\rho}^{RS}(z(\lambda), y^k, v^k) \\
y^{k+1} &= \underset{y \in \mathcal{Y}}{\operatorname{argmin}}\ \mathcal{L}_{\rho}^{RS}(z(\lambda^{k+1}), y, v^k) \\
v^{k+1} &= v^k + \rho(Az(\lambda^{k+1}) - By^{k+1})
\end{aligned}$$

respectively. From reference [126], the iterative update process utilized in Alg. 4 is guaranteed to converge when the following conditions are satisfied:

1. **Residual Convergence**: The consensus residual r^k tends to 0 when k tends to ∞.

2. **Objective Convergence**: The objective function $F(z(\lambda))$ tends to p^* as k tends to ∞.

3. **Dual Variable Convergence**: v^k tends to v^* as k tends to ∞ where v^* is a dual optimal point.

For brevity, the Lagrangian $\mathcal{L}_{\rho}^{RS}(z(\lambda), y^k, v^k)$ is denoted as $\mathcal{L}_{\rho}^{k}(z(\lambda))$ for the rest of this study. Unless otherwise specified, the convexity and differentiability of the various functions discussed in this study are referred to with respect to λ. To prove the convergence of Alg. 4, the first thing is to demonstrate that the three convergence conditions are satisfied when the following assumptions hold:

A1 : $\mathcal{L}_{\rho}^{k}(z(\lambda))$ is convex and non-decreasing with regard to $z(\lambda)$.

A2 : $F(z(\lambda))$ is differentiable with regard to $z(\lambda)$.

A3 : $z(\lambda)$ is convex, differentiable and $\frac{\partial f}{\partial \lambda} \neq 0$.

Then, practical conditions in the topological reconfiguration problem where the assumptions in A1-A3 are valid are presented.

From reference [129], the composition function $\mathcal{L}_\rho^k(z(\lambda))$ is convex providing it satisfies two conditions:

B1 : $z(\lambda)$ is a convex function.

B2 : $\mathcal{L}_\rho^k(z(\lambda))$ is convex with respect to $z(\lambda)$.

When the conditions A1-A3 are satisfied, conditions B1-B2 are satisfied and the function $\mathcal{L}_\rho^k(z(\lambda))$ is differentiable. Since $\mathcal{L}_\rho^k(z(\lambda))$ is: 1) Closed; 2) Proper; 3) Convex; and 4) Differentiable, the optimal value of λ^{k+1} can be obtained from the following:

$$0 = \frac{\partial}{\partial \lambda}\mathcal{L}_\rho^k(z(\lambda)) = [\frac{\partial F(z(\lambda))}{\partial z(\lambda)} + A^T v^k + \rho A^T(Az(\lambda) - By^k)]\frac{\partial z(\lambda)}{\partial \lambda}$$

As $\frac{\partial f}{\partial \lambda} \neq 0$ and $v^{k+1} = v^k + \rho r^{k+1}$, the above expression can be reformulated as:

$$0 = \frac{\partial F(z(\lambda))}{\partial z(\lambda)} + A^T(v^{k+1} + \rho B(y^{k+1} - y^k))$$

Since λ^{k+1} must satisfy the relation presented above, λ^{k+1} minimizes the term $F(z(\lambda)) + (v^{k+1} + \rho B(y^{k+1} - y^k)A^T z(\lambda)$. Similarly, y^{k+1} minimizes the term $-(v^{k+1})^T By$. Let (λ^*, y^*, v^*) be a saddle point for $\mathcal{L}_0^{RS}$ (i.e. $\mathcal{L}_0^{RS}(\lambda^*, y^*, v^*) \leq \mathcal{L}_0^{RS}(\lambda^{k+1}, y^{k+1}, v^*)$) where $\mathcal{L}_0^{RS}$ denotes the standard Lagrangian for $\mathcal{P}$. Then the following inequalities must be valid:

$$F(z(\lambda^{k+1})) + (v^{k+1} + \rho B(y^{k+1} - y^k))A^T z(\lambda^{k+1}) \leq$$

$$F(z(\lambda^*)) + (v^{k+1} + \rho B(y^{k+1} - y^k))A^T z(\lambda^*) \tag{6.26}$$

$$g(y^{k+1}) - (v^{k+1})^T By^{k+1} \leq g(y^*) - (v^{k+1})^T By^* \tag{6.27}$$

Summarizing Eqs. 6.26 and 6.27 as well as rearranging the terms leads to:

$$p^{k+1} - p^* \leq -(v^{k+1})^T r^{k+1} + \rho(B(y^{k+1} - y^k))^T(-r^{k+1} - B(y^{k+1} - y^*)) \tag{6.28}$$

As $Az(\lambda^*) - By^* = 0$ and $p^{k+1} = F(z(\lambda^{k+1})) + g(y^{k+1})$ respectively, the following equation holds:

$$p^* \leq p^{k+1} + v^* r^{k+1} \tag{6.29}$$

Summarizing Eqs. 6.28 and 6.29 leads to:

$$\begin{aligned} &2(v^{k+1} - v^*)^T r^{k+1} + 2\rho(B(y^{k+1} - y^k))^T r^{k+1} + \\ &2\rho(B(y^{k+1} - y^k))^T(B(y^{k+1} - y^*)) \leq 0 \end{aligned} \tag{6.30}$$

Define $H^k = \frac{1}{\rho}\|v^k - v^*\|_2^2 + \rho\|B(y^k - y^*)\|_2^2$. Then, substituting $v^{k+1} = v^k + \rho r^{k+1}$, $v^{k+1} - v^k = (v^{k+1} - v^*) - (v^k - v^*)$ and $y^{k+1} - y^k = (y^{k+1} - y^k) - (y^k - y^*)$ into the expression of $H^k - H^{k+1}$ leads to:

$$H^k - H^{k+1} \geq \rho\|r^{k+1} + B(y^{k+1} - y^k)\|_2^2 \tag{6.31}$$

As y^{k+1} minimizes $-(v^{k+1})^T By$ and $v^{k+1} - v^k$ is equal to ρr^{k+1}, the following inequality is established:

$$2\rho(r^{k+1})^T(B(y^{k+1} - y^k)) \geq 0 \tag{6.32}$$

Substituting Eq. 6.32 into Eq. 6.31 then yields the following result:

$$H^{k+1} \leq H^k - \rho\|r^{k+1}\|_2^2 - \rho\|B(y^{k+1} - y^k)\| \tag{6.33}$$

As $0 \leq H^k < \infty$ for all k, iterating Eq. 6.33 produces the following inequality:

$$\rho \sum_{k=0}^{\infty}(\rho\|r^{k+1}\|_2^2 + \rho\|B(y^{k+1} - y^k)\|) \leq H^0 \tag{6.34}$$

This inequality proves both **residual convergence** and **dual variable convergence** as it is valid if and only if r^k and $B(y^{k+1} - y^k)$ tend to 0 when $k \rightarrow$ tends to ∞. Moreover, substituting these results into Eqs. 6.28 and 6.29 leads to $p^{k+1} - p^* = 0$ as k tends to ∞ which indicates **objective convergence**.

For the condition A1 to hold, the term $\mathcal{L}_\rho^k(f(\lambda))$ must be convex and non-decreasing with respect to $f(\lambda)$. The convexity condition is satisfied if $F(f(\lambda))$ is convex with respect to $f(\lambda)$. Moreover, the non-decreasing condition is satisfied if the following is true:

$$\frac{\partial F(f(\lambda))}{\partial f(\lambda)} + A^T v^k + \rho A^T (A f(\lambda) - B y^k) \geq 0, \ \forall f(\lambda) \tag{6.35}$$

This inequality is valid when $\frac{\partial F(f(\lambda))}{\partial f(\lambda)} + A^T v^k > 0$ and the value of ρ is sufficiently small. Since the objective function $F(f(\lambda))$ of the reconfiguration problem $\mathcal{P}_{TR}$ is linear with respect to $f(\lambda)$, it is differentiable with respect to $f(\lambda)$ and therefore the condition A2 is satisfied. Then, the conditions under which A3 is valid are derived. Denote Eqs. 6.24 and 6.25 as $f_{ig}^a(\lambda_{ig})$ and $f_{ij}^b(\lambda_{ij})$ respectively. $f(\lambda)$ is $f_{ig}^a(\lambda_{ig})$ for every $(i, g) \in \mathcal{E}_s$ and $f_{ij}^b(\lambda_{ij})$ for every $(i, j) \in \mathcal{E}$. From the formulation of $f_{ig}^a(\lambda_{ig})$, it can be concluded that it is convex and differentiable providing Q_{ig}, u_{ig} and λ_{ig} for every $(i, g) \in \mathcal{E}_s$ satisfy either one of the following two conditions:

C1 : $Q_{ig} + u_{ig} > 0$ and $\lambda_{ig} - Q_{ig} > 0$.

C2 : $Q_{ig} + u_{ig} < 0$ and $\lambda_{ig} - Q_{ig} < 0$.

Moreover, it can be concluded that $f_{ig}^a(\lambda_{ig}) \geq 0$ is a necessary but not sufficient condition for the convexity of $f_{ig}^a(\lambda_{ig})$. Furthermore, the derivative of $f_{ig}^a(\lambda_{ig})$ is nonzero providing $Q_{ig} + u_{ig} \neq 0$ is satisfied. Next, since the single constraint in $\mathcal{P}_x^{ij}$ represents the line power constraint in Eq. 2.19, w_{ij} is a zero vector and G_{ij} is composed of the following components:

$$G_{ij} = \begin{bmatrix} 0 & I_{|\Phi_{ij}|} & 0 & 0 \\ 0 & 0 & 0 & 0 \\ 0 & 0 & I_{|\Phi_{ij}|} & 0 \\ 0 & 0 & 0 & I_{|\Phi_{ij}|} \end{bmatrix}$$

As such, $f_{ij}^{b}(\lambda_{ij})$ expands to be:

$$\begin{bmatrix} -\frac{1}{\rho} I_{|\Phi_{ij}|} & -\frac{2\lambda_{ij}}{\rho^2} I_{|\Phi_{ij}|} & -\frac{2\lambda_{ij}^2}{\rho^2(\rho-\lambda_{ij})} I_{|\Phi_{ij}|} & 0 \\ 0 & -\frac{1}{\rho} I_{|\Phi_{ij}|} & -\frac{\lambda_{ij}}{\rho(\rho-\lambda_{ij})} I_{|\Phi_{ij}|} & 0 \\ 0 & 0 & -\frac{1}{2(\rho-\lambda_{ij})} I_{|\Phi_{ij}|} & 0 \\ 0 & 0 & 0 & -\frac{1}{2(\rho-\lambda_{ij})} I_{|\Phi_{ij}|} \end{bmatrix} u_{ij}$$

According to reference [130], a vector-valued function is convex providing the second derivatives of all elements of the function output vector are positive. As such, $f_{ij}^{b}(\lambda_{ij})$ is both convex and differentiable if either one of the following two conditions are satisfied for all $(i, j) \in \mathcal{E}$:

D1 : $\lambda_{ij} - \rho > 0$ and $u_{ij} > 0$.

D2 : $\lambda_{ij} - \rho < 0$ and $u_{ij} < 0$.

6.4 Simulations on Practical DNs

To verify the convergence and optimality characteristics of Alg. 4, practical simulations are conducted on realistic DN settings and present comparative studies with the state-of-the-art in topology reconfiguration. Since the majority of bus loads residing in the 76 bus DN are either single-phase or two-phase loads, this DN is a highly unbalanced system. The simulations presented here are conducted on a 100 MW, 4.16 KV 76-bus DN which is based on the IEEE 123-bus feeder [131]. The radial topology of the 76-bus DN is illustrated in Fig. 6.2 where the fixed and the switchable lines are expressed as solid black lines and dotted red lines respectively. From Fig. 6.2, the 76-bus DN contains 5 switchable lines which are denoted as $|\mathcal{E}|_s = \{l_{73}, l_{74}, l_{75}, l_{76}, l_{77}\}$. As such, the

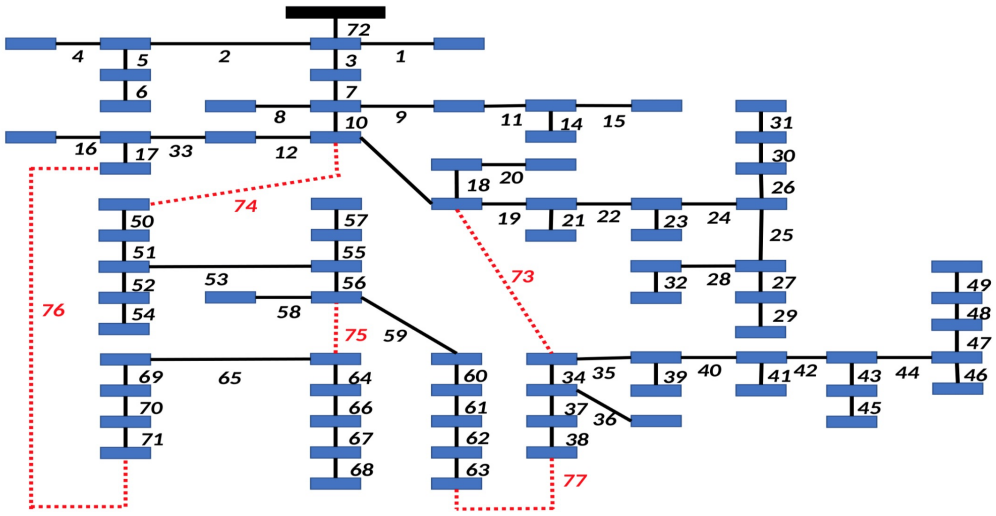

Figure 6.2: Topology of the 76-Bus DN ©2021 IEEE.

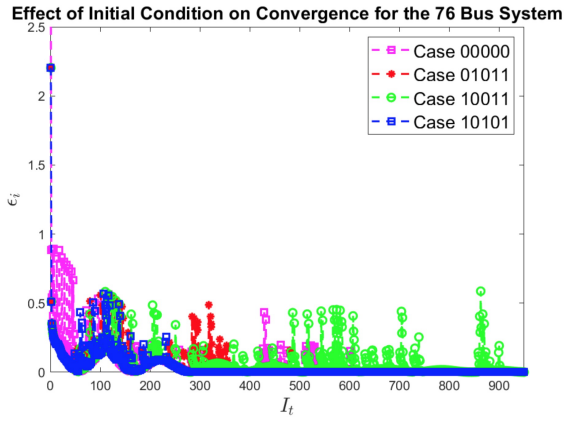

Figure 6.3: Impact of Initial Topology ©2021 IEEE.

activation/deactivation of the switchable lines in the 76-bus DN can lead to $2^5 = 32$ different DN topologies. For clarity and brevity of representation, the topology of the 76-bus DN is denoted in terms of the statuses of its switchable lines. For instance, the DN topology where only l_{73}, l_{75} and l_{76} are active is referred to as 10110. Moreover, the upper and lower bounds for bus voltage magnitudes in this DN are set to 0.95 p.u. and 1.05 p.u. respectively. The parameters ρ and ϵ are set to 10^3 and 1×10^{-3} respectively for the 76-bus DN.

In Figs. 6.4a-6.4e and 6.3, the convergence characteristics of Alg. 4 are investigated for the 76-bus DN. In these figures, I_t is the iteration number defined for Alg. 4 which refers to the number of times the system state variables are computed at every bus in the DN. Figs. 6.4a-6.4e present the evolution of the y-layer switching variables (i.e. β^y) associated with the switchable lines in the DN when the Initial Topology (IT) 01011 is adopted. From these figures, it can be observed that the switching variables alternate between 0 and 1 during the convergence of Alg. 4 and the radial constraints presented in Eqs. 6.8 and 6.9 are always satisfied. Moreover, the topology produced by Alg. 4 is 11010 which is the optimal topology for the reconfiguration problem ascertained via the brute force approach. As such, it can be concluded that Alg. 4 examines a number of radial topologies before converging to the optimal topology. Fig. 6.3 demonstrates the effects of different ITs on the convergence of the proposed algorithm by tracking the evolution of consensus residual (i.e. $\|Ax - By\|_2^2$). It can be observed from this figure that Alg. 4 converges for all ITs examined. Moreover, Alg. 4 leads to the optimal topology 11010 for all ITs examined. From the theoretical constructs established in the previous section, Alg. 4 is capable of convergence to the globally optimal topology regardless of IT. Hence, the theoretical performance guarantees of Alg. 4 are verified by the simulations. Furthermore, Fig. 6.3 demonstrates that Alg. 4 converges to an equilibrium within 1000 iterations for randomly selected ITs. To infer the overall computing time for Alg. 4, it is first noted that Alg. 4 requests every bus in the DN to sequentially perform the x-layer, y-layer and z-layer updates as well as information exchanges with its peers. From Eqs. 6.18 -6.20, the x-layer and y-layer updates solve two QCQP-1 problems while the v-layer update computes a simple mathematical relation. According to reference [132], the update process associated with each layer can be completed within a fraction of a millisecond with the computational capabilities available in standard distributed intelligent devices. From reference [133], the information exchange process can be completed within 100 milliseconds as typical delays in wireless communication processes ranges from 8 ms to 30 ms. As such, each iteration will be completed within 0.3 seconds and the computing time for Alg. 4 is within $1000 * 0.3s/60\text{s} = 5\text{min}$ for the 76-bus DN.

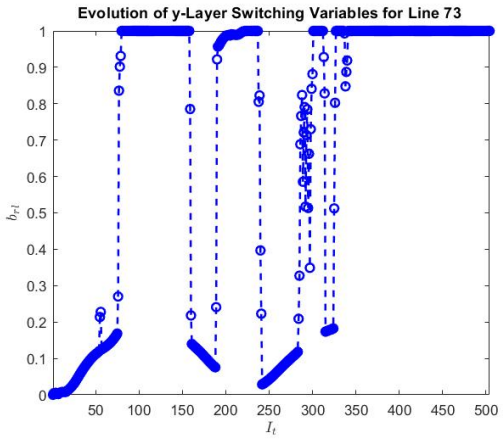

(a) Variable Evolution for Line 73.

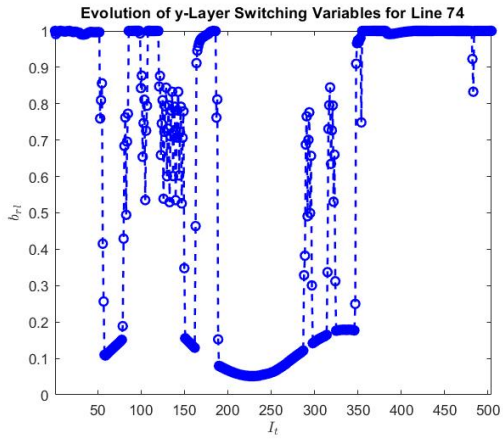

(b) Variable Evolution for Line 74.

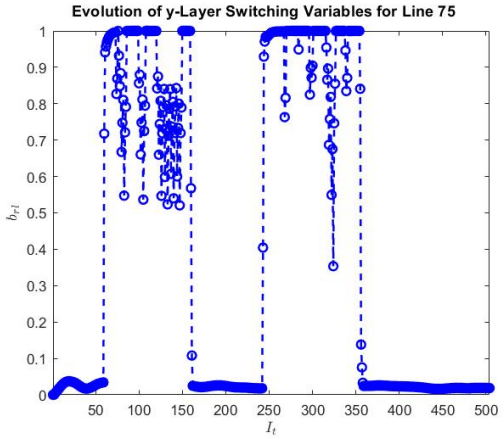

(c) Variable Evolution for Line 75.

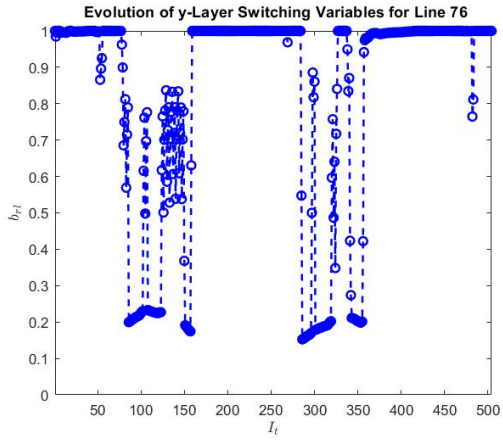

(d) Variable Evolution for Line 76.

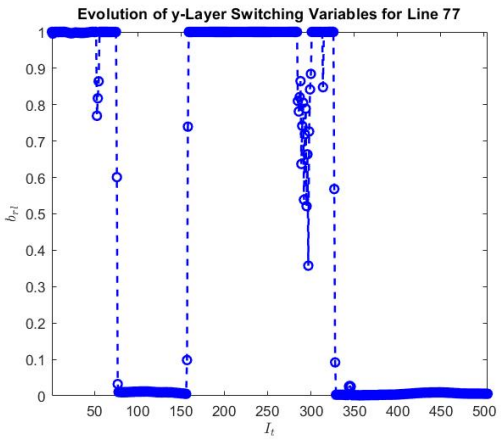

(e) Variable Evolution for Line 77.

Figure 6.4: Convergence Study for Alg. 4 under IT 01011.

6.5 Comparative Analysis

	Alg. 4	**[67, 75]**	**[70]**	**[71]**	**[76, 77]**	**[54, 78]**	**[5], [55]**
Optimization Method	QCQP	MISOCP, MILP	SOCP	MISDP	MISOCP, MINLP	QCQP, SOCP	Meta-Heuristic
Constraint Relaxations	Nearly balanced voltage, zero power product	No DER in DN, Balanced DN	One redundant switch, Balanced DN	Rank-1 constraint	Bus voltage 1 p.u, Balanced DN	No Power Loss, Balanced DN	None
Optimality Conditions	Strong Duality Gap	Strong Duality Gap	Strong Duality Gap	Strong Duality Gap	Strong Duality Gap	Strong Duality Gap	N/A
Computational Complexity	$O(\|\mathcal{B}\|)$)	$O(\|\mathcal{B}\|^3)$	$O(\|\mathcal{B}\|^3)$	$O(\|\mathcal{B}\|^3)$	$O(\|\mathcal{B}\|^3)$	$O(\|\mathcal{B}\|^3)$	$O(\|\mathcal{B}\|^3)$

Table 6.1: Comparison with Existing Work ©2021 IEEE.

Next, a three-fold comparative study between Alg. 4 and the existing proposals is presented. First, the differences and similarities between Alg. 4 and some state-of-the-art reconfiguration methods discussed in Section. 1.2.3 are presented in Table 6.1. Then, the performance of Alg. 4 is compared with the FNSGA algorithm introduced in reference [55] through simulations conducted on practical distribution systems. Finally, Alg. 4 is compared with the decentralized reconfiguration technique of Alg. 3 and give a brief summary on their respective advantages and disadvantages.

Table 6.1 compares four aspects of reconfiguration algorithms: 1) The optimization technique adopted (e.g. QCQP, Second Order Cone Programming (SOCP), etc.); 2) Assumptions on the physical networks (e.g. balanced DN, etc.); 3) Convergence and optimality guarantees (e.g. strong duality gap); and 4) Computational complexity. The methods presented in this table can be classified into two categories depending on the optimization techniques they employ. The proposals belonging to the first category (e.g. Alg. 4, [54, 67, 75] and [78]) relax the constraints associated with practical networks to transform the reconfiguration problem into tractable formulations (e.g.

MINLP, MISOCP) that can be exactly solved through convex relaxation. However, these relaxations can also lead to suboptimal or even infeasible solutions for practical DNs especially when the solutions obtained are close to stable operating limits. For instance, the methods proposed in references [67] and [75] may lead to violations of radial constraints for DNs with DERs. Also, the solution produced by the reconfiguration technique introduced in [71] is feasible only if it satisfies three non-convex rank-1 constraints that needs to be checked separately from the convex formulation. Moreover, most proposals in DN reconfiguration (e.g. references [76] and [78]) are based on the assumption that the network is a perfectly balanced system where bus voltage magnitudes at with different phases are identical. The NPF model utilized in this chapter is based on the assumptions that the voltage values are nearly balanced and the power product between phases are negligible. As such, the NPF model presents a more accurate description of the load flow relation in practical DNs than the NPF model adopted in the previous chapter. From the actual sensor measurements presented in reference [68], the error produced by these assumptions is negligible for practical DNs. Comparing with the convex state-of-the-art, this proposal is more tractable as it always leads to feasible radial topology configurations and performs well for both balanced and unbalanced networks. Reconfiguration methods in the second category (e.g. [5] and [55]) adopt meta-heuristic techniques that preserves the DN constraints and produces near-optimal solutions. However, their convergence to optimality is not guaranteed.

In Table. 6.1, the computational complexity of an algorithm refers to the asymptotic convergence performance of the optimization technique adopted by that algorithm. Alg. 4 employs the technique of ADMM to establish consensus amongst the solutions of the $|\mathcal{B}|$ sub-problems computed by each bus in parallel. According to reference [134], ADMM based computation techniques for DNs that include up to 2065 buses achieve linear convergence in terms of the total number of sub-problems (i.e. number of buses). In Alg. 4, the complexity associated with solving each quadratic sub-problem depends on the total number of optimization variables present in the sub-problem. Since the number of variables is much smaller than the total number of buses in the DN, the computational complexity associated with solving each sub-problem is constant (i.e. $O(1)$).

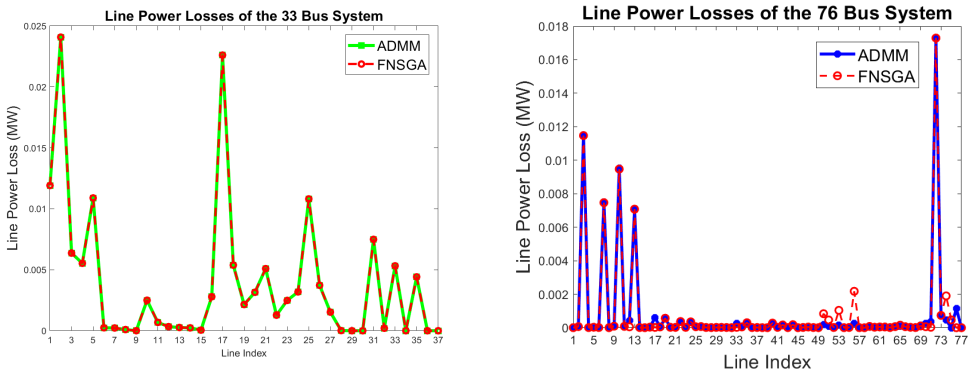

(a) 33 bus system. (b) 76 bus system.

Figure 6.5: Comparative study with FNSGA ©2021 IEEE.

Therefore, Alg. 4 entails an overall computational complexity of $O(|\mathcal{B}|)$. This result is further validated by simulation studies conducted on the 33-bus and 76 bus test systems. Alg. 4 converges within 575 and 1000 iterations for the 33-bus and 76 bus test systems respectively. As such, the computational complexity of Alg. 4 increases linearly with regard to the number of buses in the DN. Proposals based on centralized convex optimization techniques such as those in references [75] [70] and [78] are associated with the computation complexity of $O(|\mathcal{B}|^3)$ since these methods rely on convex solvers such as SeDuMi that are typically associated with cubic convergence in terms of the total number of optimization variables in the problem [135]. What is more, Meta-heuristic methods such as reference [55] approach the reconfiguration problem by iteratively generating sets of candidate solutions and choosing the best candidate from each set. From reference [136], the complexity associated with computing each candidate solution is $O(|\mathcal{B}|^3)$. Therefore, the complexity associated with algorithms in this category is $O(|\mathcal{B}|^3)$.

Next, Alg. 4 is applied to minimize the power loss along each line in the DN and compare its performance with the FNSGA through simulations conducted on the 33 bus and 76 bus test systems. Fig. 6.5a illustrates the power losses at each line in the 33-bus DN for the topologies obtained from Alg. 4 and FNSGA. For this case, both algorithms converge to the optimal topology of the reconfiguration problem. As such, both algorithms result in the same power losses for each DN line. It can be observed from this figure that although the FNSGA algorithm does not guarantee convergence to the global optima, it can result in the optimal solution in certain networks like the

33-bus DN. Our algorithm has also resulted in the optimal topology configuration as expected. Then, Fig. 6.5b illustrates the power loss at each line in the 76-bus system for both algorithms. For this test system, Alg. 4 results in the optimal topology configuration which is associated with a cumulative power loss of 0.0616 MW whereas FNSGA converges to a near-optimal solution with a cumulative power loss of 0.0642 MW. This result serves to illustrate the efficacy of the optimal reconfiguration algorithm as Alg. 4 results in the optimal solution whereas the FNSGA algorithm results in a sub-optimal solution for the same DN setting.

Then, a brief comparison between Alg. 4 and the decentralized reconfiguration algorithm in Alg. 3 is presented. Comparing with Alg. 3, Alg. 4 is associated with superior theoretical performance bounds as Alg. 4 is guaranteed to converge to the global optima of the reconfiguration problem whereas Alg. 3 only guarantees convergence to local optima. On the other hand, Alg. 3 is typically associated with superior convergence rate. From Fig. 5.2b, Alg. 3 converges within 4 and 5 iterations for the IEEE 33-bus and 69-bus test systems respectively. This is significantly lower than those associated with Alg. 3 for similarly sized systems (i.e. 575 iterations for the 33-bus test system and 1000 iterations for the 76-bus test system).

6.6 Chapter Summary

This chapter proposes a topology reconfiguration algorithm that accounts for the non-linear interdependencies in practical DNs so that the operation constraints of the DN can be maintained. For tractable solution of the reconfiguration problem, the original problem is decomposed into QCQP-1 subproblems that can be exactly resolved with convex relaxation techniques based on additive separability, Schur's complement and S-procedure. The convergence characteristics of the proposed algorithm have been demonstrated via simulations conducted on both balanced and unbalanced practical DNs as well as comparative studies with the state-of-the-art.

Chapter 7

Conclusions and Future Work

7.1 Dissertation Summary

This dissertation has introduced several regulation algorithms for addressing key challenges to the voltage profiles of DNs that are caused by the rapid proliferation of DERs. The proven models elaborated in Chapter 2 allow for tractable formulations of regulation algorithms while capturing the interdependencies in multiphase radial DNs. Utilizing the AMI and SCADA technologies prevalent in modern smart DNs as well as the cyber-enabled smart devices detailed in Chapter 1, these algorithms enhance the voltage profile of DN through voltage monitoring, analysis and improvement.

In Chapter 3, a distributed monitoring technique of voltage profile in the DN is proposed. Leveraging the cyber-physical nature of the grid, the monitoring technique equips smart components in the DN with the ability to monitor the changing voltage profiles in a collaborative and adaptive manner. In this technique, theoretical constructs associated with social learning are employed to design the iterative information exchange process between neighboring buses in the DN. This exchange process allows the buses in the DN to reach a consensus regarding the voltage profile in real-time. Then, this consensus information is used by smart power entities in the DN to make local integration decisions of ALEs that heed physical grid constraints. Thus, the distributed

architecture employed by this technique reduces the heavy computation overhead commonly associated with large-scale coordination and data processing by offloading them to cyber-enabled smart buses. The performance of this technique is verified via both theoretical studies and simulations conducted on the IEEE 33-bus practical DN. This technique is published in reference [81] as a conference paper.

In Chapter 4, a technique for data-driven PLF is presented where the technique makes no assumption on the power flow relations and requires no knowledge of specific parameters of the DN such as impedance and topology. This is accomplished through modelling the power flow relations in the DN with GP emulators, whose performance depends heavily on the structure of the kernels they adopt. An ideal kernel for the emulator results in greater efficiency during the training and inferencing stages and prevents issues such as over-fitting to the training dataset. In this technique, the design process for the emulator kernel is first formulated as a bi-level optimization problem which is NP-hard as it includes both discrete variables and non-convex constraints. Then, this problem is resolved with a best response strategy refinement process based on theoretical constructs from potential games. The convergence guarantees of this iterative algorithm are established via potential game theoretic constructs. Moreover, the approximating properties of the GP emulator are proved using the universal approximation theorem and the representer theorem. Simulations showcasing the performance of the proposed emulator are then conducted on the practical IEEE 33-bus, 37-bus and 123-bus DNs. This technique is published in reference [82] as a journal paper.

In Chapter 5, a distributed DN topology reconfiguration technique for voltage profile improvement is presented. Leveraging the communication capacities of the modern smart grid, the proposed reconfiguration technique equips the DN with the capability to accommodate highly fluctuating power entities such as EVs and DGs through effective coordination among intelligent buses. In this technique, individual buses in the DN infer the state of the system through communications with their neighbours and make local actuation decisions based on this information. The convergence guarantees and the optimality conditions of this algorithm are derived from theoreti-

cal constructs associated with potential games and discrete concavity. From the simulation results conducted on practical DNs in Chapter 5, this reconfiguration technique can adapt to the variations in voltage profile caused by load fluctuations in real-time and balance the loads across the feeder. This technique is published in reference [83] as a journal paper.

In Chapter 6, a topology reconfiguration algorithm based on convex relaxation techniques is introduced. Leveraging theoretical constructs from ADMM, Schur's complement and additive separability, the proposed technique proactively mitigates the inefficiencies in the power grid through a distributed scheme where each bus in the DN iteratively solves a subproblem of the topology reconfiguration problem. Utilizing decomposition methods based on ADMM and additive separability, the proposed technique decomposes the reconfiguration problem into subproblems that can be resolved with information available to each bus. Moreover, the non-convexities present in these subproblems are resolved through the application of relaxation techniques based on Schur's complement. The convergence and performance guarantees for the proposed algorithm are also established. Furthermore, the convergence properties of the algorithm are illustrated with simulation studies conducted on practical DNs. This technique is published in reference [84] as a journal paper.

7.2 Future Work

Here, the future directions for the research topics presented in this dissertation are expanded upon. For the monitoring algorithm presented in Chapter 3, a direction of future research is to explore how cyber vulnerabilities in a small subset of buses in the DN can be exploited to spread faulty information to the entire DN. From the results established in Chapter 3, local variables at any bus can be propagated to the rest of the DN through iterative information exchanges with its neighbours. As such, one possible method for adversary to propagate faulty information from a subset of buses to the rest of DN would be through the hijacking of the iterative information exchanges instrumental to distributed voltage improvement algorithms such as those presented in Chapters 5

and 6. Another direction of future research is to design the threshold value for ALE integration (i.e. τ) with machine learning techniques. One possible way to accomplish that is to model the relationship between the threshold value and the cumulative capacity of ALE in the DN with the GP emulator adopted in Chapter 4. For the PLF technique presented in Chapter 4, one direction is to extend the kernel design technique introduced in this work to data-driven methods based on neural networks. Similar to the GP emulator, the performance of neural networks is heavily affected by a number of hyper-parameters such as the number of layers used and the type of activation function adopted. As such, the proposed kernel design method can be extended to tuning the hyper-parameters of neural networks. For the reconfiguration technique introduced in Chapter 5, a direction of future research is considering DN topology planning for guaranteeing discrete concavity for the reconfiguration problem. As the algorithm in Chapter 5 leads to the global optimal solution for the reconfiguration problem when the discrete concavity condition is satisfied, such research direction can lead to better optimality guarantees for the algorithm. For the reconfiguration technique proposed in Chapter 6, a direction of future research is to extend the exact convex relaxation technique for QCQP-n problems derived for this work to other non-convex problems in power system optimization such as the optimal power flow problem and the service restoration problem. Another direction would be to extend the QCQP-n relaxation technique to non-convex and non-quadratic constraints. Another direction for extending the reconfiguration techniques is to combine them with the PLF method introduced in Chapter 4 to study their performances under probabilistic power injections. The majority of existing proposals in reconfiguration such as references [55, 56, 57] only consider deterministic power injections. As such, reconfiguration under probabilistic power injection would be a notable improvement over the state-of-the-art.

Appendix A

Network Parameters for DNs

This appendix presents the bus and line parameters for the DNs studied in this dissertation. These DNs are the balanced IEEE 33-bus DN, the balanced IEEE 69-bus DN, the balanced Brazilian 136-bus DN, the unbalanced 37-bus DN and the unbalanced 123-bus DN. The IEEE 33-bus, 69-bus, 37-bus and 123-bus DNs are detailed in reference [131] and the Brazilian 136-bus DN is introduced in reference [122]. For the balanced IEEE 33-bus and 69-bus as well as the Brazilian 136-bus networks, the bus parameters presents are the real and reactive loads at each bus. Also, the line parameters presented are the resistance and reactance at each power-delivering line in the DN. For the unbalanced IEEE 37-bus and 123-bus networks, the bus parameters are the real and reactive loads for each phase associated with every bus in the DN. Moreover, the line parameters are the length and line type of each line as well as the resistance and reactance matrices associated with each line type.

Bus Index	Real Load (kW)	Reactive Load (kVar)	Bus	Real Load (kW)	Reactive Load (kVar)
1	0	0	18	90	40
2	100	60	19	90	40
3	90	40	20	90	40
4	120	80	21	90	40
5	60	30	22	90	40
6	60	20	23	90	50
7	200	100	24	420	200
8	200	100	25	420	200
9	60	20	26	60	25
10	60	20	27	60	25
11	45	30	28	60	20
12	60	35	29	120	70
13	60	35	30	200	600
14	120	80	31	150	70
15	60	10	32	210	100
16	60	20	33	60	40
17	60	20			

Table A.1: Bus Parameters for the IEEE 33-Bus DN.

Line	Resistance (Ohm)	Reactance (Ohm)	Line	Resistance (Ohm)	Reactance (Ohm)
(2,1)	0.0922	0.047	(21,20)	0.4095	0.4784
(3,2)	0.493	0.2511	(22,21)	0.7089	0.9373
(4,3)	0.366	0.1864	(23,3)	0.4512	0.3083
(5,4)	0.3811	0.1941	(24,23)	0.898	0.7091
(6,5)	0.819	0.707	(25,24)	0.896	0.7011
(7,6)	0.1872	0.6188	(26,6)	0.203	0.1034
(8,7)	0.7114	0.2351	(27,26)	0.2842	0.1447
(9,8)	1.03	0.74	(28,27)	1.059	0.9337
(10,9)	1.044	0.74	(29,28)	0.8042	0.7006
(11,10)	0.1966	0.065	(30,29)	0.5075	0.2585
(12,11)	0.3744	0.1238	(31,30)	0.9744	0.963
(13,12)	1.468	1.155	(32,31)	0.3105	0.3619
(14,13)	0.5416	0.7129	(33,32)	0.341	0.5302
(15,14)	0.591	0.526	(8,21)	2	2
(16,15)	0.7463	0.545	(15,9)	2	2
(17,16)	1.289	1.721	(22,12)	2	2
(18,17)	0.732	0.574	(33,18)	0.5	0.5
(19,2)	0.164	0.1565	(29,25)	0.5	0.5
(20,19)	1.5042	1.3554			

Table A.2: Line Parameters for the IEEE 33-Bus DN.

Bus Index	Real Load (kW)	Reactive Load (kVar)	Bus	Real Load (kW)	Reactive Load (kVar)
1	0	0	36	26	18.6
2	0	0	37	26	18.6
3	0	0	38	0	0
4	0	0	39	24	17
5	0	0	40	24	17
6	2.6	2.2	41	1.2	1
7	40.4	30	42	0	0
8	75	54	43	6	4.3
9	30	22	44	0	0
10	28	19	45	39.2	26.3
11	145	104	46	39.2	26.3
12	145	104	47	0	0
13	8	5.5	48	79	56.4
14	8	5.5	49	384.7	274.5
15	0	0	50	384.7	274.5
16	45.5	30	51	40.5	28.3
17	60	35	52	3.6	2.7
18	60	35	53	4.3	3.5
19	0	0	54	26.4	19
20	1	0.6	55	24	17.2
21	114	81	56	0	0
22	5.3	3.5	57	0	0
23	0	0	58	0	0
24	28	20	59	100	72
25	0	0	60	0	0
26	14	10	61	1244	888
27	14	10	62	32	23
28	26	18.6	63	0	0
29	26	18.6	64	227	162
30	0	0	65	59	42
31	0	0	66	18	13
32	0	0	67	18	13
33	14	10	68	28	20
34	19.5	14	69	28	20
35	6	4			

Table A.3: Bus Parameters for the IEEE 69-Bus DN.

Line	Resistance (Ohm)	Reactance (Ohm)	Line	Resistance (Ohm)	Reactance (Ohm)
(2,1)	0.0005	0.0012	(39,38)	0.0304	0.0355
(3,2)	0.0005	0.0012	(40,39)	0.0018	0.0021
(4,3)	0.0015	0.0036	(41,40)	0.7283	0.8509
(5,4)	0.0251	0.0294	(42,41)	0.31	0.3623
(6,5)	0.366	0.1864	(43,42)	0.041	0.0478
(7,6)	0.381	0.1941	(44,43)	0.0092	0.0116
(8,7)	0.0922	0.047	(45,44)	0.1089	0.1373
(9,8)	0.0493	0.0251	(46,45)	0.0009	0.0012
(10,9)	0.819	0.2707	(47,4)	0.0034	0.0084
(11,10)	0.1872	0.0619	(48,47)	0.0851	0.2083
(12,11)	0.7114	0.2351	(49,48)	0.2898	0.7091
(13,12)	1.03	0.34	(50,49)	0.0822	0.2011
(14,13)	1.044	0.34	(51,8)	0.0928	0.0473
(15,14)	1.058	0.3496	(52,51)	0.3319	0.114
(16,15)	0.1966	0.065	(53,9)	0.174	0.0886
(17,16)	0.3744	0.1238	(54,53)	0.203	0.1034
(18,17)	0.0047	0.0016	(55,54)	0.2842	0.1447
(19,18)	0.3276	0.1083	(56,55)	0.2813	0.1433
(20,19)	0.2106	0.069	(57,56)	1.59	0.5337
(21,20)	0.3416	0.1129	(58,57)	0.7837	0.263
(22,21)	0.014	0.0046	(59,58)	0.3042	0.1006
(23,22)	0.1591	0.0526	(60,59)	0.3861	0.1172
(24,23)	0.3463	0.1145	(61,60)	0.5075	0.2585
(25,24)	0.7488	0.2475	(62,61)	0.0974	0.0496
(26,25)	0.3089	0.1021	(63,62)	0.145	0.0738
(27,26)	0.1732	0.0572	(64,63)	0.7105	0.3619
(28,3)	0.0044	0.0108	(65,64)	1.041	0.5302
(29,28)	0.064	0.1565	(66,11)	0.2012	0.0611
(30,29)	0.3978	0.1315	(67,66)	0.0047	0.0014
(31,30)	0.0702	0.0232	(68,12)	0.7394	0.2444
(32,31)	0.351	0.116	(69,68)	0.0047	0.0016
(33,32)	0.839	0.2816	(59,50)	2	2
(34,33)	1.708	0.5646	(21,13)	2	2
(35,34)	1.474	0.4873	(65,27)	2	2
(36,3)	0.0044	0.0108	(44,11)	0.5	0.5
(37,36)	0.064	0.1565	(16,46)	0.5	0.5
(38,37)	0.1053	0.123			

Table A.4: Line Parameters for the IEEE 69-Bus DN.

Bus Index	Real Load (kW)	Reactive Load (kVar)	Bus	Real Load (kW)	Reactive Load (kVar)
1	0	0	35	396.735	193.96
2	0	0	36	0	0
3	47.78	19.01	37	181.152	88.56
4	42.55	16.93	38	242.172	118.395
5	87.02	34.62	39	75.32	36.82
6	311.31	123.855	40	0	0
7	148.869	59.23	41	1.25	0.53
8	238.672	94.96	42	6.27	2.66
9	62.3	24.79	43	0	0
10	124.598	49.57	44	117.88	49.97
11	140.175	55.77	45	62.67	26.57
12	116.813	46.47	46	172.285	73.03
13	249.203	99.15	47	458.556	194.388
14	291.447	115.952	48	262.962	111.473
15	303.72	120.835	49	235.761	99.94
16	215.396	85.7	50	0	0
17	198.586	79.01	51	109.215	46.3
18	0	0	52	0	0
19	0	0	53	72.81	30.87
20	0	0	54	258.473	109.57
21	30.13	14.73	55	69.17	29.32
22	230.972	112.92	56	21.84	9.26
23	60.26	29.46	57	0	0
24	230.972	112.92	58	20.53	8.7
25	120.507	58.92	59	150.548	63.82
26	0	0	60	220.687	93.55
27	56.98	27.86	61	92.38	39.16
28	364.665	178.281	62	0	0
29	0	0	63	226.693	96.1
30	124.647	60.94	64	0	0
31	56.98	27.86	65	294.016	116.974
32	0	0	66	83.02	33.03
33	85.47	41.79	67	83.02	33.03
34	0	0	68	103.77	41.29

Table A.5: Bus Parameters for the Brazilian 136-Bus DN (1).

Bus Index	Real Load (kW)	Reactive Load (kVar)	Bus	Real Load (kW)	Reactive Load (kVar)
69	176.408	70.18	103	9.07	3.84
70	83.02	33.03	104	2.09	0.89
71	217.917	86.7	105	16.735	7.09
72	23.29	9.27	106	1506.522	638.634
73	5.08	2.02	107	313.023	132.694
74	72.64	28.9	108	79.83	33.84
75	405.99	161.523	109	51.32	21.76
76	0	0	110	0	0
77	100.182	42.47	111	202.435	85.82
78	142.523	60.42	112	60.82	25.78
79	96.04	40.71	113	45.62	19.34
80	300.454	127.366	114	0	0
81	141.238	59.87	115	157.07	66.58
82	279.847	118.631	116	0	0
83	87.31	37.01	117	250.148	106.041
84	243.849	103.371	118	0	0
85	247.75	105.025	119	69.81	29.59
86	0	0	120	32.07	13.6
87	89.88	38.1	121	61.08	25.89
88	1137.28	482.108	122	0	0
89	458.339	194.296	123	94.62	46.26
90	385.197	163.29	124	49.86	24.38
91	0	0	125	123.164	60.21
92	79.61	33.75	126	78.35	38.3
93	87.31	37.01	127	145.475	71.12
94	0	0	128	21.37	10.45
95	74	31.37	129	74.79	36.56
96	232.05	98.37	130	227.926	111.431
97	141.819	60.12	131	35.61	17.41
98	0	0	132	249.295	121.877
99	76.45	32.41	133	316.722	154.842
100	0	0	134	333.817	163.199
101	51.32	21.76	135	249.295	121.877
102	59.87	25.38	136	0	0

Table A.6: Bus Parameters for the Brazilian 136-Bus DN (2).

Line	Resistance (Ohm)	Reactance (Ohm)	Line	Resistance (Ohm)	Reactance (Ohm)
(2,1)	0.33205	0.76653	(41,40)	0.11819	0.27283
(3,2)	0.00188	0.00433	(42,41)	2.96288	1.01628
(4,3)	0.22324	0.51535	(43,41)	0.00188	0.00433
(5,4)	0.09943	0.22953	(44,43)	0.06941	0.16024
(6,5)	0.15571	0.35945	(45,44)	0.81502	0.42872
(7,6)	0.16321	0.37677	(46,44)	0.06378	0.14724
(8,7)	0.11444	0.26417	(47,46)	0.13132	0.30315
(9,7)	0.05675	0.05666	(48,47)	0.06191	0.14291
(10,9)	0.52124	0.27418	(49,48)	0.11444	0.26417
(11,9)	0.10877	0.1086	(50,49)	0.28374	0.28331
(12,11)	0.39803	0.20937	(51,50)	0.28374	0.28331
(13,11)	0.91744	0.31469	(52,49)	0.04502	0.10394
(14,11)	0.11823	0.11805	(53,52)	0.02626	0.06063
(15,14)	0.50228	0.26421	(54,53)	0.06003	0.13858
(16,14)	0.05675	0.05666	(55,54)	0.03002	0.06929
(17,16)	0.29379	0.15454	(56,55)	0.02064	0.04764
(18,1)	0.33205	0.76653	(57,53)	0.10881	0.25118
(19,18)	0.00188	0.00433	(58,57)	0.25588	0.1346
(20,19)	0.22324	0.51535	(59,58)	0.41699	0.21934
(21,20)	0.10881	0.25118	(60,59)	0.50228	0.26421
(22,21)	0.71078	0.37388	(61,60)	0.3317	0.17448
(23,21)	0.18197	0.42008	(62,61)	0.20849	0.10967
(24,23)	0.30326	0.15952	(63,48)	0.13882	0.32047
(25,23)	0.02439	0.0563	(64,1)	0.0075	0.01732
(26,25)	0.04502	0.10394	(65,64)	0.27014	0.62362
(27,26)	0.01876	0.04331	(66,65)	0.3827	0.88346
(28,27)	0.11823	0.11805	(67,66)	0.33018	0.7622
(29,28)	0.02365	0.02361	(68,67)	0.3283	0.75787
(30,29)	0.18954	0.0997	(69,68)	0.17072	0.39409
(31,30)	0.39803	0.20937	(70,69)	0.55914	0.29412
(32,29)	0.05675	0.05666	(71,69)	0.05816	0.13425
(33,32)	0.09477	0.04985	(72,71)	0.7013	0.3689
(34,33)	0.41699	0.21934	(73,72)	1.02352	0.53839
(35,34)	0.11372	0.05982	(74,71)	0.06754	0.15591
(36,32)	0.07566	0.07555	(75,74)	1.32352	0.45397
(37,36)	0.3696	0.19442	(76,1)	0.01126	0.02598
(38,37)	0.26536	0.13958	(77,76)	0.72976	1.68464
(39,36)	0.05675	0.05666	(78,77)	0.22512	0.51968
(40,1)	0.33205	0.76653	(79,78)	0.20824	0.48071

Table A.7: Line Parameters for the Brazilian 136-Bus DN (1).

Line	Resistance (Ohm)	Reactance (Ohm)	Line	Resistance (Ohm)	Reactance (Ohm)
(80,79)	0.0469	0.10827	(119,105)	0.32267	0.74488
(81,80)	0.6195	0.61857	(120,119)	0.14633	0.33779
(82,81)	0.34049	0.33998	(121,120)	0.12382	0.28583
(83,82)	0.56862	0.29911	(122,1)	0.01126	0.02598
(84,82)	0.10877	0.1086	(123,122)	0.6491	1.49842
(85,84)	0.56862	0.29911	(124,123)	0.04502	0.10394
(86,1)	0.01126	0.02598	(125,124)	0.5264	0.18056
(87,86)	0.41835	0.96575	(126,124)	0.02064	0.04764
(88,87)	0.10499	0.13641	(127,126)	0.53071	0.27917
(89,87)	0.43898	1.01338	(128,126)	0.09755	0.2252
(90,89)	0.0752	0.02579	(129,128)	0.11819	0.27283
(91,90)	0.07692	0.17756	(130,128)	0.13882	0.32047
(92,91)	0.33205	0.76653	(131,130)	0.04315	0.09961
(93,92)	0.08442	0.19488	(132,131)	0.09192	0.2122
(94,93)	0.1332	0.30748	(133,132)	0.16134	0.37244
(95,94)	0.2932	0.29276	(134,133)	0.37832	0.37775
(96,95)	0.21753	0.21721	(135,134)	0.39724	0.39664
(97,96)	0.26482	0.26443	(136,135)	0.2932	0.29276
(98,94)	0.10318	0.23819	(74,8)	0.13132	0.30315
(99,98)	0.13507	0.31181	(25,10)	0.26536	0.13958
(100,1)	0.00938	0.02165	(84,16)	0.14187	0.14166
(101,100)	0.16884	0.38976	(136,39)	0.08512	0.08499
(102,101)	0.11819	0.27283	(52,26)	0.04502	0.10394
(103,102)	2.28608	0.78414	(97,51)	0.14187	0.14166
(104,102)	0.45587	1.05236	(99,56)	0.14187	0.14166
(105,104)	0.696	1.60669	(121,63)	0.0394	0.09094
(106,105)	0.45774	1.05669	(80,67)	0.12944	0.29882
(107,106)	0.20298	0.26373	(132,80)	0.01688	0.03898
(108,107)	0.21348	0.27737	(136,85)	0.3317	0.17448
(109,108)	0.54967	0.28914	(105,92)	0.14187	0.14166
(110,109)	0.54019	0.28415	(130,91)	0.07692	0.17756
(111,108)	0.0455	0.05911	(104,91)	0.07692	0.17756
(112,111)	0.47385	0.24926	(105,93)	0.07692	0.17756
(113,112)	0.86241	0.45364	(133,93)	0.07692	0.17756
(114,113)	0.56862	0.29911	(121,97)	0.26482	0.26443
(115,109)	0.77711	0.40878	(48,111)	0.49696	0.64567
(116,115)	1.08038	0.5683	(77,127)	0.17059	0.08973
(117,110)	1.09933	0.57827	(78,129)	0.05253	0.12126
(118,117)	0.47385	0.24926	(99,136)	0.2932	0.29276

Table A.8: Line Parameters for the Brazilian 136-Bus DN (2).

Bus Index	Real A (kW)	Reactive A (kVar)	Real B (kW)	Reactive B (kVar)	Real C (kW)	Reactive C (kVar)
701	140	70	140	70	350	175
712	0	0	0	0	85	40
713	0	0	0	0	85	40
714	17	8	21	10	0	0
718	85	40	0	0	0	0
720	0	0	0	0	85	40
722	0	0	140	70	21	10
724	0	0	42	21	0	0
725	0	0	42	21	0	0
727	0	0	0	0	42	21
728	42	21	42	21	42	21
729	42	21	0	0	0	0
730	0	0	0	0	85	40
731	0	0	85	40	0	0
732	0	0	0	0	42	21
733	85	40	0	0	0	0
734	0	0	0	0	42	21
735	0	0	0	0	85	40
736	0	0	42	21	0	0
737	140	70	0	0	0	0
738	126	62	0	0	0	0
740	0	0	0	0	85	40
741	0	0	0	0	42	21
742	8	4	85	40	0	0
744	42	21	0	0	0	0

Table A.9: Bus Parameters for the IEEE 37-Bus DN.

Line	Length (mile)	Line Type	Line	Length (mile)	Line Type
(702,701)	0.1818144	722	(736,710)	0.2424192	724
(705,702)	0.075756	724	(741,711)	0.075756	723
(713,702)	0.0681804	723	(740,711)	0.037878	724
(703,702)	0.2499948	722	(704,713)	0.0984828	723
(727,703)	0.0454536	724	(718,714)	0.0984828	724
(730,703)	0.113634	723	(707,720)	0.1742388	724
(714,704)	0.0151512	724	(706,720)	0.113634	723
(720,704)	0.151512	723	(744,727)	0.0530292	723
(742,705)	0.0606048	724	(709,730)	0.037878	723
(712,705)	0.0454536	724	(734,733)	0.1060584	723
(725,706)	0.0530292	724	(737,734)	0.1212096	723
(724,707)	0.1439364	724	(710,734)	0.0984828	724
(722,707)	0.0227268	724	(738,737)	0.075756	723
(733,708)	0.0606048	723	(711,738)	0.075756	723
(732,708)	0.0606048	724	(728,744)	0.037878	724
(731,709)	0.113634	723	(729,744)	0.0530292	724
(708,709)	0.0606048	723	(701,799)	0.3503715	721
(735,710)	0.037878	724			

Table A.10: Line Parameters for the IEEE 37-Bus DN

Line Type	Resistance Matrix (Ohm/mile)	Reactance Matrix (Ohm/mile)
721	$\begin{bmatrix} 0.2926 & 0.0673 & 0.0337 \\ & 0.2646 & 0.0673 \\ & & 0.2926 \end{bmatrix}$	$\begin{bmatrix} 0.1973 & -0.0368 & -0.0417 \\ & 0.19 & -0.0368 \\ & & 0.1973 \end{bmatrix}$
722	$\begin{bmatrix} 0.4751 & 0.1629 & 0.1234 \\ & 0.4488 & 0.1629 \\ & & 0.4751 \end{bmatrix}$	$\begin{bmatrix} 0.2973 & -0.0326 & -0.0607 \\ & 0.2678 & -0.0326 \\ & & 0.2973 \end{bmatrix}$
723	$\begin{bmatrix} 1.2936 & 0.4871 & 0.4585 \\ & 1.3022 & 0.4871 \\ & & 1.2936 \end{bmatrix}$	$\begin{bmatrix} 0.6713 & 0.2111 & 0.1521 \\ & 0.6326 & 0.2111 \\ & & 0.6713 \end{bmatrix}$
724	$\begin{bmatrix} 2.0952 & 0.5204 & 0.4926 \\ & 2.1068 & 0.5204 \\ & & 2.0952 \end{bmatrix}$	$\begin{bmatrix} 0.7758 & 0.2738 & 0.2123 \\ & 0.7398 & 0.2738 \\ & & 0.7758 \end{bmatrix}$

Table A.11: Line Types for the IEEE 37-Bus DN.

Bus Index	Real A (kW)	Reactive A (kVar)	Real B (kW)	Reactive B (kVar)	Real C (kW)	Reactive C (kVar)
1	40	20	0	0	0	0
2	0	0	20	10	0	0
4	0	0	0	0	40	20
5	0	0	0	0	20	10
6	0	0	0	0	40	20
7	20	10	0	0	0	0
9	40	20	0	0	0	0
10	20	10	0	0	0	0
11	40	20	0	0	0	0
12	0	0	20	10	0	0
16	0	0	0	0	40	20
17	0	0	0	0	20	10
19	40	20	0	0	0	0
20	40	20	0	0	0	0
22	0	0	40	20	0	0
24	0	0	0	0	40	20
28	40	20	0	0	0	0
29	40	20	0	0	0	0
30	0	0	0	0	40	20
31	0	0	0	0	20	10
32	0	0	0	0	20	10
33	40	20	0	0	0	0
34	0	0	0	0	40	20
35	40	20	0	0	0	0
37	40	20	0	0	0	0
38	0	0	20	10	0	0
39	0	0	20	10	0	0
41	0	0	0	0	20	10
42	20	10	0	0	0	0
43	0	0	40	20	0	0

Table A.12: Bus Parameters for the IEEE 123-Bus DN (1).

Bus Index	Real A (kW)	Reactive A (kVar)	Real B (kW)	Reactive B (kVar)	Real C (kW)	Reactive C (kVar)
45	20	10	0	0	0	0
46	20	10	0	0	0	0
47	35	25	35	25	35	25
48	70	50	70	50	70	50
49	35	25	70	50	35	20
50	0	0	0	0	40	20
51	20	10	0	0	0	0
52	40	20	0	0	0	0
53	40	20	0	0	0	0
55	20	10	0	0	0	0
56	0	0	20	10	0	0
58	0	0	20	10	0	0
59	0	0	20	10	0	0
60	20	10	0	0	0	0
62	0	0	0	0	40	20
63	40	20	0	0	0	0
64	0	0	75	35	0	0
65	35	25	35	25	70	50
66	0	0	0	0	75	35
68	20	10	0	0	0	0
69	40	20	0	0	0	0
70	20	10	0	0	0	0
71	40	20	0	0	0	0
73	0	0	0	0	40	20
74	0	0	0	0	40	20
75	0	0	0	0	40	20
76	105	80	70	50	70	50
77	0	0	40	20	0	0
79	40	20	0	0	0	0
80	0	0	40	20	0	0
82	40	20	0	0	0	0
83	0	0	0	0	20	10
84	0	0	0	0	20	10

Table A.13: Bus Parameters for the IEEE 123-Bus DN (2).

Bus Index	Real A (kW)	Reactive A (kVar)	Real B (kW)	Reactive B (kVar)	Real C (kW)	Reactive C (kVar)
85	0	0	0	0	40	20
86	0	0	20	10	0	0
87	0	0	40	20	0	0
88	40	20	0	0	0	0
90	0	0	40	20	0	0
92	0	0	0	0	40	20
94	40	20	0	0	0	0
95	0	0	20	10	0	0
96	0	0	20	10	0	0
98	40	20	0	0	0	0
99	0	0	40	20	0	0
100	0	0	0	0	40	20
102	0	0	0	0	20	10
103	0	0	0	0	40	20
104	0	0	0	0	40	20
106	0	0	40	20	0	0
107	0	0	40	20	0	0
109	40	20	0	0	0	0
111	20	10	0	0	0	0
112	20	10	0	0	0	0
113	40	20	0	0	0	0
114	20	10	0	0	0	0

Table A.14: Bus Parameters for the IEEE 123-Bus DN (3).

Line	Length (mile)	Line Type	Line	Length (mile)	Line Type
(2,1)	0.03314325	10	(250,30)	0.037878	2
(3,1)	0.0473475	11	(32,31)	0.056817	11
(7,1)	0.056817	1	(15,34)	0.018939	11
(4,3)	0.037878	11	(36,35)	0.1231035	8
(5,3)	0.06155175	11	(40,35)	0.0473475	1
(6,5)	0.0473475	11	(37,36)	0.056817	9
(8,7)	0.037878	1	(38,36)	0.0473475	10
(12,8)	0.04261275	10	(39,38)	0.06155175	10
(9,8)	0.04261275	9	(41,40)	0.06155175	11
(13,8)	0.056817	1	(42,40)	0.0473475	1
(14,9)	0.08049075	9	(43,42)	0.094695	10
(34,13)	0.0284085	11	(44,42)	0.037878	1
(18,13)	0.15624675	2	(45,44)	0.037878	9
(11,14)	0.0473475	9	(47,44)	0.0473475	1
(10,14)	0.0473475	9	(46,45)	0.056817	9
(16,15)	0.07102125	11	(48,47)	0.0284085	4
(17,15)	0.0662865	11	(49,47)	0.0473475	4
(19,18)	0.0473475	9	(50,49)	0.0473475	4
(21,18)	0.056817	2	(51,50)	0.0473475	4
(20,19)	0.06155175	9	(151,51)	0.094695	4
(22,21)	0.09942975	10	(53,52)	0.037878	1
(23,21)	0.0473475	2	(54,53)	0.02367375	1
(24,23)	0.1041645	11	(55,54)	0.05208225	1
(25,23)	0.05208225	2	(57,54)	0.0662865	3
(26,25)	0.0662865	7	(56,55)	0.05208225	1
(28,25)	0.037878	2	(58,57)	0.0473475	10
(27,26)	0.05208225	7	(60,57)	0.1420425	3
(31,26)	0.04261275	11	(59,58)	0.0473475	10
(33,27)	0.094695	9	(61,60)	0.1041645	5
(29,28)	0.056817	2	(62,60)	0.0473475	12
(30,29)	0.0662865	2			

Table A.15: Line Parameters for the IEEE 123-Bus DN (1).

Line	Length (mile)	Line Type	Line	Length (mile)	Line Type
(63,62)	0.03314325	12	(92,91)	0.056817	11
(64,63)	0.0662865	12	(93,91)	0.04261275	6
(65,64)	0.08049075	12	(94,93)	0.05208225	9
(66,65)	0.06155175	12	(95,93)	0.056817	6
(68,67)	0.037878	9	(96,95)	0.037878	10
(72,67)	0.05208225	3	(98,97)	0.05208225	3
(97,67)	0.0473475	3	(99,98)	0.1041645	3
(69,68)	0.05208225	9	(100,99)	0.056817	3
(70,69)	0.06155175	9	(450,100)	0.151512	3
(71,70)	0.05208225	9	(102,101)	0.04261275	11
(73,72)	0.05208225	11	(105,101)	0.05208225	3
(76,72)	0.037878	3	(103,102)	0.06155175	11
(74,73)	0.0662865	11	(104,103)	0.132573	11
(75,74)	0.075756	11	(106,105)	0.04261275	10
(77,76)	0.075756	6	(108,105)	0.06155175	3
(86,76)	0.132573	3	(107,106)	0.10889925	10
(78,77)	0.018939	6	(109,108)	0.0852255	9
(79,78)	0.04261275	6	(300,108)	0.18939	3
(80,78)	0.08996025	6	(110,109)	0.056817	9
(81,80)	0.08996025	6	(111,110)	0.10889925	9
(82,81)	0.0473475	6	(112,110)	0.02367375	9
(84,81)	0.12783825	11	(113,112)	0.09942975	9
(83,82)	0.0473475	6	(114,113)	0.06155175	9
(85,84)	0.08996025	11	(35,135)	0.07102125	4
(87,86)	0.0852255	6	(1,149)	0.075756	1
(88,87)	0.03314325	9	(52,152)	0.075756	1
(89,87)	0.05208225	6	(67,160)	0.0662865	6
(90,89)	0.04261275	10	(101,197)	0.0473475	3
(91,89)	0.04261275	6			

Table A.16: Line Parameters for the IEEE 123-Bus DN (2)

Line Type	Resistance Matrix (Ohm/mile)	Reactance Matrix (Ohm/mile)
1	$\begin{bmatrix} 0.4576 & 0.1560 & 0.1535 \\ & 0.4666 & 0.1580 \\ & & 0.4615 \end{bmatrix}$	$\begin{bmatrix} 1.0780 & 0.5017 & 0.3849 \\ & 1.0482 & 0.4236 \\ & & 1.0651 \end{bmatrix}$
2	$\begin{bmatrix} 0.4666 & 0.1580 & 0.1560 \\ & 0.4615 & 0.1535 \\ & & 0.4576 \end{bmatrix}$	$\begin{bmatrix} 1.0482 & 0.4236 & 0.5017 \\ & 1.0651 & 0.3849 \\ & & 1.0780 \end{bmatrix}$
3	$\begin{bmatrix} 0.4615 & 0.1535 & 0.1580 \\ & 0.4576 & 0.1560 \\ & & 0.4666 \end{bmatrix}$	$\begin{bmatrix} 1.0651 & 0.3849 & 0.4236 \\ & 1.0780 & 0.5017 \\ & & 1.0482 \end{bmatrix}$
4	$\begin{bmatrix} 0.4615 & 0.1580 & 0.1535 \\ & 0.4666 & 0.1560 \\ & & 0.4576 \end{bmatrix}$	$\begin{bmatrix} 1.0651 & 0.4236 & 0.3849 \\ & 1.0482 & 0.5017 \\ & & 1.0780 \end{bmatrix}$
5	$\begin{bmatrix} 0.4666 & 0.1560 & 0.1580 \\ & 0.4576 & 0.1535 \\ & & 0.4615 \end{bmatrix}$	$\begin{bmatrix} 1.0482 & 0.5017 & 0.4236 \\ & 1.0780 & 0.3849 \\ & & 1.0651 \end{bmatrix}$
6	$\begin{bmatrix} 0.4576 & 0.1535 & 0.1560 \\ & 0.4615 & 0.1580 \\ & & 0.4666 \end{bmatrix}$	$\begin{bmatrix} 1.0780 & 0.3849 & 0.5017 \\ & 1.0651 & 0.4236 \\ & & 1.0482 \end{bmatrix}$
7	$\begin{bmatrix} 0.4576 & 0 & 0.1535 \\ & 0 & 0 \\ & & 0.4615 \end{bmatrix}$	$\begin{bmatrix} 1.0780 & 0 & 0.3849 \\ & 0 & 0 \\ & & 1.0651 \end{bmatrix}$
8	$\begin{bmatrix} 0.4576 & 0.1535 & 0 \\ & 0.4615 & 0 \\ & & 0 \end{bmatrix}$	$\begin{bmatrix} 1.0780 & 0.3849 & 0 \\ & 1.0651 & 0 \\ & & 0 \end{bmatrix}$
9	$\begin{bmatrix} 1.3292 & 0 & 0 \\ & 0 & 0 \\ & & 0 \end{bmatrix}$	$\begin{bmatrix} 1.3475 & 0 & 0 \\ & 0 & 0 \\ & & 0 \end{bmatrix}$
10	$\begin{bmatrix} 0 & 0 & 0 \\ & 1.3292 & 0 \\ & & 0 \end{bmatrix}$	$\begin{bmatrix} 0 & 0 & 0 \\ & 1.3475 & 0 \\ & & 0 \end{bmatrix}$
11	$\begin{bmatrix} 0 & 0 & 0 \\ & 0 & 0 \\ & & 1.3292 \end{bmatrix}$	$\begin{bmatrix} 0 & 0 & 0 \\ & 0 & 0 \\ & & 1.3475 \end{bmatrix}$
12	$\begin{bmatrix} 1.5209 & 0.5198 & 0.4924 \\ & 1.5329 & 0.5198 \\ & & 1.5209 \end{bmatrix}$	$\begin{bmatrix} 0.7521 & 0.2775 & 0.2157 \\ & 0.7162 & 0.2775 \\ & & 0.7521 \end{bmatrix}$

Table A.17: Line Types for the IEEE 123-Bus DN.

Bibliography

[1] H. Farhangi, "The path of the smart grid", *IEEE Power and Energy Magazine*, vol. 8, no. 1, pp. 18-28, 2010.

[2] Y. Xue, M. Starke, J. Dong, M. Olama, T. Kuruganti, J. Taft, and M. Shankar, "On a future for smart inverters with integrated system functions" *IEEE PEDG 2018*, June 2018.

[3] Y. Sun, X. Chen, S. Yang, Rusli, K. J. Tseng, and G. Amaratunga, "Micro PMU based monitoring system for active distribution networks", *IEEE PEDS 2017*, December 2017.

[4] M. Baran and F. Wu, "Network reconfiguration in distribution systems for loss reduction and load balancing", *IEEE Transactions on Power Delivery*, vol. 4, no. 2, pp. 1401-1407, 1989.

[5] F. Ding, and K. A. Loparo, "Feeder reconfiguration for unbalanced distribution systems with distributed generation: A hierarchical decentralized approach", *IEEE Transactions on Power Systems*, vol 31, no. 2, pp. 1633-1642, 2016.

[6] K. Shahid, K. Nainar, R. L. Olsen, F. Iov, M. Lyhne and G. Morgante, "On the use of common information model for smart grid applications-A conceptual approach", *IEEE Transactions on Smart Grid*, vol. 12, no. 6, 2021.

[7] J. W. Simpson-Porco and F. Bullo, "Distributed monitoring of voltage collapse sensitivity indices", *IEEE Transactions on Smart Grid*, vol. 7, no. 4, 2016.

[8] Y. Yuan, K. Dehghanpour and Z. Wang, "Mitigating smart meter asynchrony error via multi-objective low rank matrix recovery", *IEEE Transactions on Smart Grid*, vol. 12, no. 5, 2021.

[9] B. Borkowska, “Probabilistic load flow”, *IEEE Transactions on Power Apparatus and Systems*, vol. pas-93, issue, 3, 1974.

[10] P. L. Donti, Y. Liu, A. J. Schmitt, A. Bernstein, R. Yang and Y. Zhang, “Matrix completion for low-observability voltage estimation”, *IEEE Transactions on Smart Grid*, vol. 11, no. 3, 2020.

[11] D. Pinney, C. Miller, and T. Lovas, “Costs and benefits of smart feeder switching: quantifying the operating value of SFS”, *NRECA-DOE Smart Grid Demonstration Project*, May 2014.

[12] A. Kulmala, M. Alonso, S. Repo, H. Amaris, A. Moreno, J. Mehmedalic and Z. Al-Jassim, “Hierarchical and distributed control concept for distribution network congestion management”, *IET Generation, Transmission and Distribution*, vol. 11, no. 3, 2017.

[13] W. An, J. J. Ma, H. Y. Zhou, H. S. Chen, X. Jun and X. Jian “Application of an Integrated Protection and Control System for Smart Distribution Grid Based on PTN and 4G LTE Communication”, *IEEE ICSGSC 2019*, June 2019.

[14] J. Zhao, J. Zhu, H. Wei, H. Weng and W. Du “Research on the Large-scale Application of 5G in Smart Distribution Network”, *IEEE ITNEC 2021*, October 2021.

[15] V. C. Gungor, D. Sahin, T. Kocak, S. Ergut, C. Buccella, C. Cecati, and G. P. Hancke, “Smart grid technologies: communication technologies and standards”, *IEEE Transactions on Industrial Informatics*, vol. 7, no. 4, November 2011.

[16] L. Wenpeng, D. Sharp, and S. Lancashire, “Smart grid communication network capacity planning for power utilities, *Proc. IEEE PES, Transmission Distrib. Conf. Expo*, April, 2010.

[17] Mathur, R. Mohan., and Rajiv K. Varma. “Thyristor-Based facts controllers for electrical transmission systems”, IEEE Press, 2002.

[18] A. Cichon, T. Boczar, P. Fracz and D. Zmarzly, "Detection of defects in on-load-tap-changers using acoustic emission method", *IEEE International Symposium on Electrical Insulation*, 2012.

[19] J. W. Simpson-Porco and F. Bullo, "Distributed monitoring of voltage collapse sensitivity indices", *IEEE Transactions on Smart Grid*, vol. 7, no. 4 2016.

[20] X. Liu, X. Zhang and V. Venkatasubramanian "Distributed voltage security monitoring in large power systems using synchrophasors", *IEEE Transactions on Smart Grid*, vol. 7, no. 2, 2016.

[21] H. Lee, S. Niddodi, A. Srivastava, and D. Bakken, "Decentralized voltage stability monitoring and control in the smart grid using distributed computing architecture". *IEEE Industry Applications Society Annual Meeting*, 2016.

[22] C. Chen, J. Wang, and S. Kishore, "A distributed direct load control approach for large scale residential demand response", *IEEE Transactions on Power System*, 29(5): 2219-2228, 2014.

[23] G. Olguin, F. Vuinovich and M. H. J. Bollen "An optimal monitoring program for obtaining voltage sag system indexes", *IEEE Transactions on Power Systems*, vol. 21, no. 1, 2006.

[24] H. Yang, X. Shi, R. B. Qiu, X. He, Q. Ai and Z. Wang "Monitoring data factorization of high renewable energy penetrated grids for probabilistic static voltage stability assessment", *IEEE Transactions on Smart Grid*, vol. 13, no. 2, 2022.

[25] T. Wu, Y-J. A. Zhang and H. Wen "Voltage stability monitoring based on disagreement-based deep learning in a time-varying environment", *IEEE Transactions on Power Systems*, vol. 36, no. 1, 2021.

[26] M. Ghafouri, M. Au, M. Kassouf, M. Debbabi, C. Assi and J. Yan "Detection and mitigation of cyber attacks on voltage stability monitoring of smart grids", *IEEE Transactions on Smart Grid*, vol. 11, no. 6, 2020.

[27] S. Lu, S. Repo, D. D. Giustina, F. A-C. Figuerola, A. Löf and M. Pikkarainen "Real-time low voltage network monitoring-ICT architecture and field test experience", *IEEE Transactions on Smart Grid*, vol. 6, no. 4, 2015.

[28] Y. Xu, Z. Hu, L. Mili, M. Korkali, and X. Chen, "Probabilistic power-flow calculation based on a novel Gaussian process emulator", *IEEE Transactions on Power Systems*, to appear.

[29] Y. Yang, Z. Yang, J. Yu, B. Zhang, Y. Zhang and H. Yu, "Fast Calculation of probabilistic power flow: A model based deep learning approach", *IEEE Transactions on Smart Grid*, vol. 11, no. 3, May 2020.

[30] H. Yu, C. Y. Chung, K. P. Wong and J. H. Zhang, "Probabilistic load flow evaluation with hybrid Latin Hypercube sampling and Cholesky decomposition", *IEEE Transactions on Power System*, vol. 24, no. 2, 2009.

[31] J. Huang, Y. Xue, Z. Y. Dong, and K. P. Wong, "An adaptive importance sampling method for probabilistic optimal power flow", *IEEE Power Energy Society General Meeting*, Detroit, MI, USA, 2011.

[32] A. A. Eajal. A. El-Awady, E. F. El-Saadany, K. Ponnambalam, A. Al-Durra, A. S. Al-Sumaiti and M. M. A. Salama, " A Bayesian approach to the reliability analysis of renewables-dominated islanded DC microgrids", *IEEE Transactions on Power Systems*, vol. 36, no. 5, 2017.

[33] Y. Xu, M. Korkali, L. Mili, X. Chen and L. Min, " Risk assessment of rare events in probabilistic power flow via hybrid multi-surrogate method", *IEEE Transactions on Smart Grid*, vol. 11, no. 2, 2020.

[34] A. M. L. da Silva and A. M. de Castro, " Risk assessment in probabilistic load flow via Monte Carlo simulation and cross-entropy method", *IEEE Transactions on Power Systems*, vol. 34, no. 2, 2019.

[35] G. Zhou, R. Bo, L. Chien, X. Zhang, S. Yang and D. Su, " GPU-accelerated algorithm for online probabilistic power flow", *IEEE Transactions on Power Systems*, vol. 33, no. 1, 2018.

[36] M. M. A. Abdelaziz, " OpenCL-accelerated probabilistic power flow for active distribution networks", *IEEE Transactions on Sustainable Energy*, vol. 9, no. 3, 2018.

[37] Z. Ren, K. Wang, W. Li, L. Jin and Y. Dai, "Probabilistic power flow analysis of power systems incorporating tidal current generation", *IEEE Transactions on Sustainable Energy*, vol. 8, no. 3, 2017.

[38] M. E. Nassar, A. A. Hamad, M. M. A. Salama and E. F. El-Saadany, "A novel load flow algorithm for islanded AC/DC hybrid microgrids", *IEEE Transactions on Smart Grid*, vol. 10, no. 2, 2019.

[39] C. Liu, K. Sun, B. Wang and W. Yu, "Probabilistic power flow analysis using multidimensional holomorphic embedding and generalized cumulants", *IEEE Transactions on Power Systems*, vol. 33, no. 6, 2018.

[40] M. Nijhuis, M. Gibescu and S. Cobben, "Gaussian mixture based probabilistic load flow for LV-network planning", *IEEE Transactions on Power Systems*, vol. 32, no. 4, 2017.

[41] M. Jia, Y. Wang, C. Shen and G. Hug, "Privacy-preserving distributed probabilistic power flow", *IEEE Transactions on Power Systems*, vol. 36, no. 2, 2021.

[42] C. Lin, Z. Bie, C. Pan and S. Liu, "Fast cumulant method for probabilistic power flow considering the nonlinear relationship of wind power generation", *IEEE Transactions on Power Systems*, vol. 35, no. 4, 2020.

[43] J. Luo, L. Shi and Y. Ni, "Uncertain power flow analysis based on evidence theory and affine arithmetic", *IEEE Transactions on Power Systems*, vol. 33, no. 1, 2018.

[44] R. Allan and R. Billinton, "Probabilistic assessment of power systems", *Proceedings of IEEE*, vol. 88, no. 2, 2000.

[45] C. D. Zuluaga and M. A. Álvarez, "Bayesian probabilistic power flow analysis using Jacobian approximate Bayesian computation", *IEEE Transactions on Power Systems*, vol. 33, no. 5, 2018.

[46] J. Laowanitwattana and S. Uatrongjit "Probabilistic power flow analysis based on partial least square and arbitrary polynomial chaos expansion", *IEEE Transactions on Power Systems*, vol. 37, no. 2, 2022.

[47] C. Lin, Z. Bie. C. Pan and S. Liu, "Considering the nonlinear relationship of wind power generation", *IEEE Transactions on Power Systems*, vol. 35, no. 4, 2020.

[48] G. Gruosso, R. S. Netto, L. Daniel and P. Maffezzoni, "Joined probabilistic load flow and sensitivity analysis of distribution networks based on polynomial chaos method", *IEEE Transactions on Power Systems*, vol. 35, no. 1, 2020.

[49] H. Nosratabadi, M. Mohammadi and A. Kargarian, "Nonparametric probabilistic unbalanced power flow with adaptive kernel density estimator", *IEEE Transactions on Smart Grid*, vol. 10, no. 3, 2019.

[50] C-C. Yang and Y-Y. Hsu, "Estimation of line flows and bus voltages using decision trees", *IEEE Transactions on Power Systems*, vol. 9, no. 3, August 1994.

[51] P. Amid and C. Crawford, "A cumulant-tensor based probabilistic load flow method", *IEEE Transactions on Power Systems*, vol. 33, no. 5, 2018.

[52] M. Aien, M. Fotuhi-Firuzabad and F. Aminifar, "Probabilistic load flow in correlated uncertain environment using unscented transformation", *IEEE Transactions on Power Systems*, vol. 27, no. 4, 2012.

[53] J. Tang, F. Ni, F. Ponci and A. Monti, "Dimension-adaptive sparse grid interpolation for uncertainty quantification in modern power systems: Probabilistic power flow", *IEEE Transactions on Power Systems*, vol. 31, no. 2, 2016.

[54] J. A. Taylor, and E. S. Hover,"Convex models of distribution system reconfiguration", *IEEE Transactions on Power Systems*, vol. 27, no. 3, pp. 1407-1413, 2012.

[55] A. M. Eldurssi, and R. M. O'Connell, "A fast nondominated sorting guided genetic algorithm for multi-objective power distribution system reconfiguration problem", *IEEE Transactions on Power Systems*, vol. 30, no. 2, pp. 593-601, 2015.

[56] V. Roberge, M. Tarbouchi and F. A. Okou, "Distribution system optimization on graphics processing unit", *IEEE Transaction on Smart Grid* vol. 8, no. 4, pp. 1689-1699, 2017.

[57] A. Asrari, S. Lotfifard and M. Ansari, "Reconfiguration of smart distribution systems with time varying loads using parallel computing", *IEEE Transactions on Smart Grid*, vol. 7, no. 6, 2010.

[58] S. Chen, W. Hu, and Z. Chen, "Comprehensive cost minimization in distribution networks using segmented time feeder reconfiguration and reactive power control of distributed generators", *IEEE Transactions on Power Systems*, vol. 31, no. 2, pp. 983-993, 2016.

[59] R. S. Rao, K. Ravindra, K. Satish, "Power loss minimization in distribution system using network reconfiguration in the presence of distributed generation", *IEEE Transactions on Power Systems*, vol. 28, no. 1, February 2013.

[60] A. Swarnkar, N, Gupta and K. Niazi, "Adapted ant colony optimization for efficient reconfiguration of balanced and unbalanced distribution system for loss minimization", *Swarm and Evolutionary Computation* vol. 1, no. 3, pp. 129-137, 2011.

[61] A. Mendes, N. Boland, P. Guiney and C. Riveros "Switch and tap-changer reconfiguration of distribution networks using evolutionary algorithms", *IEEE Transactions on Power Systems*, vol. 28, no. 1, 2013.

[62] A. Mendes, N. Boland, P. Guiney and C. Riveros "Switch and tap-changer reconfiguration of distribution networks using evolutionary algorithms", *IEEE Transactions on Power Systems*, vol. 28, no. 1, 2013.

[63] W. Huang, W. Zheng and D. J. Hill "Distribution network reconfiguration for short-term voltage stability enhancement: An efficient deep learning approach", *IEEE Transactions on Smart Grid*, vol. 12, no. 6, 2021.

[64] W. Zheng, W. Huang, D. J. Hill and Y. Hou "An adaptive distributionally robust model for three-phase distribution network reconfiguration", *IEEE Transactions on Smart Grid*, vol. 12, no. 2, 2021.

[65] T. Zhong, H-T. Zhang, Y. Li, L. Liu and R. Lu "Bayesian learning-based multi-objective distribution power network reconfiguration", *IEEE Transactions on Smart Grid*, vol. 12, no. 2, 2021.

[66] H. Ahmadi, and J. R. Marti, "Linear Current Flow Equations With Application to Distribution Systems Reconfigurations", *IEEE Transactions on Power Systems*, vol. 30, no. 4, pp. 2073-2080, 2015.

[67] R. A. Jabr, R. Singh, and B. C. Pal, "Minimum loss network reconfiguration using mixed-integer convex programming", *IEEE Transactions on Power Systems*, vol. 27, no. 2, 2012.

[68] L. Gan, and S. H. Low, "Convex relaxations and linear approximation for optimal power flow in multiphase radial networks", *Power Systems Computation Conference*, August 18-22, 2014, Wroclaw, Poland.

[69] A. B. Jusoh, The instability effects of constant power loads, PECon 2004. Proceedings, Kuala Lumpur, Malaysia.

[70] Q. Peng, Y. Tang, and S. H. Low, "Feeder reconfiguration in distribution networks based on convex relaxation of OPF", *IEEE Transactions on Power Systems*, vol. 30, no.4, 2015.

[71] Y. Liu, J. Li, L. Wu, "Coordinated Optimal Network Reconfiguration and Voltage Regulator/DER Control for Unbalanced Distribution Systems", *IEEE Transactions on Smart Grid*, 2018.

[72] T. Altun, R. Madani, A. P. Yadav, A. Nasir and A. Davoudi, "Optimal reconfiguration of DC Networks", *IEEE Transactions on Power Systems* vol. 35, no. 6, 2020.

[73] M. Nick, R. Cherkaoui and M. Paolone, "Optimal planning of distributed energy storage systems in active distribution networks embedding grid reconfiguration", *IEEE IEEE Transactions on Power Systems*, vol. 33, no. 2, 2018.

[74] H. Sekhavatmanesh and R. Cherkaoui, "A novel decomposition solution approach for the restoration problem in distribution networks", *IEEE Transactions on Power Systems*, vol. 35, no. 5, 2020.

[75] C. Lee, C. Liu, S. Mehritra, and Z. Bie, "Robust distribution in network reconfiguration", *IEEE Transactions on Smart Grid*, vol. 6, no. 2, pp. 836-842, 2015.

[76] H. Sekhavatmanesh and R. Cherkaoui, "Analytical Approach for Active Distribution Network Restoration Including Optimal Voltage Regulation", *IEEE Transactions on Power Systems*, vol. 34, no. 3, 2019

[77] H. A. Ahmed and M. M. A. Salama,"Energy Management of AC/DC Hybrid Distribution Systems Considering Network Reconfiguration", *IEEE Transactions on Power Systems*, vol. 34, no. 6, 2019.

[78] Y. Song, Y. Zheng, T. Liu, S. Lei and D. Hill, "A New Formulation of Distribution Network Reconfiguration for Reducing the Voltage Volatility Induced by Distributed Generation", *IEEE Transactions on Power Systems*, vol. 35, no. 1, 2020.

[79] F. J. RodrÃguez, S. Fernandez, I. Sanz, M. Moranchel and E. J. Bueno, "Distributed approach for smart grids reconfiguration based on the OSPF routing protocol", *IEEE Transactions on Industrial Informatics*, vol. 12, no. 2, pp. 864-871, 2016.

[80] T. Taylor and D. Lubkeman, "Implementation of heuristic search strategies for distribution feeder reconfiguration", *IEEE Transactions on Power Delivery*, vol. 5, no. 1, pp. 239-246, 1990.

[81] J. Liu, P. Srikantha, "Distributed Assimilation of Grid Conditions and Load Integration via Social Learning", *2018 IEEE Global Conference on Signal and Information Processing (GlobalSIP)*, November 26-29, 2018, Anaheim, CA.

[82] J. Liu, P. Srikantha, "Kernel Structure Design for Data-Driven Probabilistic Load Flow Studies", *IEEE Transactions on Smart Grid*, to appear.

[83] J. Liu, P. Srikantha, "Decentralized Topology Reconfiguration in Multiphase Distribution Networks", *IEEE Transactions on Signal and Information Processing over Networks*, early access.

[84] J. Liu, P. Srikantha, "Adaptive Topology Reconfiguration in Smart Distribution Networks", *IEEE Transactions on Signal and Information Processing over Networks*, vol. 7, 2021.

[85] R. D. Zimmerman, C. E. Murillo-Snchez abd R. J. Thomas, "MATPOWER: Steady-state operations, planning and analysis tools for power systems research and education", *IEEE Transactions on Power Systems, vol. 26, no. 1, 2011.*

[86] R. C. Dugan, "Reference Guide: The open distribution system simulator (OpenDSS)", EPRI, 2016.

[87] J. Glover, M. Sarma and T. Overbye, "Power system design and analysis" Thompson-Engineering*, 2011.*

[88] S. Sun, B. Liang, M. Dong, and J. Taylor, "Phase balancing using energy storage in power grids under uncertainty", IEEE Transactions on Power Systems*, vol. 31, no. 5, pp. 3891-3903, 2016.*

[89] A. Camacho, M. Castilla, J. Miret, L. G. de Vicua, and G. L. M. Andros, "Control strategy for distribution generation inverters to maximize the voltage support in the lowest phase during voltage sags", IEEE Transactions on Industrial Electronics*, vol. 65, no. 3, pp. 2346-2355, 2018.*

[90] K. Orwig, et, al. "Recent Trends in variable generation forecasting and its value to the power system" IEEE Transactions on Sustainable Energy*, vol. 6, no. 3, pp. 924-933, 2015.*

[91] R. Hidalgo, C. Abbey and G. Joos, "A review of active distribution networks enabling technologies", Power and Energy Society General Meeting (PESGM) 2010 IEEE*, 2010.*

[92] H. J. Liu, W. Shi and H. Zhu, "Distributed voltage control in distribution networks: Online and robust implementations", IEEE Transactions on Smart Grid*, vol. 9, no. 6, 2018.*

[93] R. R. Nejad, W. Sun and A. Golshani "Distributed restoration for integrated transmission and distribution system with DERs", IEEE Transactions on Power Systems*, vol. 34, no. 6, 2019.*

[94] G. Gruosso, P. Maffezzoni, Z. Zhang and L. Daniel, "Probabilistic load flow methodology for distribution networks including loads uncertainty", International Journal of Electrical Power and Energy Systems*, 106, pp. 392-400, 2019.*

[95] R. R. Nejad and W. Sun, "Distributed load restoration in unbalanced active distribution networks", IEEE Transactions on Smart Grid*, vol. 10, no. 5, 2019.*

[96] B. Rotthier, T. V. Maerhem, P. Blockx, P. V. Bossche and J. Cappelle, "Home charging of electric vehicles in Belgium", 27th Electric Vehicle Symposium, Barcelona, Spain, November 2013.

[97] E. Yao, P. Samadi, V. W. S. Wong and R. Schober, "Residential demand side management under high penetration of rooftop photovoltaic units", IEEE Transactions on Smart Grid *, vol. 7, no. 3, 2016.*

[98] G. Li and X. Zhang, "Modeling of plug-in hybrid electric vehicle charging demand in probabilistic power flow calculations", IEEE Transactions on Smart Grid*, vol. 3, no. 1, 2012.*

[99] J. W. Shim, G. Verbic and K. Hur, "Stochastic eigen-analysis of electric power system with high renewable penetration: Impact of changing inertia on oscillatory modes", IEEE Transactions on Power Systems *, vol. 25, no. 6, 2020.*

[100] Z. Liang, H. Chen, X. Wang. S. Chen and C. Zhang, "Risk-based uncertainty set optimization method for energy management of hybrid AC/DC microgrids with uncertain renewable generation", IEEE Transactions on Smart Grid , vol. 11, no. 2, 2020.

[101] P. Billimgsley, *Probability and Measure, New York, Wiley, ISBN 0-471-0071-02.*

[102] B. Golub and M. O. Jackson, "Network structure and the speed of learning", Annals of Economics and Statistics*, (No. 107/108): 33-48, 2012.*

[103] S. Ronnberg, " Power Line Communication and Customer Equipment", Licentiate Thesis, Lulea University of Technology, Lulea, 2011.

[104] ABB Group, Distribution automation handbook*, 2011*

[105] P. T. Staats, W. M. Grady, A. Arapostathis, and R. S. Thallam, "A statistical analysis of the effect of electric vehicle battery charging on distribution system harmonic voltages", IEEE Transactions on Power Delivery*, vol. 13, no. 2, pp. 640-646, Apr. 1998.*

[106] J. R. Pillai and B. Bak-Jensen, "Impacts of electric vehicle loads on power distribution systems", Proceedings of IEEE Vehicle Power and Propulsion Conference*, Paris, France, Sep. 2010, pp. 1-6.*

[107] R. R. Richardson, M. A. Osborne, D. A. Howey "Gaussian process regression for forecasting battery state of health", Journal of Power Sources*, vol. 357, pp. 209-219, 2017.*

[108] D. K. Duvenaud, "Automatic Model Construction with Gaussian Process", Ph. D thesis, 2014.

[109] B. Colson, P. Marcotte and G. Savard, "An overview of bilevel optimization", Annals of Operation Research*, pp. 235-256, 2007.*

[110] C. A. Micchelli, Y. Xu and H. Zhang, "Universal Kernels", Journal of Machine Learning Research*, pp. 2651-2667, 2006.*

[111] B. Scholkopf, R. Herbrich and A. J. Smola, "A Generalized Representer System", Conference on Computational Learning Theory*, 2001.*

[112] S. Axler, Measure, Integration & Real Analysis *, Graduate Texts in Mathematics, Springer, 2020.*

[113] P. Pareek and H. D. Nguyen, "Gaussian Process Learning-Based Probabilistic Optimal Power Flow", IEEE Transactions on Smart Grid*, vol. 36, no. 1, 2021.*

[114] J. Lever, M. Krzywinski and N. Altman, "Model selection and overfitting", Nature Methods*, 13, pp.703-704 (2016).*

[115] A. G. De G. Matthews, M. Van Der Wilk, T. Nickson, K. Fujii, A. Boukouvalas, P. Leon-Villagra and Z. Gharamani, "GPflow: a Gaussian process library using tensorflow", The Journal of Machine Learning Research*, Jan. 2017.*

[116] K. P. Burnham, D. R. Anderson, Model Selection and Multi-Model Inference 2nd edition*, pp. 51, Springer, 2002.*

[117] H. Liu, Y. Ong, X. Shen and J. Cai, "When Gaussian Process meets big data: A Review of Scalable GPs", IEEE Transactions on Neural Networks and Learning Systems, vol. 31, no. 11, 2020.

[118] M. Marin, D. Defour and F. Milano, "Power flow analysis under uncertainty using symmetric fuzzy arithmetic", IEEE PES General Meeting*, 2014.*

[119] D. Monderer and L. Shapley, Potential games, Games and Economic Behavior, vol. 14, no. 1, pp. 1-8, 2008.

[120] T. Ui, "Discrete concavity for potential games", International Game Theory Review*, vol. 10, no. 1, pp. 1-8, 2008.*

[121] M. E. Baran and F. F. Wu, "Optimal capacitor placement of radial distribution systems", IEEE Transactions on Power Delivery*, vol. 4, no. 2, pp. 725-734, 1989.*

[122] J. R. S. Mantovani, F. Casari, and R. A. Romero, "Reconfiguração de sistemas de distribuição radiais utilizando o critério de queda de tensão, Revista Controle e Automação", Sociedade Brasileira de Au- tomática,SBA, vol. 11, no. 3, pp. 150-159, 2000.

[123] M. E. Baran and F. F. Wu, "Optimal decentralized microgrid coordination via the Schur's complement and S-procedure", IEEE Transactions on Smart*, vol. 11, no. 1, 2019.*

[124] T. Erseghe, "Distributed optimal power flow using ADMM", IEEE Transactions on Power Systems*, vol. 29, no. 5, 2014.*

[125] K. Damian, "Inference in additively separable models with a high-dimensional set of conditioning variables", University of Zurich, Department of Economics, Working Paper no. 284, 2018.

[126] S. Boyd, N. Parikh, E. Chu, B. Peleato, and J. Eckstein, "Distributed optimization and statistical learning via the alternating direction method of multipliers", Foundations and Trends in Machine Learning, vol. 3, no. 1, 2011.

[127] A. A. Ahmadi, "The S-lemma", 2016, Available: https://www.princeton.edu/~aaa/Public/Teaching/ORF523/S16/ORF523_S16_Lec12_gh.pdf

[128] S. Boyd, N. Parikh, E. Chu, B. Peleato and J. Eckstein, " Distributed optimization and statistical learning via the alternating direction method of multipliers", Foundations and Trends in Machine Learning*, vol. 3, no. 1, 2010.*

[129] S. Boyd and L. Vandenberghe. Convex Optimization*, Cambridge, UK: Cambridge university press, 2004.*

[130] J. Dattorro, Convex Optimization and Euclidean Distance Geometry*, 2006.*

*[131] K. P. Schneider, B. A. Mather, B. C. Pal, C. W. Ten, G. J. Shirek, H. Zhu, J. C. Fuller, J. L. R. Pereira, L. F. Ochoa, L. R. de Araujo, R. C. Dugan, S. Matthias, S. Paudyal, T. E. McDermott, and W Kersting, "Analytic considerations and design basis for the IEEE distribution test feeders",*IEEE Transactions on Power Systems *, vol. 33, issue. 3, 2018.*

[132] Y. Wang, T. L. Nguyen, Y. Xu, Z. Li, Q-T. Tran and R. Caire, "Cyber-physical design and implementation of distributed event-triggered secondary control in islanded microgrids", IEEE Transactions on Industry Application*, vol. 55, no. 6, pp. 5631-5642, Nov. 2019*

[133] B. Krupanek and R. Bogacz, "Investigations of transmission delays in ZigBee networks", Politechnika Slaska, Instytut Metrologii, Elektroniki i Automatyki*, vol. 1, no. 2, 2014.*

[134] Q. Peng and S. H. Low, "Distributed optimal power flow algorithm for radial networks, I: Balanced single phase case" IEEE Transactions on Smart Grid*, vol. 9, no. 1, 2018.*

[135] D. Peaucelle, D. Henrion, Y. Labit and K. Taitz, "Users guide for SeDuMi interface 1.04"

[136] A. Krishnamoorthy and D. Menon, "Matrix inversion using Cholesky Decomposition" Proc. Signal Processing Algorithms, Architectures, Arrangements and Applications*, pp. 70-72, Poznan, Poland, 2013.*